POLITECNICO DI TORINO

Department of Chemical and Materials Engineering

Master of Science Course
in Materials Engineering

Master of Science Thesis

INVESTIGATION OF A RADICAL INDUCED CATIONIC FRONTAL PHOTOPOLYMERIZATION (RICFP) IN HETEROGENEOUS SOFT POROUS MEDIA

Tutors

Prof. Marco Sangermano (Politecnico di Torino)
Dr. Yves Leterrier (EPFL)

Candidate

Daniele Maugeri

Marzo 2020

SOMMARIO DEL LAVORO DI TESI

Negli ultimi anni, il processo di fotopolimerizzazione ha acquisito sempre più importanza in base al suo valore economico ed ecologico. Moltissime applicazioni, come adesivi, rivestimenti, inchiostri e microelettronica, si basano su fotopolimeri, coprendo una vasta gamma di settori quali il biomedico e l'industriale [1]. A differenza della polimerizzazione iniziata termicamente, la fotopolimerizzazione non richiede alte temperature per attivare la reazione di crescita della catena polimerica e può essere eseguita anche a temperatura ambiente. Inoltre, le formulazioni foto-reticolabili sono prive di solventi, i tassi di produzione potrebbero essere molto elevati e il consumo di energia è molto basso se confrontato con l'indurimento termico classico. [2] Tuttavia, alcuni svantaggi devono essere considerati per il processo di fotopolimerizzazione quali i maggiori costi del materiale, la presenza di stabilizzanti che rallentano la polimerizzazione UV, la tossicità delle specie reattive e l'impossibilità di penetrazione della luce attraverso strati più profondi. Quest'ultimo problema può essere superato con il processo di polimerizzazione frontale (FP). Secondo Pojman J.A., la polimerizzazione frontale è un "*processo in cui la polimerizzazione avviene direzionalmente in una zona di reazione localizzata*", [3], [4]. In questo modo, secondo la stimolazione esterna utilizzata, viene indotto un fronte di reazione che trasforma il monomero nel polimero negli strati più profondi. Il processo complessivo coinvolto in questo studio è chiamato fotopolimerizzazione frontale cationica indotta da radicali (RICFP), definita come la combinazione di un indurimento superficiale fotoindotto della formulazione e del successivo fronte di reazione attivato termicamente che porterà alla polimerizzazione dell'intera struttura in poco tempo. L'RICFP è studiato principalmente per la produzione di compositi. Fori, cavità, o, matematicamente parlando, soluzioni di continuo rappresentano un problema enorme perché le instabilità strutturali e meccaniche ad esse collegate portano inesorabilmente a guasti, dal momento che possono essere classificati come crepe o concentratori di stress. Pertanto, sviluppare un riempitivo con un'elevata stabilità meccanica e la capacità di applicarlo in modo controllato è di fondamentale importanza. Alcune tecnologie sono ben note e ampiamente utilizzate per queste applicazioni, quali poliuretano espanso o silicone. Tuttavia, queste tecnologie richiedono tempi di applicazione lunghi, che possono anche raggiungere diverse ore, prima di ottenere il risultato finale [5], [6]. Per questo motivo, trovare una tecnologia / materiale che si adatta perfettamente alla forma dello spazio da riempire e che si indurisce in un tempo molto breve può essere molto attraente, specialmente se viene raggiunta la stabilità meccanica richiesta. Non tutte le soluzioni di continuo possono essere considerate anomalie o possibili origini del fallimento. Un esempio può essere la cavità auricolare e la necessità di produrre un auricolare personalizzato. Si possono prevedere molti vantaggi: innanzitutto un'esperienza migliore da parte dell'utente, principalmente grazie al perfetto adattamento dell'auricolare alla cavità dell'orecchio. Di conseguenza, il dispositivo non farà male quando è richiesto un uso prolungato, non cadrà frequentemente e garantirà un migliore isolamento dai rumori esterni. La tecnologia / materiale studiato può anche essere una valida alternativa alle tecnologie più recenti e avanzate nel campo delle procedure di scansione 3D che possono essere invasive e richiedere tempo [7] - [9]. In questo contesto, lo scopo di questo studio è di caratterizzare un sistema / materiale che induca l'acquisizione della forma in modo molto rapido. Il sistema / materiale dovrebbe avere due caratteri chiave: in primo luogo, deve avere la capacità di raggiungere la forma desiderata e, in secondo luogo, deve indurirsi quando si verifica uno stimolo esterno. Per quanto riguarda il primo carattere, il sistema / materiale deve essere abbastanza morbido per acquisire perfettamente la forma della cavità, mantenendola attraverso una pressione esterna e riprodurla attraverso la sua espansione. Un mezzo poroso morbido, come una schiuma, si adatta perfettamente a questi requisiti. Il secondo componente deve attivare la solidificazione della struttura, quindi è stata

selezionata una formulazione polimerizzabile ai raggi UV. In questo studio, la schiuma impregnata dalla formulazione induribile con UV è stata polimerizzata usando il processo RICFP. L'RICFP è caratterizzato da elevata esotermicità e grande produzione di gas, principalmente legati all'ebollizione della resina fotosensibile. Questo problema può portare a instabilità del fronte di polimerizzazione e a difficoltà nella conservazione della struttura. Inoltre, una maggiore quantità di gas prodotti porta a pressioni più elevate che possono essere un grosso problema quando la reazione avviene in una regione confinata come una cavità. Considerando la produzione di un auricolare su misura, la pressione aggiuntiva relativa alla produzione di gas si rifletterà sul timpano dell'utente, causando lesioni inaccettabili. Anche in altre condizioni, come una piccola cavità in un muro, la pressione prodotta genererà forze che agiranno sulla cavità inducendo ulteriori crepe. Inoltre, la temperatura è un fattore gravemente limitante quando si considera un dispositivo medico, come l'auricolare. Questa non deve raggiungere un valore superiore a 38 °C a causa dell'elevata sensibilità al calore collegata alla cavità dell'orecchio [10]. D'altra parte, se si considerano le applicazioni strutturali, i fenomeni di degradazione relativi al dispositivo studiato possono mettere in pericolo la stabilità meccanica. Nel presente studio, sono state analizzate la cinetica, la capacità di ritenzione della struttura, i fenomeni di temperatura e degradazione variando la composizione degli elementi fotosensibili e termici al fine di caratterizzare l'uso di RICFP su una schiuma poliuretanica impregnata con formulazioni polimerizzabili con UV. La serie di test condotti in questo studio fornisce una prima serie di caratterizzazione di tale sistema / materiale al fine di ottenere dati utili per ottimizzare la velocità della reazione, la velocità di produzione e per ridurre al minimo i fenomeni di degradazione. L'analisi termografica è stata condotta usando una videocamera IR per registrare le temperature coinvolte e la cinetica del fronte di propagazione. Sono state eseguite analisi termogravimetriche per studiare i fenomeni di degrado in base alle temperature registrate mediante test termografici. SEM e microscopia ottica sono stati utilizzati per riconoscere questi eventi di degrado che caratterizzano la struttura formata. Al fine di studiare in profondità i fenomeni cinetici e di conversione, si sono dimostrati potenti metodi di indagine la spettroscopia infrarossa a trasformata di Fourier (FTIR) e la (foto)calorimetria a scansione differenziale. Nella sezione 2, viene presentata una panoramica dei processi di fotopolimerizzazione, comprese le tecniche di polimerizzazione frontale. Nella sezione 3 sono descritti i metodi di indagine e la preparazione del campione. Infine, nella sezione 4 verranno presentati i risultati relativi agli obiettivi sopra menzionati. Inoltre, il processo RICFP è stato utilizzato per produrre per la prima volta un composito a fase compenetrante (IPC) utilizzando una schiuma di alluminio come mezzo poroso. Questa condizione riduce l'adattabilità alla forma della cavità, portando al contempo una vasta gamma di miglioramenti. Innanzitutto, la combinazione di una tecnica indotta dai raggi UV con la produzione di un materiale composito può condurre a vantaggi economici e ambientali ed implica la possibilità di migliorare le proprietà fisiche, chimiche e meccaniche di questa classe di materiali.

In questo studio, è stata utilizzata una resina epossidica cicloalifatica (3-4-epoxycyclohexane) methyl3'-4'-epoxycyclohexyl-carboxylate, Omnilane OC 1005 proveniente da IGM. Il fotoiniziatore impiegato (come ricevuto) è p-(octyloxyphenyl)-phenyliodonium hexafluoroantimonate, abbreviato in IOC8 SbF_6^-, proveniente da ABCR mentre l'iniziatore termico utilizzato (come ricevuto) è 1,1,2,2-Tetraphenyl-1,2-ethanediol (98%) di Acros, abbreviato in TPED. La schiuma selezionata è quella poliuretanica PU Supercell 2017 EUROFOAM prodotta dal gruppo EUROSPUMA®.

Sono state studiate in totale nove formulazioni, come illustrato nella Tabella 1, che scansionano condizioni diverse

Tabella 1: formulazioni studiate

#	IOC8 SbF6 (FOTOINIZIATORE)	TPED (INIZIATORE TERMICO)
1.	0.5%wt	0%wt
2.	1%wt	0%wt
3.	2%wt	0%wt
4.	3%wt	0%wt
5.	0.5%wt	0.5%wt
6.	0.5%wt	1.5%wt
7.	0.5%wt	3%wt
8.	1.5%wt	0.5%wt
9.	3%wt	0.5%wt

Nelle composizioni da 1 a 4. non è stato utilizzato alcun iniziatore termico mentre sono state utilizzate quantità crescenti di fotoiniziatore. Sono stati confrontati con le composizioni 5., 6. e 7. al fine di identificare qualsiasi effetto di schermatura dato dalla presenza dell'iniziatore termico nella sua minima quantità (0,5% in peso). Quindi sono state selezionate le composizioni da 5. a 9. per studiare gli effetti sui parametri del fronte risultanti dalla diversa quantità di fotoiniziatore mantenendo la minima quantità di iniziatore termico e viceversa.

La quantità più piccola di entrambi gli iniziatori è fissata allo 0,5% in peso, ponderata in 15 g della composizione complessiva. A quantità inferiori di entrambi gli iniziatori non è stato osservato alcun fronte. Tutte le formulazioni sono state agitate magneticamente a 40 ° C per 40 minuti mostrando una buona omogeneità. Una prima serie di prove è stata condotta per dimostrare che solo la presenza di entrambi gli iniziatori è adatta alla propagazione del fronte. Ad esempio, le formulazioni contenenti solo fotoiniziatore hanno prodotto solo un indurimento superficiale mentre le formulazioni contenenti solo iniziatore termico non hanno mostrato alcun tipo di polimerizzazione alla luce UV.

Il campione di schiuma, tagliato a 1,5 cm di lunghezza e con un diametro di 16 mm (tenendo presente che lo studio esamina la possibilità di realizzare un auricolare), viene immerso nella resina in uno stato compresso e quindi lasciato espandersi in modo che assorba la resina. Quindi il campione impregnato viene posto su un foglio di alluminio per eliminare la resina esterna in eccesso e successivamente posizionato sul supporto per l'irraggiamento diretto. Questa procedura è stata eseguita al fine di liberare il campione da qualsiasi contenitore (silicio, vetro o metallo) dato che questo modificherebbe il valore di emissività e altererebbe il valore di temperatura registrato, compromettendo l'indagine sui fenomeni di degradazione. Tuttavia, in relazione all'applicazione effettiva del dispositivo, deve essere considerato l'uso di un involucro esterno aggiuntivo. Questo potrebbe essere usato come uno schermo termico e agli UV, ad esempio nei casi in cui è previsto il contatto del dispositivo con la pelle. Tuttavia, questa configurazione non modifica la temperatura reale emanata durante la propagazione frontale attraverso la schiuma impregnata. Infine, in questo modo la struttura della schiuma è stata mantenuta inalterata per non indurre eterogeneità aggiuntive.

Per tutto lo studio, è stata utilizzata una lampada UV al mercurio ad alta pressione serie Omnicure 2000, Exfo-Omnicure, Canada. Le immagini termiche sono state realizzate con

una telecamera IR FLIR T450sc al fine di descrivere il comportamento del fronte. Per ogni campione sono stati fissati tre diversi punti di registrazione, in dettaglio:

- sp1: sulla superficie superiore del campione, dove dovrebbe avvenire l'inizio del fronte di polimerizzazione;

- sp2: a 0,5 cm da sp1, dove dovrebbe essere in corso un fronte di propagazione stabile di polimerizzazione;

- sp3: a 0,5 cm da sp2, dove il fronte di polimerizzazione dovrebbe passare alle stesse condizioni di sp2.

Per caratterizzare il comportamento di un fronte di propagazione della polimerizzazione, devono essere considerati tre diversi parametri: tempo di inizio del fronte (t_{start}), temperatura massima (T_{max}), velocità del fronte (V_f) e tempo di processo. Il tempo di innesco è definito come quello in cui si ha la formazione iniziale del fronte di polimerizzazione termica, in altre parole quando il fronte viene attivato e si verifica un "inizio" (la temperatura della reazione esotermica è compresa tra 250 ° C e 270 ° C, evidenziata con un colore rosso nell'immagine IR). La temperatura massima (T_{max}) è stata misurata tramite la termografia IR, registrando la temperatura massima in ciascuno dei tre punti di registrazione. Sapendo che la distanza tra sp2 e sp3 è 0,5 cm, è stato quindi possibile misurare la velocità del fronte tra di essi. Il tempo di processo viene misurato durante la registrazione dell'evoluzione del processo per tutta la lunghezza del campione (1,5 cm). Al fine di studiare il comportamento del fronte attraverso lo spessore del campione e ottenere dati utili per stabilizzare il fronte di propagazione, sono state identificate curve di temperatura rispetto al tempo (Figura 1).

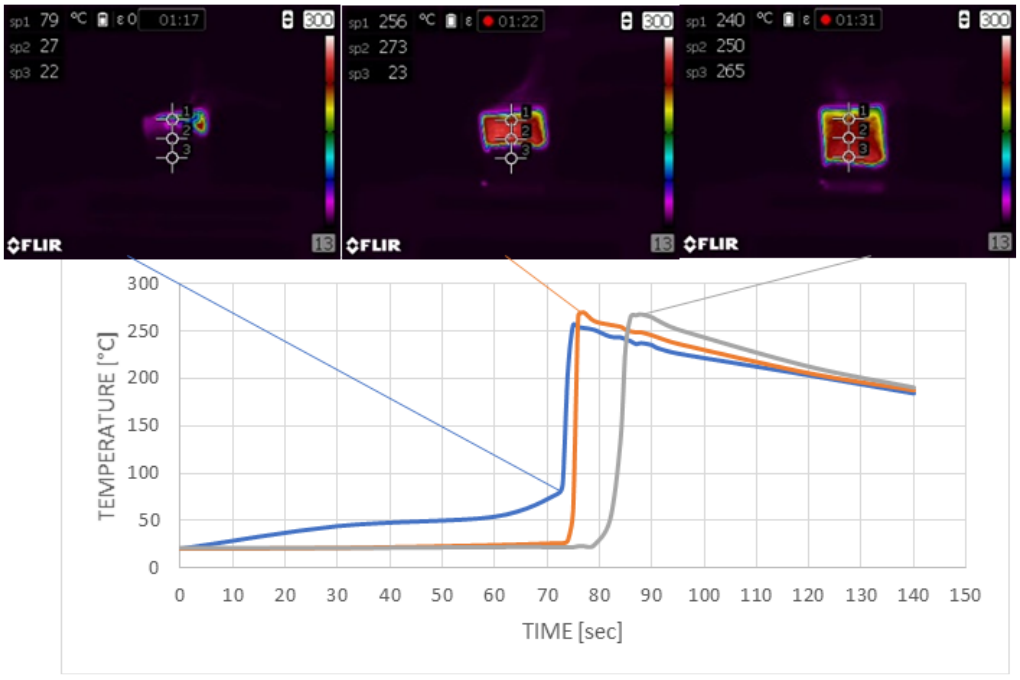

Figura 1: esempio di sviluppo del fronte di propagazione

Come riportato in letteratura, nonostante alcune anomalie, la forma delle curve è una chiara manifestazione che si è verificata una polimerizzazione frontale per tutte le composizioni. Il comportamento frontale è caratterizzato da un buon livello di omogeneità tra sp2 e sp3. Ciò ha creato le condizioni per misurare la velocità del fronte con una buona precisione usando il calcolo e la mappatura delle immagini sui fotogrammi estratti dal video registrato.

Al contrario, il comportamento del fronte è imprevedibile tra sp1 e sp2 e fortemente influenzato dalle distorsioni tra sp3 e il fondo dei campioni.

Lo studio della cinetica del fronte di propagazione è stato condotto per tutte le formulazioni, concentrandosi sul tempo di inizio del fronte e sulla sua velocità (Figura 2). Da questo grafico, è possibile concludere che il tempo di inizio del fronte può essere ridotto a una quantità maggiore di fotoiniziatore. Tuttavia, una limitazione dovrebbe essere presa in considerazione al 1,5% in peso di fotoiniziatore perché, quando viene superata tale soglia, l'effetto pelle (*skin effect*) diventa importante, portando a un ritardo del tempo di innesco del fronte. Grazie al miglioramento della reattività, la velocità del fronte aumenta quando la quantità di fotoiniziatore viene aumentata all'1,5% in peso. A quantità più elevate, si verifica una saturazione ed è visibile un plateau, quindi la velocità del fronte non è più influenzata. Questa tendenza è simile a quella studiata da Mariani et al., tuttavia i valori assoluti registrati in questo studio sono leggermente più alti, probabilmente a causa dell'uso di un diverso iniziatore termico (benzofenone).

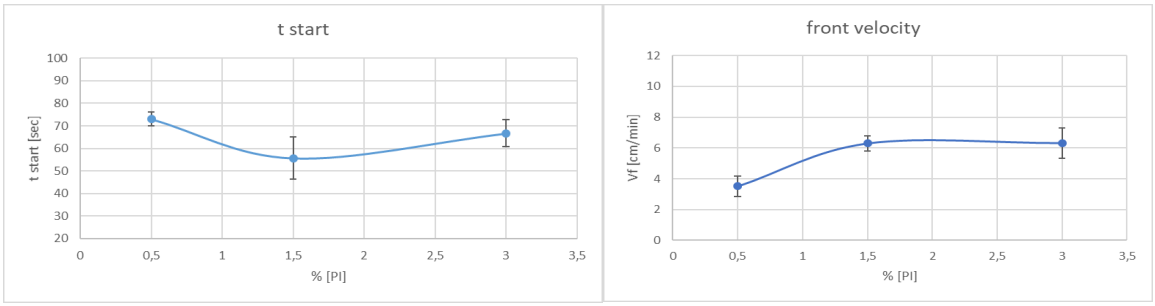

Figure 2: tempo di innesco (sinistra), velocità del fronte (destra) variando la quantità di fotoiniziatore a 40mW/cm²

Per quanto riguarda la diversa quantità di iniziatore termico, la cinetica del fronte di propagazione è diversa (Figura 3). Il tempo di innesco può essere ritardato aumentando la quantità di iniziatore termico, questo comportamento è chiaramente visibile quando la sua quantità è massima. Questo problema può essere correlato a un effetto di schermatura dell'iniziatore termico dovuto al fatto che contiene strutture cromofore o alla probabile mancanza di dissoluzione che porta a effetti di dispersione (*scattering*). La velocità del fronte aumenta aumentando la quantità dell'iniziatore termico fino all'1,5% in peso di TPED, per quantità più elevate di TPED la velocità del fronte continua ad aumentare, anche se con un gradiente basso. Ciò potrebbe essere dovuto a un "effetto di saturazione", in altre parole, dopo aver raggiunto un certo livello / soglia, la velocità del fronte non è più influenzata da una percentuale maggiore di TPED. Il risultato è parzialmente in linea con la letteratura. Sia Bomze et al. e Mariani et al. hanno registrato una maggiore velocità frontale aumentando la concentrazione dell'iniziatore termico. In particolare, Mariani et al. hanno registrato che "*per una quantità di iniziatore superiore al 3,0% in moli non sono state osservate variazioni significative nella velocità del fronte e nella temperatura massima*". Quanto riportato da Mariani et al. ed il risultato dei test condotti nel presente studio, può suggerire che la velocità del fronte non è influenzata considerevolmente dalla concentrazione dell'iniziatore termico che supera un certa soglia. È molto probabile che questa soglia sia un valore caratteristico di una formulazione specifica (resina e iniziatore termico). In questo studio, la soglia è dell'1,5% in peso.

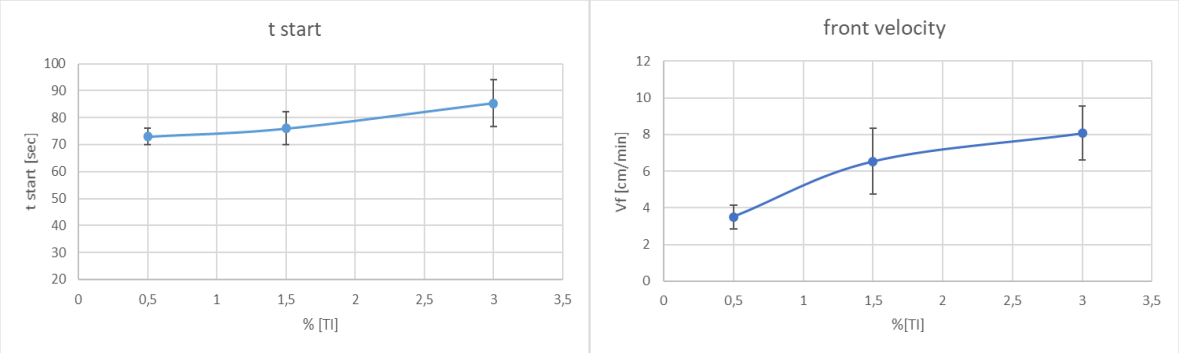

Figure 3: tempo d'innesco del fronte (sinistra) e velocità del fronte (destra) per diverse quantità di iniziatore termico a 40mW/cm²

È stato condotto uno studio sull'effetto delle diverse percentuali dei due iniziatori sul tempo di processo, un parametro chiave per determinare il tasso di produzione del processo studiato (Figura 4). Come è visibile, è possibile concludere che l'unico modo per ridurre significativamente il tempo di processo è legato alle formulazioni in cui il fotoiniziatore è compreso tra 0,5% in peso e 1,5% in peso, mentre l'iniziatore termico è mantenuto alla quantità minima dello 0,5% in peso. Ciò comporterà una diminuzione del tempo di inizio del fronte considerando che l'effetto pelle non è una condizione influente che, in questo caso, viene registrata con una maggiore quantità di fotoiniziatore. La variazione della percentuale di TPED non influisce sul tempo di processo.

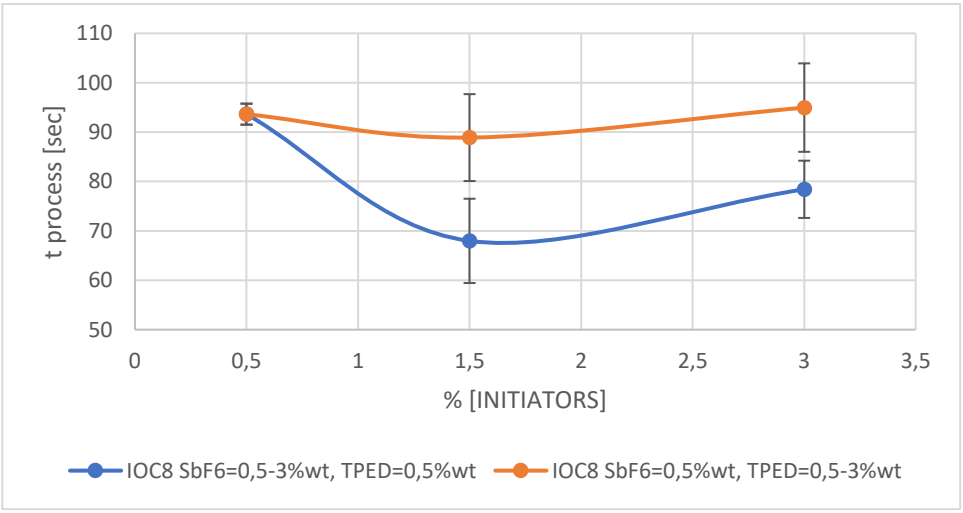

Figura 4: tempo di processo riferito ad un manufatto spesso 1,5cm

Per quanto riguarda la temperatura massima, essa è stata misurata in tutte le formulazioni (Figura 5). A una maggiore quantità di fotoiniziatore, viene indotta una maggiore esotermicità, che porta ad un aumento del valore della temperatura massima. In queste particolari condizioni, l'enorme produzione di fumi porta a molte difficoltà nella valutazione della temperatura massima, come mostrano i valori elevati relativi alle deviazioni standard (Figura 5). Tuttavia, le temperature registrate mostrano un aumento all'aumentare della quantità di fotoiniziatore, come prevedibile a causa della maggiore reattività della formulazione. Per quanto riguarda la quantità crescente di iniziatore termico, un valore massimo di temperatura viene registrato all'1,5% in peso, mentre a quantità più elevate la temperatura non ha mostrato variazioni importanti. Ancora una volta, questa tendenza è simile a quella definita da Bomze et al. [27].

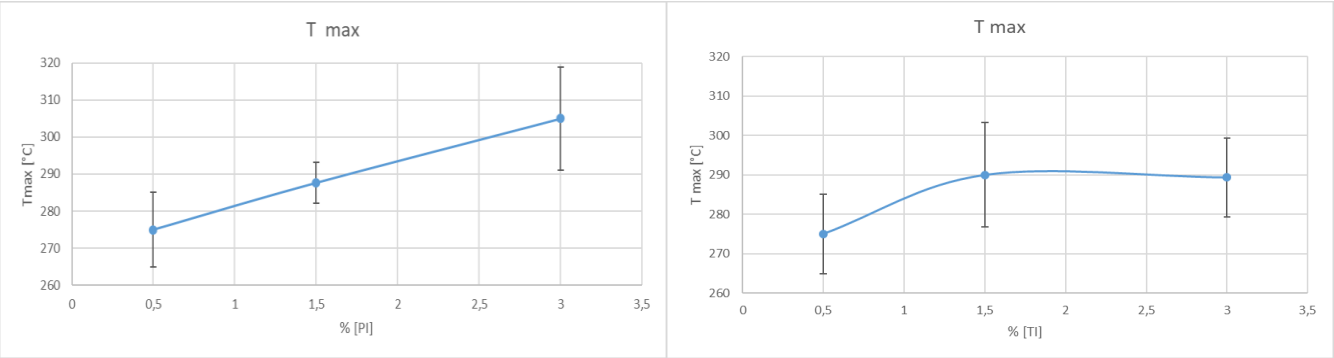

Figure 5:valutazione della massima temperatura registrata: variazione della quantità di fotoiniziatore (sinistra) e variazione della quantità di termoiniziatore (destra)

Poiché sono stati registrati valori di temperatura elevata, si è ritenuto necessario condurre indagini sui fenomeni di degrado interno. In questo modo, sono state eseguite misurazioni TGA sul comportamento di degradazione di: schiuma non riempita e resina (Figura 6).

	T_{onset}	T_{peak}
Omnilane Oc1005	239,69 °C	290,04°C
Pu Supercell 2017 Eurofoam	264,70 °C	283,03°C; 345,19 °C

Figura 6: risultati misure TGA, range di temperatura: 30-400°C, rampa:10°C/min

In tutti i test, le temperature effettive hanno raggiunto livelli superiori alla temperatura di onset. Questa condizione ha portato alla presenza di fenomeni di degradazione in tutti i campioni studiati, tranne in quello con le minori concentrazioni di iniziatori, in cui questo problema sembra essere più controllato. Tale fenomeno è stato confermato dalle immagini SEM. Le immagini mostrano che è stata mantenuta una struttura schiumosa perché durante la polimerizzazione è stato prodotto un agente schiumogeno (gas proveniente dall'ebollizione della resina). Ciò può portare a un miglioramento del comportamento di isolamento termico del materiale studiato. Tuttavia, è necessario prendere in considerazione un numero maggiore di parametri per dimostrare la sua efficace bassa conduttività termica come il controllo della porosità, che non può essere investigato nelle condizioni dei test eseguiti. Sono state eseguite misurazioni DSC per studiare la conversione in strati più profondi del campione ottenuto da RICFP. Nessuna delle formulazioni studiate ha rivelato importanti picchi esotermici identificando una reazione completa e confermando l'elevata reattività associata alla resina fotosensibile studiata.

Sono necessarie ulteriori indagini per confermare ciò che è stato sperimentato attraverso misurazioni visive del fenomeno della polimerizzazione frontale. Il contributo delle misure di Photo-DSC è fondamentale per studiare i fenomeni cinetici e di conversione della prima reazione foto-indotta. In primo luogo, l'entalpia teorica di reazione è stata calcolata tenendo conto della funzionalità del monomero utilizzato (f=2), dell'energia di attivazione (94,5 kJ/mol) e del suo peso molecolare (232,32 g/mol). Il valore calcolato è di 749,05 J/g ed utilizzato come valore di riferimento per le misure di Phot-DSC. L'attenzione è stata posta inizialmente sulla diversa quantità di IOC8 SbF6 dalla formulazione 1. alla formulazione 4. in cui non è stato aggiunto alcun iniziatore termico. Quindi, i valori di t gel e ά sono stati confrontati con la formulazione 5., 8. e 9. al fine di studiare la stessa influenza quando viene

aggiunto lo 0,5% in peso di iniziatore termico. Aumentando la quantità di IOC8 SbF6 si verifica un aumento sul gel t e una diminuzione su ȧ. Questo può essere correlato all'effetto pelle, che si verifica in queste condizioni. Inoltre, la formazione di specie aromatiche secondarie, che assorbono a lunghezze d'onda simili a quelle assorbite dal foto-iniziatore, può influire sull'efficienza di assorbimento dello stesso, riducendo la quantità di specie reattive formate [56], [57]. Nessuna differenza, specialmente nel t gel, è stata identificata quando si aggiunge lo 0,5% in peso di iniziatore termico, assumendo l'inesistenza di effetti di schermatura da parte di quest'ultimo in queste concentrazioni. Tuttavia, è visibile un aumento di ȧ confrontando la formulazione 1. (0,5% in peso di IOC8 SbF6) e la formulazione 5. (0,5% in peso di entrambi gli iniziatori foto e termici) che porta a una certa reattività causata dalla presenza aggiuntiva dell'iniziatore termico. La stessa indagine è stata condotta aumentando la quantità di TPED dallo 0% in peso (formulazione 1.) al 3% in peso (formulazione 5., 6., 7.) mantenendo costante il valore del fotoiniziatore allo 0,5% in peso. Non sono state osservate differenze per quanto riguarda il t gel, tuttavia una diminuzione del *rate* di conversione massimo è evidente con una maggiore quantità di iniziatore termico (1,5% in peso e 3% in peso) se confrontato con la formulazione con la quantità più bassa di TPED. Si ipotizza quindi la possibilità di un effetto di screening correlato alla presenza di maggiori quantità di iniziatore termico, in linea con il ritardo nel punto d'innesco precedentemente mostrato ad elevate quantità di iniziatore termico (3% in peso) attraverso le misure termografiche.

Infine, i risultati ottenuti da Photo-DSC e le misurazioni della termografia sono stati confrontati al fine di identificare una correlazione tra la fase di iniziazione e la propagazione del fronte. In particolare, sono stati tracciati t gel e tempo d'innesco, ȧ e la velocità del fronte (Figura 6). La curva arancione raffigura il comportamento dei quattro parametri tracciati con percentuali diverse di iniziatore termico: nessuna particolare relazione tra iniziazione e propagazione può essere dedotta, specialmente per quanto riguarda ȧ vs V_f. In questa condizione, il risultato può essere considerato come "una nuvola di punti". La curva blu mostra il comportamento dei quattro parametri con percentuali diverse di foto iniziatore.

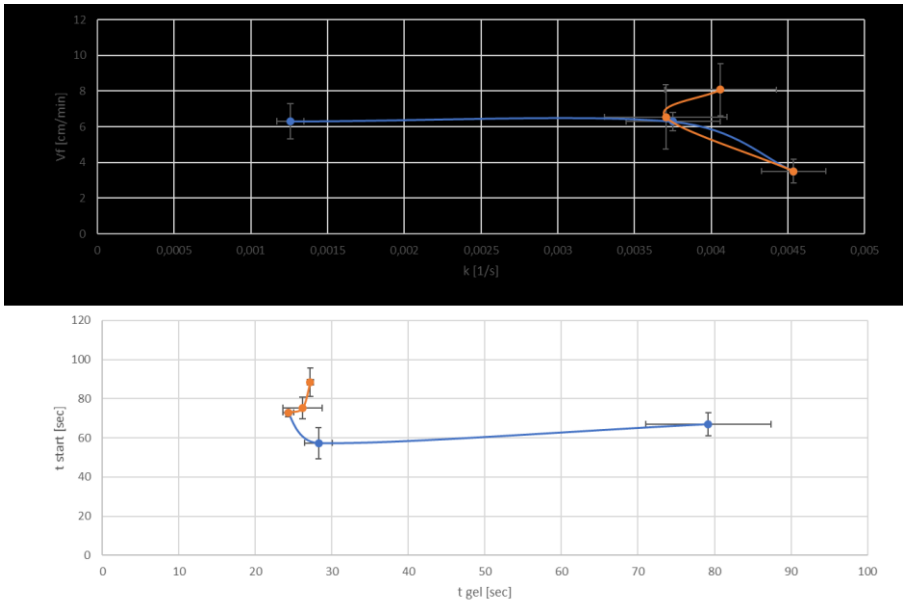

Figure 6: ȧ vsV_f (in alto). t_{start} vs t_{gel}(in basso),curva arancione: IOC8 SbF6=0,5%wt / TPED=0,5% - 3%wt. curva blu:: IOC8 SbF6=0,5% - 3%wt / TPED=0,5%wt

Il diagramma tempo d'innesco (t start) vs t gel come anche la diminuzione di ά suggerisce la presenza di un effetto pelle, che aumenta con l'aumentare delle percentuali del

fotoiniziatore. Quando la quantità di fotoiniziatore viene aumentata eccessivamente, può verificarsi un ritardo nell'innesco del fronte: questo è in linea con il crescente t gel e una diminuzione di ά. Sorprendentemente, per concentrazioni di fotoiniziatore tra lo 0,5% in peso e l'1,5% in peso, la velocità del fronte aumenta mentre diminuisce ά: ciò potrebbe essere dovuto al fatto che l'effetto pelle blocca la creazione di specie reattive attraverso lo spessore del campione, ma una maggiore creazione di specie reattive si verifica sulla sua superficie, quindi la parte iniziale della polimerizzazione è caratterizzata da una diffusione termica più lenta. Ciò può comportare sia una riduzione del tempo di avvio del fronte sia una velocità del fronte più elevata [59], [60]. Per concentrazioni superiori all'1,5% in peso, detto fenomeno non è stato registrato. Comunque, questo studio necessita un maggiore approfondimento.

Visti i fenomeni di degradazione presenti nel sistema utilizzato, una valida alternativa è quella di cambiare il mezzo poroso, utilizzando una spugna metallica per la creazione di un materiale composito a fasi interpenetranti. La possibilità di combinare i vantaggi legati alla tecnologia UV con quelli relativi ai composti a fasi interpenetranti può portare a eccezionali vantaggi economici, ecologici e tecnologici. La prima sfida è stata l'impregnazione della schiuma. Per facilitare l'impregnazione della resina attraverso il mezzo poroso, è stata selezionata una schiuma di alluminio caratterizzata da grandi dimensioni dei pori e una forma cilindrica di 3 cm di diametro. Una composizione dell'1% in peso di entrambi gli iniziatori è stata preparata seguendo il metodo proposto al fine di garantire la propagazione frontale attraverso i mezzi porosi. La schiuma è stata tagliata ad uno spessore inferiore a quello dello stampo. La formulazione è stata versata in uno stampo di silicio fino a riempire metà di essa, quindi la schiuma di alluminio è stata posizionata e spinta nello stampo per ottenere l'impregnazione degli strati più profondi. Quindi, una formulazione aggiuntiva è stata versata nello stampo per ottenere l'impregnazione in strati superficiali. Successivamente, la fonte luminosa è stata posizionata molto vicino al campione, la potenza della lampada è stata impostata al 100% e, infine, la luce è stata accesa. È stata garantita la presenza dello spessore minimo dello strato per innescare la polimerizzazione frontale che è avvenuta con successo. Il materiale ottenuto potrebbe aprire un nuovo ampio capitolo nel campo dei compositi ultraleggeri mantenendo tutti i vantaggi relativi al processo di polimerizzazione UV. Gli alti tassi di produzione prevedibili, il basso consumo di energia, le formulazioni prive di solventi e facili da produrre sono caratteristiche importanti che possono portare a notevoli benefici nella produzione di materiali compositi.

Poiché si verificano alte temperature e fenomeni di degrado, non è possibile prendere in considerazione un'applicazione valida per il sistema finale ottenuto tenendo conto anche del fatto che non è possibile raggiungere la stabilità meccanica. Inoltre, sono state osservate molte difficoltà nel tentativo di controllare il processo quali instabilità del fronte, produzione di gas e persino possibile mancanza di impregnazione. Tali difficoltà sono principalmente dovute all'eterogeneità della struttura della schiuma e al metodo di impregnazione basato solo sull'infiltrazione. Il controllo di queste proprietà porterà a un livello di precisione più elevato. Ad esempio, al fine di migliorare la fase di impregnazione, è possibile considerare una funzionalizzazione della superficie della schiuma mediante tecniche di photografting oppure sfruttando dei tensioattivi. Infine, i fenomeni di degrado e la formazione di bolle dovrebbero essere considerati attentamente in queste condizioni più critiche, specialmente per le applicazioni strutturali.

Ulteriori studi devono essere condotti al fine di identificare il miglior compromesso per questo processo, in primo luogo concentrandosi sulla quantità di iniziatore considerata e sulla relativa velocità di produzione. Secondo i risultati ottenuti dal sistema studiato, un modo per ridurre i tempi di processo e massimizzare il tasso di produzione è quello di

aumentare la quantità di fotoiniziatore. Tuttavia, questo potrebbe essere dispendioso perché il fotoiniziatore è il composto più costoso aggiunto nella formulazione.

Un altro parametro, che non è stato modificato in questo studio e mantenuto a livelli bassi per studiare possibili applicazioni che comportano il contatto con la pelle, è l'irradianza iniziale. L'aumento di questo valore porterà a un *rate* di polimerizzazione più rapido correlato alla prima parte foto-indotta del processo. Ciò ridurrà il punto di partenza del fronte portando ad un aumento del tasso di produzione.

In sintesi, lo studio ha condotto alla caratterizzazione dell'applicazione della metodologia RICFP per l'occlusione di piccole cavità con il particolare obiettivo di produrre un auricolare. La tecnica RICFP utilizzata con schiuma poliuretanica è caratterizzata da:

- certezza della realizzazione di un fronte di polimerizzazione;
- esotermicità elevata e non riducibile, questo ne impedisce l'uso per uso medico e, in particolare, rende questa tecnica inadatta alla creazione di un auricolare personalizzato;
- presenza di fenomeni irregolari e non predeterminabili nell'area di innesco;
- alte temperature di processo che portano a fenomeni di degrado della schiuma, all'ebollizione della resina con la conseguente formazione di gas caldi che mettono in pericolo l'omogeneità del prodotto polimerizzato con evidenti conseguenze negative sulla stabilità meccanica e sull'isolamento termico e acustico.

I risultati degli esperimenti di laboratorio hanno permesso di determinare che le percentuali ottimali di iniziatori sono comprese tra lo 0,5% in peso e l'1,5% in peso di fotoiniziatore, mentre l'iniziatore termico deve essere mantenuto al valore dello 0,5% in peso.

Ulteriori indagini applicate a questa domanda potrebbero essere:

- studiare una resina diversa con temperatura di ebollizione più elevata che non consenta la presenza di bolle durante l'indurimento;
- studiare un modo per ridurre la temperatura, che è principalmente correlato alla resina selezionata;
- trovare un equilibrio tra la percentuale di iniziatori e l'irraggiamento iniziale, al fine di ottenere la migliore efficienza dal processo;
- studiare come si comporta il fronte della polimerizzazione quando sono necessarie dimensioni maggiori del produttore, concentrandosi su quanto può essere alimentato e su quanto è prevista la produzione di gas e bolle;
- migliorare l'impregnazione della schiuma sfruttando le tecniche di funzionalizzazione, questo potenziamento può essere correlato a tutti i tipi di schiume usate, sia polimeriche che metalliche;
- studiare le proprietà meccaniche, fisiche e chimiche del composto di fase compenetrante prodotto con la tecnica RICFP.

Sommario

1. Introduction

In recent years, photopolymerization process has gained more and more importance according to its economic and ecological value. A wide range of application are based on photopolymers such as adhesives, coatings, inks and microelectronics, covering a wide range of applications such as biomedical and industrial sectors [1]. In contrast to thermal-initiated polymerization, photopolymerization doesn't requires high temperatures in order to activate the chain growth reaction and it can be performed even at room temperature. Furthermore, crosslinkable formulations are solvent free, production rates could be very high and energy consumption is very low if compared with classical thermal curing. [2] However, some disadvantages must be considered for the photopolymerization process such as the higher material costs, the presence of stabilizers which decelerate the UV curing, the toxicity of reactive species and the impossibility of light penetration through deeper layers. This last issue can be overcome by the frontal polymerization (FP) process. According to Pojman JA, frontal polymerization is a "*process in which polymerization occurs directionally in a localized reaction zone"*, [3], [4]. In this way, according to the used external stimulation, a reaction front is induced which transform the monomer into the polymer in deeper layers. The overall process involved in this study is called Radical Induced Cationic Frontal Photopolymerization (RICFP), defined as the combination of a photo-induced surface curing of the formulation and the subsequent thermal-activated reaction front which will lead to the polymerization of the entire structure in a short time. RICFP is mainly studied for composites production.

Holes, cavities, orifices or, mathematically speaking, breaks in continuity represents a huge issue because structural and mechanical instabilities linked to them lead inexorably to failures as soon as they can be classified as cracks or stress concentrator. Therefore, developing a filler with an high mechanical stability and the capability to apply it in a controlled way is of paramount importance. Some technologies are well known and widely used for those applications such as expanded polyurethane or silicon. However, these applications are highly time consuming because they require long application time that may range in several hours before reaching the final result [5], [6]. For that reason, finding a technology/material that fits perfectly the shape of the gap to be filled and that hardens in a very short time can be very attractive, especially if the required mechanical stability is reached. Not all breaks in continuity can be considered as anomalies or possible origins of failure. One example can be the ear cavity and the requirement of producing a personalized earbud. Lots of benefits can be envisaged: first of all a better user experience, mainly due to the perfect adaptation of the earbud to the ear cavity. As a result, the device won't hurt when a prolonged use is required, won't fall frequently and will ensure a better insulation from external noises. The studied technology/material may also be a valid alternative to the latest and most advanced technologies in the domain of 3-D scanning procedures which can be invasive and time consuming [7]-[9]. In this contest, the aim of this study is to characterize a system/material that induces the shape acquisition in a very fast way. The system/material should have two key characters: first, it must have the ability to reach the desired shape and, second, it must cure when an external stimulus occurs. Regarding the first character, the system/material must be soft enough in order to acquire perfectly the shape of the cavity, maintaining it through an external pressure and maintaining it through its expansion. A soft porous media, like a foam, fit perfectly with these requirements. Then, the second component must activate the solidification of the structure, therefore an UV-curable formulation was selected. In this study, the foam impregnated by the UV-curable formulation was cured using the RICFP process.

RICFP is characterized by high exothermicity and large production of gasses, related mostly to the boiling of the photosensitive resin. This issue may lead to front instabilities and difficulties in the structure retention. Moreover, larger amount of produced gasses leads to higher pressures which can be a big issue when the curing occurs into a confined region such as cavities. Considering the manufacturing of a custom-made earbud, the extra pressure related to gas production will be reflected on the user's earbum leading to unacceptable injuries. Also in other conditions, such as a small cavity into a wall, the produced pressure will generate forces that will act on the cavity inducing further cracks. In addition, temperature is a severe factor when a medical device is considered, such as the earbud, taking for mandatory that whatever technology is used, it must not reach a temperature higher than 38 °C due to the high heat sensitivity linked to the ear cavity [10]. On the other hand, if structural applications are considered, degradation phenomena related to the studied device may endanger the mechanical stability. In the present study, the kinetic, structure retention ability, temperature and degradation phenomena were analysed varying the composition of the photosensitive and thermal elements in order to characterize the use of RICFP on polyurethane foam impregnated with UV-curable formulations. The set of tests conducted in this study provide a first set of characterization of such a system/material in order to obtain useful data for optimising the speed of the reaction, the production rate, and for minimizing degradation phenomena. Thermographic analysis was conducted using an IR camera in order to record involved temperatures and the propagating front kinetic. Thermogravimetric analyses were performed to investigates degradation phenomena according to recorded temperatures by thermographic tests. SEM and optical microscopy were used to recognise these degradation events characterizing the formed structure. In order to deeply investigate kinetic and conversion phenomena, Fourier-transform infrared spectroscopy (FTIR) and scanning (photo) calorimetry were powerful methods. In section 2, is presented an overview of photopolymerization processes including frontal polymerization techniques is presented. In section 3 materials, methods of investigation and sample preparation are described. Finally, in section 4 will present results related to the previously mentioned goals. In addition, the RICFP process was used to produce an Interpenetrating Phase Composite (IPC) for the very first time using an aluminium foam as porous media. This condition reduces the adaptability to the shape of the cavity while leading to a wide range of improvements. First, combining an UV-induced technique with the production of a composite material, will lead to economic and environmental benefits and imply the possibility to enhance physical, chemical and mechanical properties of this class of materials.

All theoretical and experimental activities were performed between September 2019 and February 2020 at EPFL – École Polytechnique Fédérale de Lausanne, and in particularly within MX department (section de science et génie des matériaux), the LPAC (Laboratory for Processing of Advanced Composites), MHMC (Molecular and Hybrid Materials Characterization Center) and DLL (Discovery Learning Laboratory).

2. State of the art

2.1 Photopolymerization

In chemistry, photopolymerization is a technique that uses light (visible or ultraviolet - UV) to initiate and propagate a polymerization reaction to form a linear and crosslinked reaction. Incident light will indeed activate suitable initiators which create reactive species (radicals, cations, anions or weak bases). Those reactive species interact with the monomer and start the polymerization reaction. (Figure 2.1)

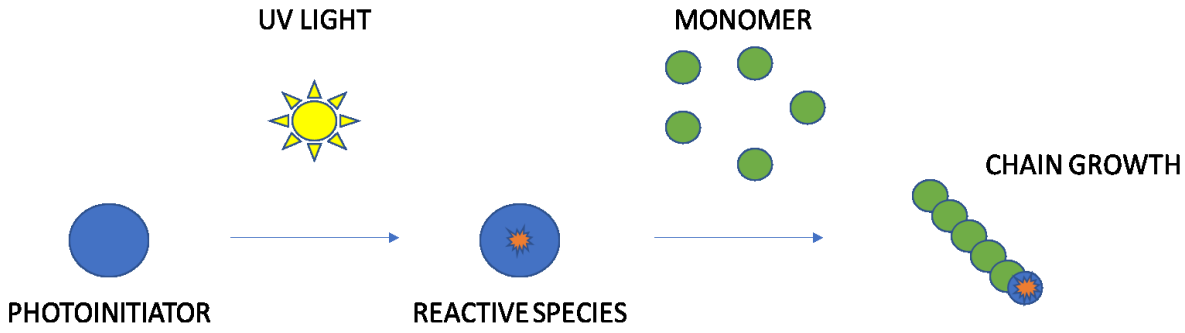

Figure2.1: photo-curing process

The main actor of the process is the light; light energy must be enough in order to trigger photo-initiator's excitation and, consequently, reactive species. Light is considered to be an optical radiation with a wave-like and corpuscular attributes characterized by its frequency (ν), its wavelength (λ) and its transported energy (E):

$$E = \frac{hc}{\lambda} = h\nu$$

These radiations can be divided according to the wavelength (λ) in UV (200-400 nm), VIS (400-700 nm) and IR (700-1000 nm).
A molecule, in this case the photo-initiator, can absorb a quantum of radiation and become energetically excited. Jablonski's diagram (Figure 2.2) is a perfect representation of the excitation process associated with light absorption. When the energy related to the quantum of radiation absorbed is higher than the difference in energy between the singlet ground state S_0 and the excited singlet state S_2, electrons excitation occurs. These electrons tend to lose some of their energy, and this may generate excited triplet states and, finally, reactive species due to subsequent H abstraction and cleavage.

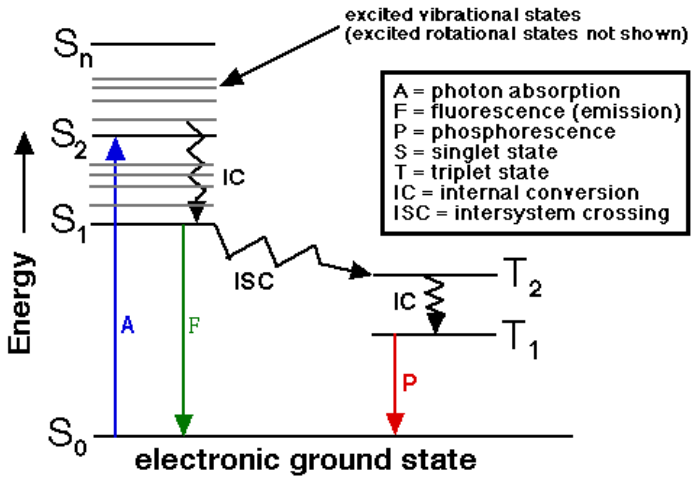

Figure 2.2: Jablonski's diagram [11]

Photosensitive resins can be divided in various kinds, according to the final properties considered. The two main categories are free radical and cationic systems, which can be defined as acrylic and epoxy resins:

- Acrylates, they are resins which can be cured through a free-radical photopolymerization process. Although this is the most used system in industry, because of the large availability of monomers and initiators, epoxy monomers gained more attention over the past decades, especially in composites production;
- Epoxy, these resins are widely used in many industrial fields because of their mechanical, adhesion, chemical resistance, low shrinkage on cure and simplicity of fabrication. The existence of one or two epoxy groups is their principal feature which can be present in the body of the monomer, even though they are usually terminal (Figure 2.3).

According to the number of epoxy rings present in the monomer's structure, epoxides can be categorised as monofunctional, difunctional or epoxy pre-polymers (or higher oligomers). Moreover, the non-epoxy part can be divided in aliphatic, cycloaliphatic or highly aromatic hydrocarbon. Generally, they react with a rearrangement polymerization process, from which they get the low shrinkage property. Curing of the epoxy monomers into polymers is led by catalyst or polyfunctional cross-linking agents (sometimes by both). However, catalytic substances are the most used and they can be divided in ammines and acids. Ammine-hardening reactions can be described as catalytic process or by bridge creation across the monomer. They can be primary, secondary (both reactive hardeners) and tertiary (catalyst) ammines. The curing reaction can be described as a three-step reaction in which firstly there is the opening of the first epoxy ring by the presence of a more reactive hydrogen linked to a nitrogen, then a second ammine is produced. This will lead to the opening of the second epoxy ring and, finally, the intramolecular bonding occurs. A third reaction occurs too, which is the formation of an alcohol; however, this can be considered negligible with respect to the first two. Generally, they are fast curing, they have good chemical resistance, but they are mostly skin-sensitive. Acid anhydrides are sometimes preferred because of their longer pot-life, low peak exotherm and minimal irritating action. Acid curing reactions are generally preceded by the reaction of the anhydride group and subsequent formation of a carboxylic group. Afterwards, the created carboxylic group react with the epoxy ring identifying its opening [12].

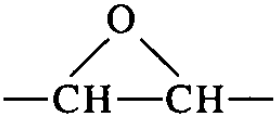

Figure 2.3: epoxy ring [12]

One of the most important and most employed resin is bis-phenol A and epichlorhydrin derived epoxy resin, Bisphenol A diglycidyl ether (BADGE, Figure 2.4). As a matter of fact, most of the studies on RICFP process were made using this kind of resin [13], [14], mostly due to the absence of bubbles.

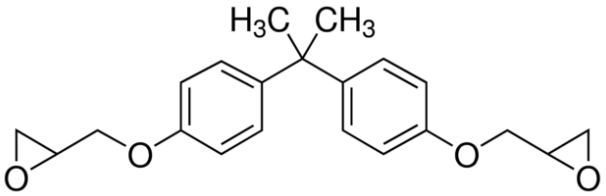

Figure 2.4: BADGE monomer [13]

However, this may be not the best choice due to the resin's lower reactivity and high viscosity (it must be maintained at 50°C and far from light sources). Moreover, the presence of the ether group near the epoxy ring may lead to a competition between the oxygen present in the epoxy ring and the ether itself, lowering the reactivity (figure 2.5).

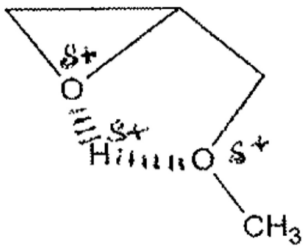

Figure 2.5: oxygen competition

Finally, for the considered application, high viscosity may be a killing factor, not allowing a proper foam impregnation.

2.1.1 Free radical photopolymerization

Free radical photopolymerization is the most used process. The photo-initiating system contains at least the photoinitiator, but addition of a photosensitizer may also be considered. These compounds, as stated in the previous chapter, must absorb light [15], [16]. Upon excitation, the photo-initiator becomes excited and generates a radical (M•) as a reactive species and, finally, through the reaction with the monomer (generally an acrylate), the curing process take place (Figure 2.4) creating the 3D crosslinked structure (P**)**.

Figure2.4: photo-curing process in free radical systems

According to the availability of a variety of photoinitiators, which can be selected in relationship with the wavelength of the used light, this system can be used in a wide range of applications. However, oxygen inhibition can be considered as an important drawback for this application.

2.1.2 Cationic Photopolymerization

Recently, significant advances have been made in the practical application of cationic photo-polymerization, a process that is gaining more and more interest not only into the scientific community, but also into the industrial sectors as a good alternative to acrylate systems [16]. In cationic photopolymerization, onium salts are used as photoinitiators. Their direct homolytic/heterolytic decomposition followed by hydrogen transfer reactions leads to a proton. This proton interacts with the cationic monomer making the curing process possible (Figure 2.5).

Figure 2.5: photo-curing process in cationic systems

This process, if compared to the well-known free radical one, has gained more interest for many reasons. First, rapidity and oxygen insensitivity make these systems extremely interesting. Important advantages that should be considered are the ability to continue the reaction even when the light is switched off (the so-called "*dark reaction*" [17]), the solvent free formulations, energy saving, high production speed, low substrate heating, application versatility, high scratch, chemical and abrasion resistance, strain, and solvent resistance, superior toughness, absence of toxicity, low irritation properties in curable systems and, finally, a lower shrinkage after curing [18], [19]. However, some disadvantages must be considered too. Cationic UV-curing can be inhibited by moisture and basis, cured products may contain acids and counter anion impurities, which can present some risks if exposed to the skin. Finally, the principal drawback that can be considered in both systems is the inability of curing in deeper layers due to lack of light penetration when first crosslinked polymer is formed on the surface of the sample. However, in the cationic UV-curing, dark reactions generate active centres that are essentially non-terminating and that have the ability to interact with monomer's region that are not directly interested by UV. This may lead to the curing of unexposed monomer, even though such a process requires long time and high temperatures since the diffusion coefficient is relatively low [20], [21].
These drawbacks will be solved through a new and outstanding process, the frontal polymerization, which will be discussed in the next chapter. Table 1 sums-up comparisons between two principal UV-curing processes.

Table 1 : UV-curing processes' comparison

Property	Radical	Cationic
Polymerization rate	High	Moderate/High
Oxygen sensitivity	Substantial	Absent
Volume change on cure	Large	Negligible
Adhesion	Moderate/Good	Good
Postcure	Absent	Strong
Chemical resistance	Moderate/Good	Good
Irritant properties of the monomers	High	Absent

Cationic photoinitiators can be divided in three categories: diaryliodonium salt, triarylsulfonium salt and phenacylsulfonium salt as Figure 2.6 shows.

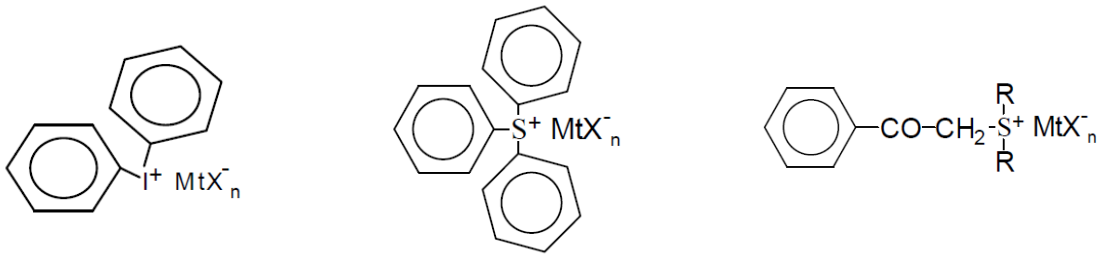

Figure 2.6: Left. diaryliodonium salt, centre: triarylsulfonium salt, right: phenacylsulfonium salt

They can be described according to their anatomy, in which the cation (I^+ or S^+) is the UV absorber part due to the presence of chromophores and the anion (MtX^-_n) will not interact with the light and will release the acid influencing reactive species' propagation. Bigger acids correspond to lower nucleophilic behaviour which means higher reactivity. Different kind of anions can be selected such as SbF_6^-, AsF_6^-, PF_6^-, BF_4^-, listed from the most reactive to the less one [17].

2.2 Frontal Polymerization

As previously discussed, the main drawback related to UV-curing processes is the inability to reach deep layers and creating three-dimensional thick crosslinked structure. This issue can be overcome by the frontal polymerization (FP) process.

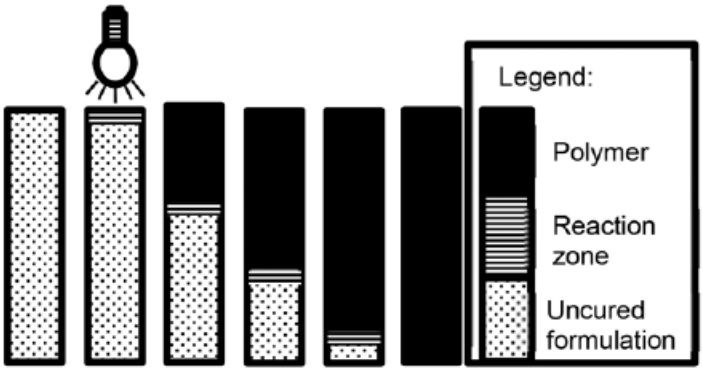

Figure 2.5: front propagation [22]

Many research fields are particularly interested in this process, especially in composite manufacturing, thanks to the very low process time and the capacity of maintaining high mechanical properties if compared to classical thermal curing [13],[14]. Different kind of FP can be considered depending on the way in which the external stimulation is used in order to trigger the polymerization front and on the used initiators. In following chapters, some of them are expounded.

2.2.1 Thermal frontal polymerization

Pojman, 2012, identified this process as the most studied process in frontal polymerization techniques. The very first studies on FP conducted on thermal frontal polymerization were performed on methyl methacrylate, with benzoyl peroxide as the initiator, that was

polymerized under drastic pressure conditions (>3000atm) [23], [24]. High pressure was used in order to reduce the difference in viscosity between the monomer and the polymer which may lead to convective motions (convective breakdown), due to monomer boiling, which can alter front propagation. This technology has gained more and more interest during recent decades thanks to unusual advantages such as high performance, environmental safety and purity of the resultant products [25]. Pojman recognizes conditions in which the front of polymerization can be triggered. Since it is a thermal-activated reaction, the essential criterion is that the heat produced by the reaction itself must exceed the heat loss by the system. Particularly, the system must react slowly at room temperature (low reaction rate) and must have a huge heat release during front propagation (high reaction rate) and high activation energy. If these conditions are confirmed, the front can start and propagate ideally without limitation in thickness.

2.2.2. Radical Induced Cationic Frontal Photo-Polymerization (RICFP)

As stated in the previous chapter, the main limitation in UV-curable systems is the depth of cure, which is common on both free-radical and cationic formulations. In order to overcome this issue, Radical Induced Cationic Frontal Photopolymerization (RICFP) can be considered as the best solution. This special technique is the result of the combination between Frontal Polymerization (FP) and Radical Induced Cationic Polymerization (RICP). In this way, many advantages must be considered such as the possibility to trigger the reaction with an UV-light source, low reagents cost, lower reaction time if compared with other techniques and lower energy consumption. The reaction mechanism has been fully reported by Mariani et al. [26]. In RICP technique, the onium salt is dissociated by the reaction with radicals instead of light irradiation. However, the overall mechanism involves the initial photo-excitation of the onium salt and then the resulting excited singlet state with both heterolytic and homolytic cleavages (Figure 2.6).

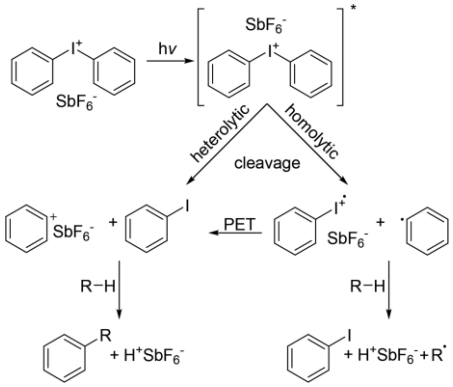

Figure 2.6: photo-initiator cleavage [27]

As Mariani et al. stated, "*free-radical, cation, and cation-radical species are simultaneously formed. The cationic species interact with a proton source, usually the monomer (M), to generate a very strong Brønsted acid HMtX_n*". Afterwards, "*initiation of polymerization takes place by the protonation of the monomer and this is followed by the addition of other monomer molecules thus resulting in chain growth. The aryl radicals interact with monomers … by abstracting a hydrogen atom. In these reactions, secondary radical species are generated …. Redox interaction of these radical species with the diaryliodonium salts give rise to carbocations and an unstable diaryliodine radical. In a subsequent reaction, the diaryliodine radical decays irreversibly to generate an aryl iodide and an aryl-free radical*". These reactive species will restart the cycle, resulting in a very rapid generation of many reactive cationic species due to a non-photochemical process. In the RICFP process performed in this study, the first photochemical step will induce the surface curing with the aforementioned process. Taking advantage of the exothermicity of the curing reaction, free

radical from a classic thermal initiator (RTI) are generated which will interact with the cationic initiator (PAG) restarting the cycle (Figure 2.7). Consequently, due to the thermal activation, the polymerization of the monomer occurs in deeper parts of the sample where the light is not able to penetrate.

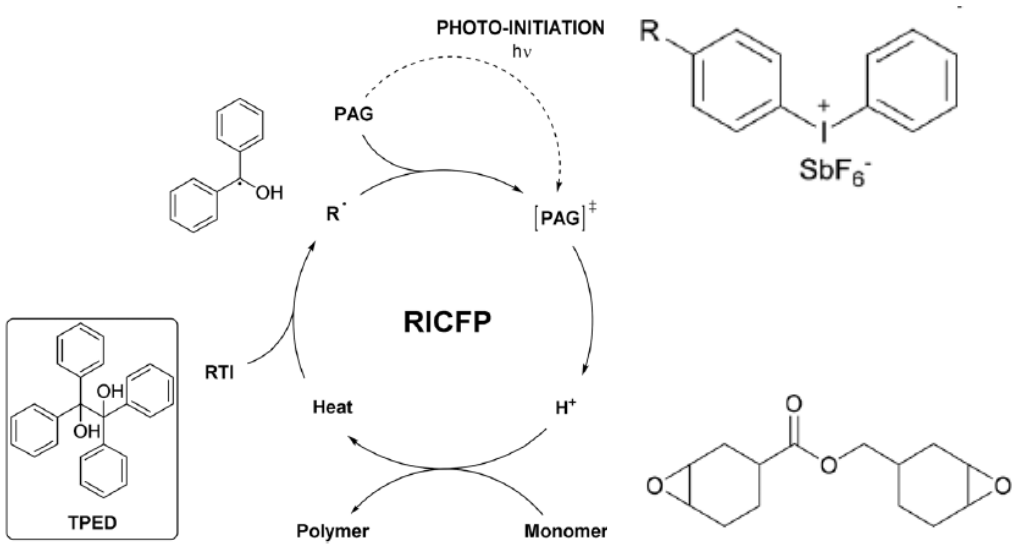

Figure 2.7: RICFP process [28], modified with the photo initiator and the monomer used in this study

Anyway, boundary conditions proposed in order to guarantee the front to start must be considered in this system too. If the dissipated heat is quite large, e.g. higher than the energy required for frontal polymerization, then the front is unable to start and propagate because the cleavage of the thermal initiator won't take place. [28]

2.2.3. Other Techniques

Pojman (2012) described other FP techniques which can be considered according to the way in which the front is activated. First, photofrontal polymerization, in which a continuous input of irradiation (in this case UV-light) is used in order to obtain a propagating front. First experiment was conducted for the photopolymerization of acrylamide in weightlessness which was essential in order to link the behaviour of the position of the front to the UV absorption as a function of depth of penetration which was both logarithmic. Secondly, isothermal frontal polymerization, in which a localized polymerization propagates from a solid polymer piece into a solution of its monomer and a thermal radical initiator. This kind of FP can be considered as the slowest among all the others. Finally, cryogenic frontal polymerization. This fascinating method was conducted in multiple systems including acetaldehyde, formaldehyde, cyclopentadiene, and methyl methacrylate. Operating in a range of temperature between 4 and 77K, the irradiation is given by gamma radiations. So, the heat generated from the surface will start the front. However, front identification is due to temperature and density gradients which will break the subsequent layer of the frozen monomer generating the reaction zone.

2.3 Kinetic of polymerization

Many factors must be considered when a photoinitiated process is involved. Firstly, the efficiency of the photoinitiator. This value can be divided in the quantum yield of photoinitiation (number of starting polymer chains per photons absorbed) and quantum yield of polymerization (number of monomer units polymerized per photon absorbed).
In this way is possible to identify the rate of the photoinduced initiation step (2.1)

$$R_i = \Phi_i I_{abs} \tag{2.1}$$

Where Φ_i is the quantum yeld of initiation and I_{abs} is the absorbed photon flux. After that, it is possible to determine the rate of polymerization R_p (2.2):

$$R_p = k_p[M]\sqrt{\frac{\phi_i I_{abs}}{k_t}} \tag{2.2}$$

Were k_p and k_t are the propagation rate constant and the termination rate constant respectively $[L * mol^{-1} * s^{-1}]$, [M] is the monomer concentration.
The absorbed photon flux can be obtained considering the Lambert-Beer law equation (2.3):

$$I'_{abs} = I_0 - I_0 e^{-\alpha[A]D} \tag{2.3}$$

Where I_0 is the initial incident irradiance, α is the light absorption coefficient of the material, [A] is the photoinitiator concentration and D is the irradiated sample thickness.
Deriving this value respect to the sample thickness, it is possible to define the change of the absorbed photon flux in function of D (2.4):

$$I_{abs} = \frac{dI'_{abs}}{dD} = \alpha[A]I_0 10^3 e^{-\alpha[A]D} \tag{2.4}$$

Where the 10^3 coefficient is due to the change from $L * cm^{-3} * s^{-1}$ to $L * mol^{-1} * s^{-1}$.
Now, regrouping equation (2.2) and equation (2.4) it is possible to obtain the polymerization kinetic at a distance D, therefore the light attenuation by increasing the thickness of the system (2.5).

$$R_p = k_p[M]\sqrt{\frac{\phi_i \alpha[A]I_0 10^3 e^{-\alpha[A]D}}{k_t}} \tag{2.5}$$

The overall reaction is identified in three steps: a first initiation step, when reactive species are produced, a second propagation step, where the polymer chains grow and a final termination step. These steps can be illustrated plotting the rate of polymerization, or the conversion, with the exposure time (Figure 2.8).

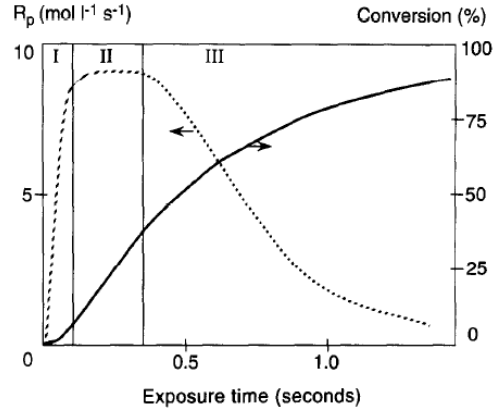

Figure 2.8: conversion (full line) and rate of polymerization (dashed line) versus time during photocuring

As illustrated in previous equations, the rate and degree of polymerization is influenced principally by the monomer concentration, the photoinitiator concentration (and its quantum yield) and the light intensity. However, further optimization must be considered in order to reach the best result. For example, photobleaching initiators are preferred due to their ability to form products which absorb less light than the precursor itself. Other additives such as photosensitizers, fillers or other initiators should be considered carefully according to their nature and concentration because of the possibility to absorb more light than the photoinitiator used, reducing the curing properties or delaying the starting point of the front of polymerization. This is the so-called screening or shield effect. Moreover, this effect can be present when a not optimum initiator concentration is selected [29], [30]. This effect, referred as skin effect, can be recorded at high amount of photoinitiator, leading to an enhanced reaction on the surface of the sample associated with a decrease in the rate of polymerization in deeper layers of the material

2.4 Foams and interpenetrating phase composites

Foams are multi-phase composite materials constitute of a solid phase, its surface and a gaseous phase, named pores. Generally, the filler of this composite is determined by chemical or physical foaming in a wide range of foaming procedure [31], [32]. They can be divided in different categories depending on an open cell structure, in which cells are not completely encapsulated, a closed cell structure, in which cells are sealed off so air doesn't get inside the structure, and a mix of the two structures. Porosity, which depends on size, shape interconnection and distribution of pores, will influence drastically the foam properties [33]. In this way, distinction between different structures must be made according to their mechanical properties. They can be considered as hard materials which don't deform when stress is applied or soft materials which can be deformed easily. One way to identify materials deformability, or their ability to absorb and disperse energy, is to consider their tan(δ). Higher tan(δ) means that the material is no more able to recover his original shape once the deformation is induced [34]. So, this behaviour can be related to closed cell structures. On the other hand, lower tan(δ) means a noticeable elastic behaviour and the possibility to recover the original structure after deformation (Figure 2.9).

Figure 2.9: Left-soft foam before compression. Centre-deformation with a glass plate. Right- recovery

In this study, soft open cell foam is chosen because they can be easily squeezed and expand in order to make acquisition of every shape possible and because they can be penetrated by gasses or liquids to make possible absorption of formulations. More specifically, low tan(δ) must be considered (approximately 0,1) in order to improve the moulding process and shape attainment due to photosensitive resin's hardening. Foam liquid impregnation must be considered as a key factor. Impregnation is the result of both the natural process, typical of porous media, of absorption by the effect of the capillarity of the pores, and of the sucking effect deriving from the expansion of the sponge in resuming its shape after crushing. Obviously, only open cell foams must be evaluated since closed cell foams are impossible to impregnate. The mechanical response of such heterogeneous structure is complex and depends on many factors. First, in order to permit a good impregnation of the porous media,

the size of the pores is very important, and it must be balanced. This will induce the resin to be soaked up by the foam itself while letting the foam expand back properly. Second, permeability of the porous media and liquid viscosity influence the correct foam impregnation. According to Washburn law, that consider the classical capillary effect, all these parameters and conditions can be illustrated (2.6):

$$\frac{l^2}{t} = \frac{\alpha k_0 P_c}{\mu} \tag{2.6}$$

Where l is the penetration length, t the time, α is a dimensionless constant, k_0 is the characteristic permeability, P_c is the capillary pressure and μ is the viscosity of the fluid. According to this equation, if the viscosity of the liquid is reduced, the ratio between the penetration length and time increases (considering constant the capillary pressure), this means a reduction of the time needed to the fluid to cover the penetration length. This condition leads to a better liquid flow thorough the porous media but also to a faster drainage, feature that must be carefully controlled especially when big porous structures are required. On the other hand, when liquid viscosity is high the reverse condition occurs, but in this case the effective permeability of the liquid in the porous media must be considered. In any case, according to the impregnation method used, capillarity or infiltration procedure, the fluid behaviour differs. In this study, in which an infiltration method was used, other conditions are considered: how the foam is compressed and how it recovers the original shape, the possibility of fluid exit from the boundaries of the porous media and the effective liquid penetration into the foam. It is self-evident that a combination of all these features must be considered, leading to a not uniform and barely predictable behaviour. In order to improve liquid penetration into the porous media and make its behaviour more linear, some solutions can be implemented. For example, a surfactant can be employed. Defined as a "surface active agent", they can change the properties of the involved surfaces, especially foam's surface tension, and refine the impregnation step [35]. In addition, photografting can be a powerful tool in order to functionalize the foam surface making it hydrophilic and improving the impregnation step and its resin retention [36]. Temperature stability is a key parameter of polymeric foams. Processes characterized by high temperature levels will lead to the foam degradation and all related problems, e.g. the drop of the mechanical properties. As stated in the introduction, metallic foams used as a host for the curable formulation can be considered as a good alternative in order to avoid degradation phenomena. However, in these systems other applications should be considered, taking into account that the processes lead to the production of a completely different class of materials. Since the metallic foam don't degrade during curing, an interpenetrating dual-phase system composed by the cured epoxy resin and the metallic part is formed. This condition will identify a class of materials called by L.D. Wegner and L.J. Gibson "interpenetrating phase composites" (IPCs) [37]. They have an improvement for three main properties such as Young modulus, strength and coefficient of thermal expansion if compared to their not interpenetrating system counterparts. However, the best benefit related to this class of materials doesn't correspond to the ability to improve one single property, but it is related to their greater capacity to extract the best advantages from properties related to each constituent. This feature will lead to an improved competence in combining all different properties. Moreover, the possibility to improve a certain property is related to the contiguity of the phase responsible of this improvement. For example, one application may require high yield strength and energy absorption. This is a case in which the material used must be tough and have high impact protection. In this way, the contiguity of high yield strength phase is important to achieve the first property. On the other hand, by assuring the contiguity of high energy absorption phase, the second property is obtained. This can be the case of an aluminium-cured epoxy

IPC in which the metallic phase is characterized by high yield strength associated with low energy absorption and, vice versa, the epoxy phase. If the contiguity is obtained, an enhancing on the correspondent properties will occur, leading to many advantages and benefits. Other parameters should be considered such as the ratio between the higher value and the lower value of the considered property. Higher differences, such as higher ratios, are linked to larger property's enhancement as the theoretical bounds are largely separated. This is significant when absolute values of the studied property of each material differs with an order of magnitude. On the other hand, when this condition is not fulfilled, phases' volume fraction become more relevant. Little work has been done related to this field, especially in metal-polymer systems [38], [39]. It has been demonstrated that an increasing in energy absorption and compressive strength occurs while maintaining system's lightness. These features may lead to outstanding advantages in some application in which the impact protection, durability, lightness and safety issue must be highly optimized such as aircraft production [40]. Cited technologies are referred to a thermal curing of the epoxy part of the composite which can be time consuming and cost intensive as stated in section 2.1. In this work, an IPC has been produced for the first time taking advantage of the Radical Induced Cationic Frontal Photo-polymerization.

This technique will exploit all the advantages related to an UV induced technique which may lead to outstanding benefits reducing manufacturing and operational costs. In this field, further studies should be conducted regarding the interconnectivity and interface characteristic, modelling system's mechanical behaviour and impregnation processes.

3. Materials and Methods

3.1 Materials

In this chapter will be presented both the materials used in this study as well as some others generally used for the RICFP process.

3.1.1 Photosensitive epoxy resins

In this study, a cycloaliphatic epoxy resin (3-4-epoxycyclohexane) methyl3'-4'-epoxycyclohexyl-carboxylate, Omnilane OC 1005 by IGM resins is choosen. In Table 2., viscosities of two different BADGE resin (Araldite MY-790-1, Huntsman and Amperg 26, Gurit) and the used cycloaliphatic epoxy resin are compared.

Table 2. Viscosity comparison

	Amperg 26	**Araldite MY-790-1**	**Omnilane OC 1005**
Viscosity at 25°C [cP]	1050	4000-5500	180-450

The used resin is suitable for use with many solvents and can be cured with anhydride acids at high temperature. It has a long storage life (12 months in appropriate storage conditions) and it is used for a wide range of applications such as graphic arts, metal coatings, plastic coatings, electronics, adhesives and many other. In figure 3.1, monomer formula and curing steps are illustrated. Furthermore, the low viscosity leads to the possibility to add in the formulation an high amount of inorganic compounds and make their dissolution easier.

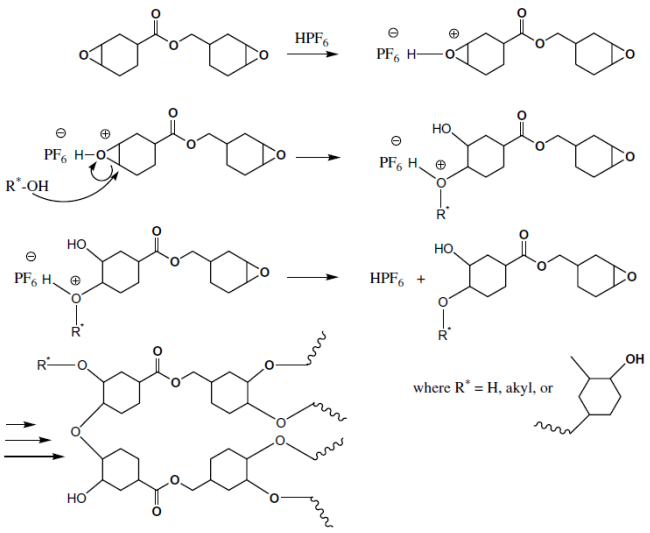

Figure 3.1: cycloaliphatic epoxy monomer and curing steps [41]

3.1.2 Photoinitiator

The inititator used (as received) for this study is p-(octyloxyphenyl)-phenyliodonium hexafluoroantimonate, abbreviated in IOC8 SbF_6^-, from ABCR which is, as stated before, the most reactive compound. Despite its outstanding behaviour, it found very low industrial application due to antimoniate presence. For this reason, only photoinititators containing

PF_6^- have had industrial attentions so far. However, photoinitiator's absorption is a fundamental feature in order to make the UV curing successful. For example, the diaryliodonium salt can absorb radiation between 220 and 280 nm. In order to improve light absorption to the system, photosensitizer or free-radical photoinitiators can be used. These compounds can absorb UV-light, and its energy, at higher wavelength. In this way, they can transfer it to the cationic photoinitiator, "shifting" its absorption (Figure 3.2).

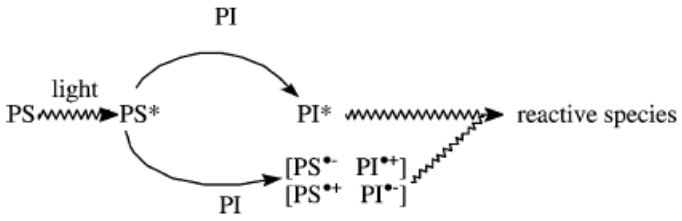

Figure 3.2: absorption shifting given by the activator (A), e.g. photosensitizer [42]

3.1.3 Thermal Initiator

As stated in section 2.2.2., taking advantage of the heat produced by the exothermicity of the photoinitiated cationic curing, there is the possibility to cleave the thermal initiator which is added to the formulation (Figure 3.3). The thermal initiator used in this study (as received) is 1,1,2,2-Tetraphenyl-1,2-ethanediol (98%) from Acros, abbreviated as TPED or benzopinacol. This chemical belongs to the C-C label compounds family. Formed reactive radicals are able to cleave the cationic photo initiator forming further acid. Bomze D. et all. studied a wide range of thermal initiators, concluding that only this (and probably even a slightly different compound, TPED-Si) was suitable for the frontal polymerization in BADGE. However, Mariani et all. concluded FP successfully with a formulation containing approximately the same photoinitiator and Benzophenone (BPO) as thermal initiator in cycloaliphatic epoxy resin.

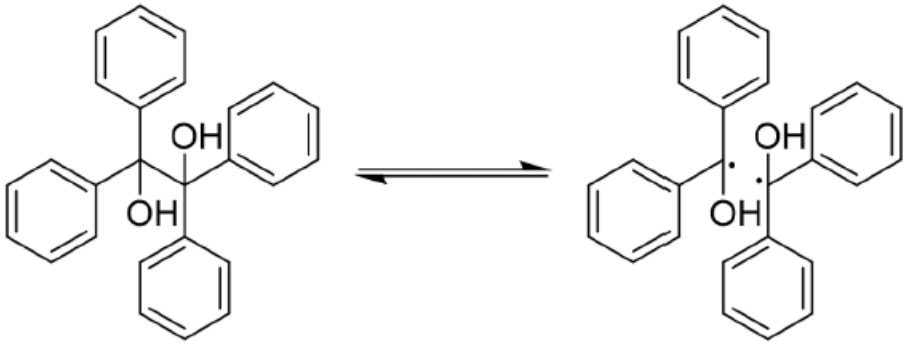

Figure 3.3: TPED cleavage [26]

A cationic latent thermal initiator, Ytterbium (III) trifluoromethanesulfonate 99%, is also tested that generate a propagating front in deeper layers.

3.1.4. Foam

The selected foam for this study is the polyurethane PU Supercell 2017 EUROFOAM foam produced by EUROSPUMA® group (Figure 3.4, left). His density is 20 kg/m^3 while the hardness ranges 1.7kPa (ILD 40% / N – ISO 2439: 75.00 ± 17.00) as stated in the EUROSPUMA® group website [43]. The dimension of pores was approximated at 100 μm. Low density, low tan(δ) (approximately 0,1), excellent light propagation makes the studied

foam ideal for impregnation, mould, shape acquisition properties and absence of light absorption. However, according to the high temperature related to the studied process, foam degradation may occur. For this reason, one test on an aluminium foam was conducted (Figure 3.4, right). This can open a wide range of possibilities regarding ultra-lightweight composites materials. However, for this application the impregnation method must be improved for those cases in which the foam cannot be squeezed. In order to facilitate the impregnation step, an aluminium foam composed of big pores was selected.

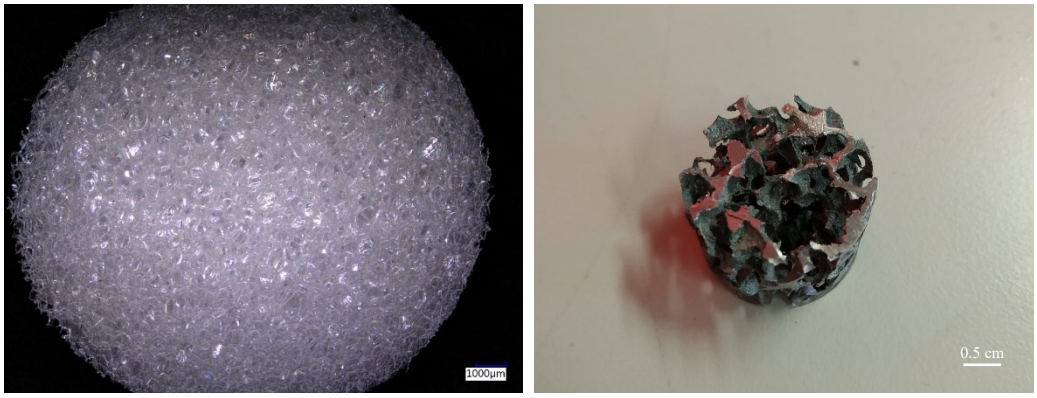

Figure 3.4: polymeric foam (left), aluminium foam (right)

3.2 Studied formulations and sample preparation

3.2.1. Formulations

A total of nine formulations were studied, as Table 3 illustrates, scanning different conditions.

Table 3: studied formulations

#	IOC8 SbF6 (PHOTOINITIATOR)	TPED (THERMAL INITIATOR)
1.	0.5%wt	0%wt
2.	1%wt	0%wt
3.	2%wt	0%wt
4.	3%wt	0%wt
5.	0.5%wt	0.5%wt
6.	0.5%wt	1.5%wt
7.	0.5%wt	3%wt
8.	1.5%wt	0.5%wt
9.	3%wt	0.5%wt

In compositions from 1. to 4. no thermal initiator was used while increasing amounts of photoinitiator were used. They were compared with composition 5., 6., and 7. in order to identify any shield effect given by the presence of the thermal initiator in its smallest amount (0,5%). Then compositions from 5. to 9. were selected in order to study the effects on the front parameters resulting from the different amount of photoinitiator maintaining the smallest amount of thermal initiator and vice versa.

The smallest amount of both initiators is set at 0,5%wt, weighted in 15g of the overall composition. At lower amounts of both initiators no front has been observed. All the formulations were stirred at 40°C for 40 minutes showing a good homogeneity (Figure 3.5).

A first proof of fact has been conducted in order to demonstrate that only the presence of both initiators is suitable for the propagation of the front. For instance, formulations containing photoinitiator only identified a surface curing. On the other hand, formulations containing only thermal initiator didn't show any kind of polymerization under UV light.

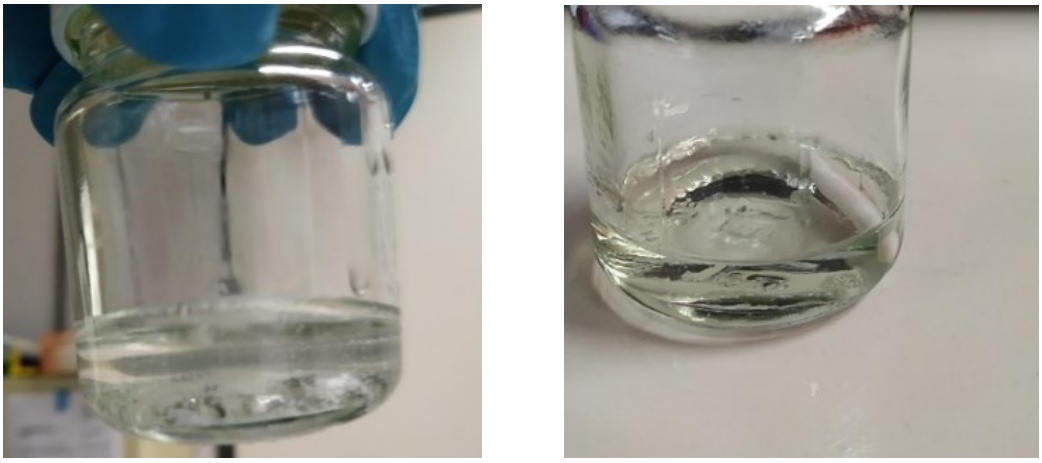

Figure 3.5: formulation before (left) and after (right) stirring at 40°C

3.2.2. Foam Impregnation

As mentioned in section 2.4, the foam was selected according to its ability to be squeezed easily in order to make the impregnation simpler. In this way, the foam sample, cut at 1,5 cm length and with diameter of 16 mm (bearing in mind that the study investigate the possibility to realize a earbud), is immersed into the resin in a compressed state and then let expand back so that it absorbs the resin. Then the impregnated sample is placed on an aluminium foil in order to eliminate the excess external resin and subsequently placed on the support for direct irradiation (figure 3.6). This procedure has been made in order to let the sample free from any container because using any kind of mould such as silicon, glass or metal, will change the emissivity value and will alter the recorded temperature value, compromising the investigation in degradation phenomena. However, in relation to the actual application of the device, the use of an additional external bladder must be considered. This could be used as a temperature and UV shield, for example when skin contact of the device occurs. Nevertheless, this configuration wouldn't modify the real temperature emanated during the front propagation through the impregnated foam. Moreover, in this way the foam structure has been maintained unaltered in order not to induce additional heterogeneities.

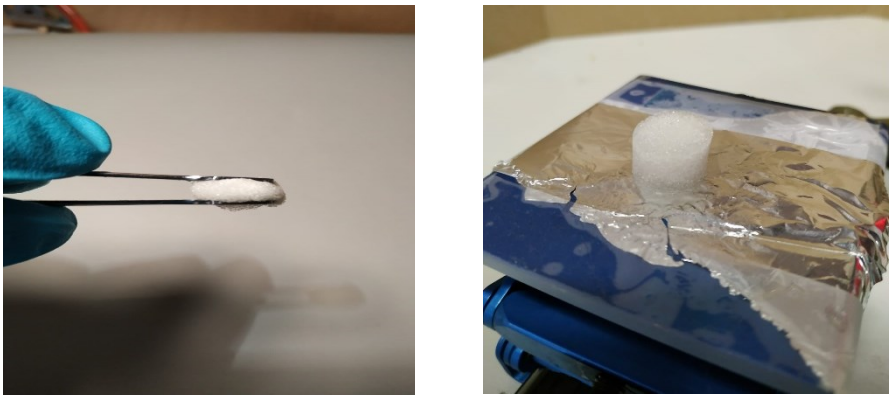

Figure 3.6: compressed state (left), impregnated foam (right)

3.3 Methods of investigation

3.3.1. UV lamp

For all the experiment, an high pressure mercury UV lamp Omnicure series 2000, Exfo-Omnicure, Canada, was used. Its broad spectral output makes this lamp suitable for a wide range of applications. Figure 3.7 illustrates the power spectrum of the lamp used from the lamp technical sheet. Knowing the power spectrum of the lamp and the absorption spectrum of the photoinitiator used can be very important in order to make possible the curing, or at least to optimize it. In this way, the two spectra should overlap, leading to the previously discussed light absorption of the cationic initiator chromophore part.

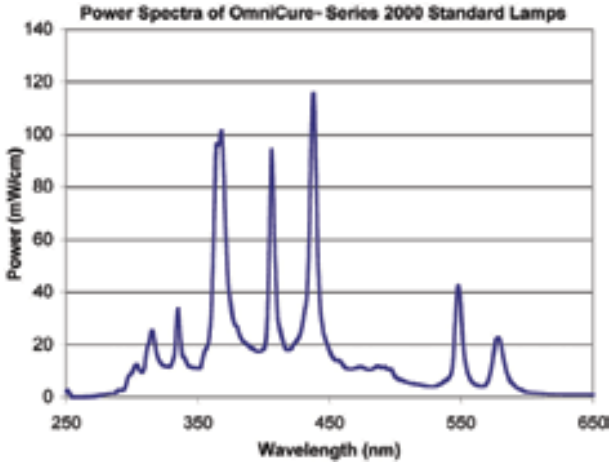

Figure 3.7: omnicure series 2000 power spectra

3.3.2. Infrared (IR) thermography

In order to characterize the behaviour of a propagating front of polymerization, three different parameters must be considered: starting time of the front (t_{start}), maximum temperature (T_{max}), front velocity (V_f) and process time. In literature, some attempts were made using a silicon mould with thermocouples located in different position and a meter in order to record maximum temperature, front velocity and starting time. In this study, an IR camera FLIR T450sc, provided by FIMAP (Laboratory of Photonic Materials and Fiber Devices), (Figure 3.8) is used in order to describe the front behaviour. Three recording spots are identified in three different position of the sample, in details:

- sp1: at the upper surface of the sample, where front start should occur;
- sp2: at 0,5cm from sp1, where a polymerization stable propagating front should be ongoing;
- sp3: at 0,5 cm from sp2, where the polymerization front should pass with the same condition as in sp2.

Figure 3.8: (left) FLIR T450sc [44], (right) three-point measurement, the white square represents the studied region

Starting point of the front is considered the initial formation of the thermal polymerization front, in other word when the front is triggered and an "onset" occurs; this happens in a point of the upper portion of the sample, when the polymerization process starts, the temperature of the exothermic reaction is comprised between 250 °C and 270 °C, highlighted with red colour in the IR image. For all samples, the starting point was located in the space between sp1 and sp2. As the start of the front was on, the light was switched off because the front propagated independently from the UV-radiation. The **maximum temperature** (T_{max}) was measured via the IR thermography, recording the maximum temperature registered at each of the three sp. The **front propagation velocity** (V_f) was calculated by the video recorded. All videos showed the front passing through sp2 and, maintaining the same conditions (temperature between 250 °C and 270°C or higher), through sp3. Knowing that the distance between sp2 and sp3 is 0,5 cm, it was then possible to calculate the front velocity between sp2 and sp3. This was taken as the front propagation velocity. The **process time** is measured during the registration of the process evolution throughout the sample length (1,5 cm), it may also be calculated as (3.1):

$$t_{process} = t_{start} + \frac{h}{V_f} \tag{3.1}$$

Several critical values must be considered in thermographic analysis. First, material emissivity or emittance, ε, which influence tremendously the real temperature of the object T_{obj}, as equation 3.2 illustrate:

$$T_{obj} = \sqrt{\frac{W_{tot} - (1-\varepsilon) * \tau_{env} * \sigma * (T_{ref})^4 - (1-\tau_{env}) * \sigma * (T_{env})^4}{\varepsilon * \tau_{env} * \sigma}} \tag{3.2}$$

Where, τ_{env} is transmissivity of the atmosphere between the object and the camera, σ is the Stefan–Boltzmann constant (5.67 x 10^{-8} W/m^2K^{-4}), W_{tot} is the total radiation entering the thermal camera which is considered as the sum of the radiation emitted and reflected by the object (W_{obj}, W_{ref}) and the radiation emitted by the atmosphere (W_{atm}) as equation 3.3 illustrates:

$$W_{tot} = W_{obj} + W_{ref} + W_{atm} \tag{3.3}$$
$$W_{obj} = \varepsilon * \sigma * \tau_{env} * (T_{obj})^4$$
$$W_{ref} = (1-\varepsilon) * \sigma * \tau_{env} * (T_{ref})^4$$
$$W_{atm} = \sigma * (1-\tau_{env}) * (T_{env})^4$$

Not proper choice in emissivity value can bring to inaccurate temperature values. This coefficient can be obtained indirectly knowing firstly the object temperature by using a thermocouple. However, considering that a very fast reaction takes place, it can be very difficult to extract this value. Despite this obstacle, maintaining high emissivity value during the measurement can be a good approximation considering that the value referred to the object studied is high [45]. Regarding polyurethane foams, the emissivity is quite high, for this reason the value chosen for all the measurements is the same (ε=0,9, [46]). Reflected temperature, T_{ref}, and environmental temperature, T_{env} are important parameters too. Reflected temperature, which is the background radiation reflected off the studied object, can have a big influence over the recorded temperature. An approximation has been made for this value too and the same value of the environmental temperature was selected.

The final setup is illustrated in Figure 3.9 in which the camera is placed 22,5 cm from the impregnated foam. The distance between the sample and the optical lightguide linked to the high-pressure mercury lamp is calibrated in order to ensure an initial irradiance of 40mW/cm² on the surface of the sample. Impregnated foam sample diameter is 16mm and the thickness is 15mm.

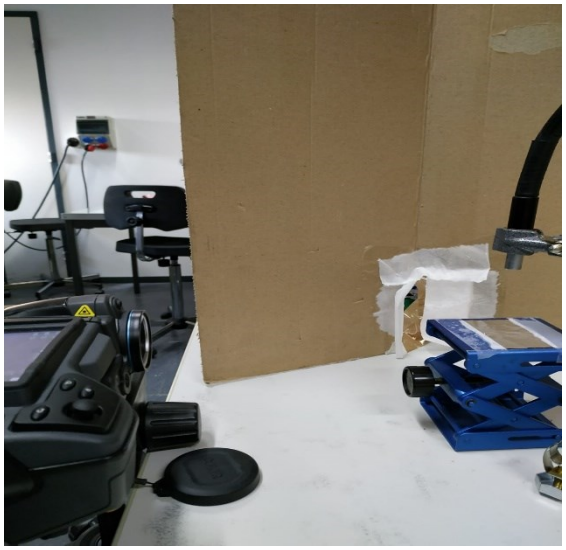

Figure 3.9: IR camera setup

The initial irradiance is captured with a Silver line UV radiometer showed in Figure 3.10 from Con-Trol-Cure® it is functional between 230nm and 410nm wavelength with a 2cm small cylinder chip which convert the power density to the total energy density. The precision of the device is about 0,2 mW/cm² when x1 magnification is used.

Figure 3.10: radiometer used to measure initial irradiance I_o

3.3.3 FTIR (Fourirer-Transform Infrared Spectroscopy)

First characterization of conversion in the first layer of the surface has been made through FTIR-ATR measurements. Spectra interpretation and assignment of the bands is very critical when speaking of in-situ monitoring processes as conversion. This feature can be more difficult regarding epoxy formulations, in which more than one component can be identified. Regarding epoxies, the most important behaviour is related to the oxirane functional group, well known as epoxy ring. Difference on the electronegativity between carbon and oxygen atoms lead to carbon electrophilicity. So, ring opening occurs when

nucleophiles are present in the formulation such as a strong Brønsted acid [47]. The detection by IR spectroscopy of the oxirane ring is due to its polarity. Four different peaks have been considered in order to study the conversion phenomena before and after photopolymerization [48], [49], [50]:

- 787.82 cm^{-1} : epoxy ring
- 1075.31 cm^{-1}: polymerized polyether structure
- 3435.25 cm^{-1}: stretch of the hydroxyl groups
- 1435 cm^{-1} : Methylene group, reference

The measurements were done with Attenuated Total Reflection (ATR) methodology, that operates by measuring the changes that occur in an internally reflected IR beam when the beam meets a sample. An IR beam is directed onto an optically dense crystal with a high refractive index at a certain angle. This internal reflectance creates an evanescent wave that extends beyond the surface of the crystal into the sample held in contact with the crystal. This wave is attenuated in IR regions where the sample absorbs energy. Then, the attenuated beam returns to the crystal and exits its opposite end, directed to the detector. Finally, the detected interferogram signal can be used as the final IR spectrum. The used device is a Nicolet 6700 from ThermoFisher Scientific with an ATR-golden gate accessory, used in MHMC laboratory (Figure 3.11). The spectra were acquired with 32 scans and a resolution of 4 cm^{-1} in the range of 4000 to 650 cm^{-1} [51].

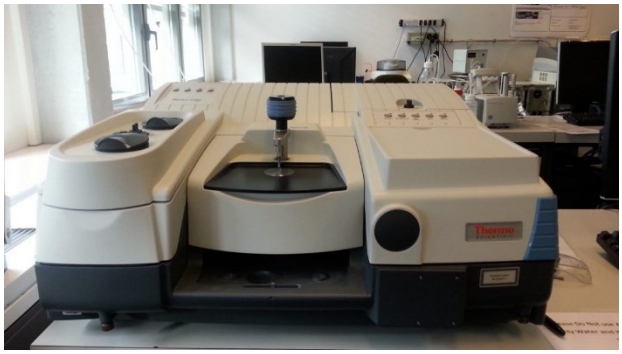

Figure 3.11: Nicolet 6700 from ThermoFisher Scientific

3.3.4. Photo-DSC (Differential Scanning Photo-calorimetry) measurements

Photo-DSC analysis are widely used in order to identify conversion and kinetic phenomena in UV curable systems [48], [49], [50]. By detecting the heat of polymerization released during UV curing, it is possible to obtain information regarding the rate of polymerization, conversion degree, gelation and vitrification steps. In this study, the focus will be mainly on gel time and maximum conversion rate. In correspondence of the gel time *gelation*, one of the two principal structural transformation, occurs. This is defined as the time in which the viscosity of the formulation increases to infinite leading to a drastic decrease of the reactivity. This identifies a macroscopic change in the material, passing from a liquid-like to solid-like behaviour. In a molecular point of view, the mass required to create an interconnected system is reached. It can be said that one big molecule is formed throughout the system (Figure 3.12).

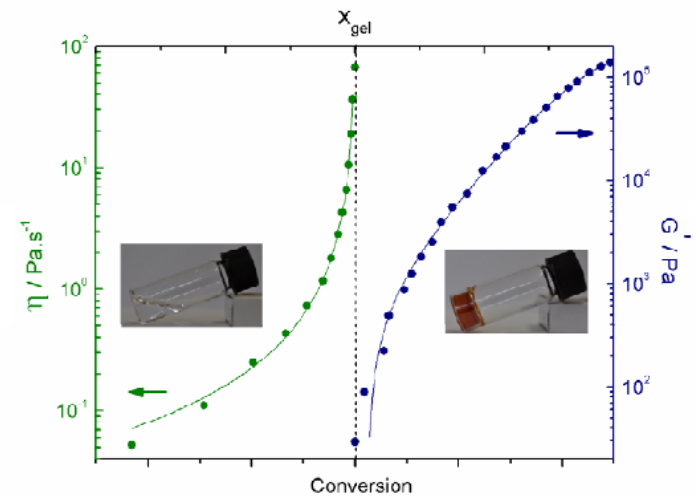

Figure 3.12: viscosity and modulus VS time at gel point [52]

Another important transformation that must be considered is vitrification. In this step, the formulation is transformed from a liquid or gel like material into a glassy material and covalent bonds are formed. In this way the monomer loses the ability to be converted into the polymer structure while the reactivity drops dramatically. Nevertheless, vitrification is a temperature dependent transformation and polymerization can restart at higher temperatures [52]. For the analysis, about 8,5 mg of the formulation are weighted and placed carefully in an open aluminium pan located into the chamber with an empty open aluminium pan as a reference. Then the measurement starts and, after 30 seconds, the light (with an irradiance of 40 mW/cm^2) is switched on for 200 seconds. The same experiment is repeated on the same sample in order to obtain the baseline heat flow to be subtracted to the initial curve, orange and blue curve respectively in Figure 3.13.

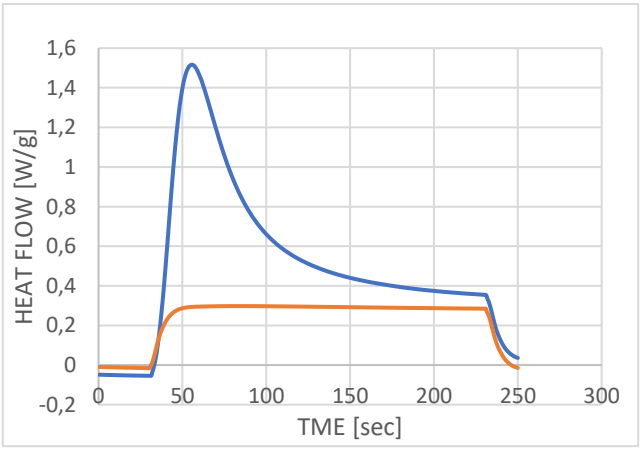

Figure 3.13: Thermogram of the curing resin (epoxy+0,5% of IOC8SbF6, blue curve) and cured resin (orange curve) at 40 mW/cm²

The gel time is considered as the time in which the maximum value of the heat flow is recorded during the measurement. At this value, the maximum conversion rate (ȧ) is considered as the ratio between the maximum heat flow value and the calculated enthalpy of reaction. So, the kinetic of the very first photoexcited process is studied (Figure 3.14).

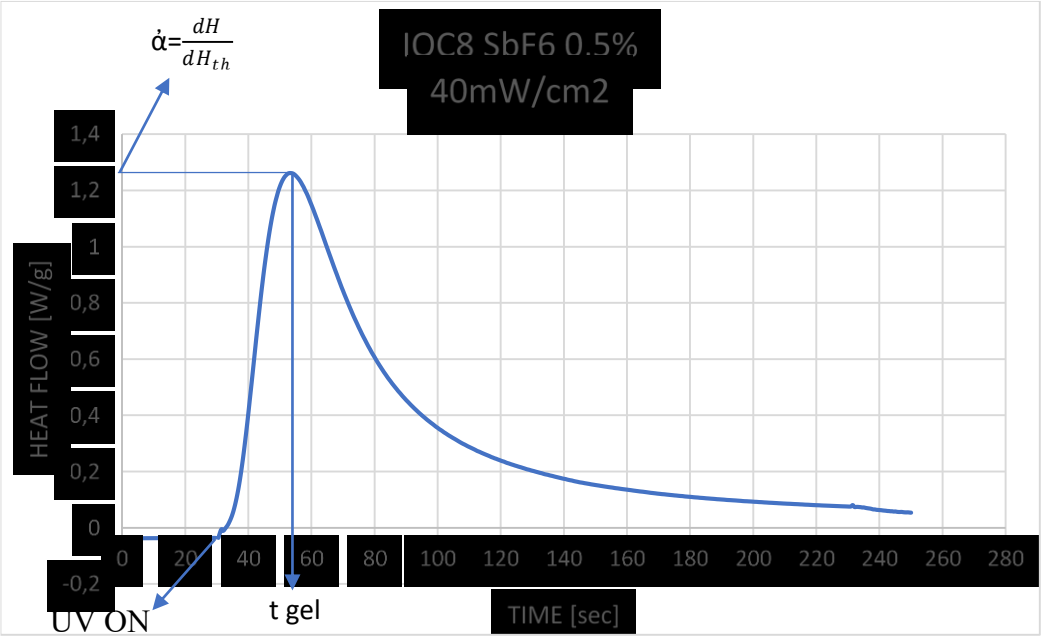

Figure 3.14: Photo-DSC curve, Top: maximum conversion rate, Bottom: gel time

The Photo-DSC instrument used is DSC Q100, Ta instrument, USA which needed a first calibration step in order to pass from the DSC mode to the Photo-DSC configuration. The samples were irradiated with a dual light guide connected to the high-pressure mercury lamp. Tests were repeated in triplicate.

3.3.5. Differential Scanning Calorimetry (DSC) measurements

This technique is largely used in order to visualize temperatures in which matter transformations occurs. The instrument used for the analysis, the DSC-Q100 from TA instruments, present in LPAC laboratory (Figure 3.15), is the same used for Photo-DSC analysis but in DSC mode. Two aluminium pans, one empty as reference and one containing the sample (5-15mg) are placed into the crucible and heated at a constant heating rate. Then the instrument records the value of the heat difference required to maintain pans at the same temperature. While the heat capacity of the material changes during different transformation, the observed heat flow will be different too. Generally, three different temperatures can be recorded through DSC measurement:

- T_g: glass transition temperature recorded as an inflection in the DSC thermogram. This is a range of values but normally the inflection point is considered
- T_c: crystallization temperature, generally linked to an exothermic peak (up) which represent the energy released by the amorphous part of the formulation
- T_m: melting point, it is considered as an endothermic peak related to the melting of the polymer structure.

Experiments were conducted in two subsequent scans from 0°C to 200°C with a heating rate of 20 °C/min. Cured samples were all taken at 1 cm deep from the surface. The first scan investigates the presence of exothermic peaks, which can be related to a possible incomplete reaction. The second scan investigates the glass transition temperature and check if the reaction is complete.

Figure 3.15: DSC Q100, TA instrument

3.3.6. Thermogravimetric Analysis (TGA)

Thermogravimetric analysis is a powerful technique when dealing with degradation. Taking into account that temperature-sensitive materials are used, first the foam, this method of investigation assumes high importance. TGA 4000 from Perkin Elmer, placed in MHMC laboratory, is the instrument used for this characterization (Figure 3.16).

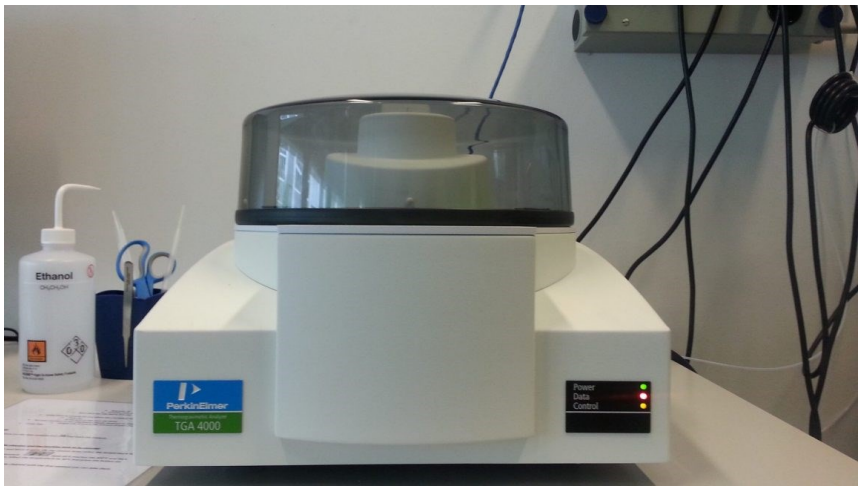

Figure 3.16: TGA 4000 from Perkin Elmer

During the experiment, weight decrease while the temperature is increased at a constant heating rate is recorder in order to identify two characteristic temperature:

- T_{onset}: temperature at which the material degradation starts
- T_{peak}: minimum peak temperature extrapolated from the derivative of the output curve.

Temperature ranges from 30°C to 400°C and 30°C to 500°C was used during the experiments with an heating rate of 10 °C/min. Tests were conducted on the foam, the photosensitive resin without initiators and the complete formulation.

3.3.7. SEM and optical microscopy

As soon as conversion, kinetic and degradation phenomena was studied, the focus moved to the structure of the samples in order to identify conditions in which the system can be

considered as optimized. In this way, two conditions were studied, the one in which the material seems to be less degraded and the worst condition observed. For this purpose, a TM-1000 SEM (Figure 3.17, left) for electron microscopy images and a Keyence VHX-5000 (Figure 3.17, right) for optical images, both present in DLL laboratory, were used. Images were taken at the surface and at 1 cm depth of the sample.

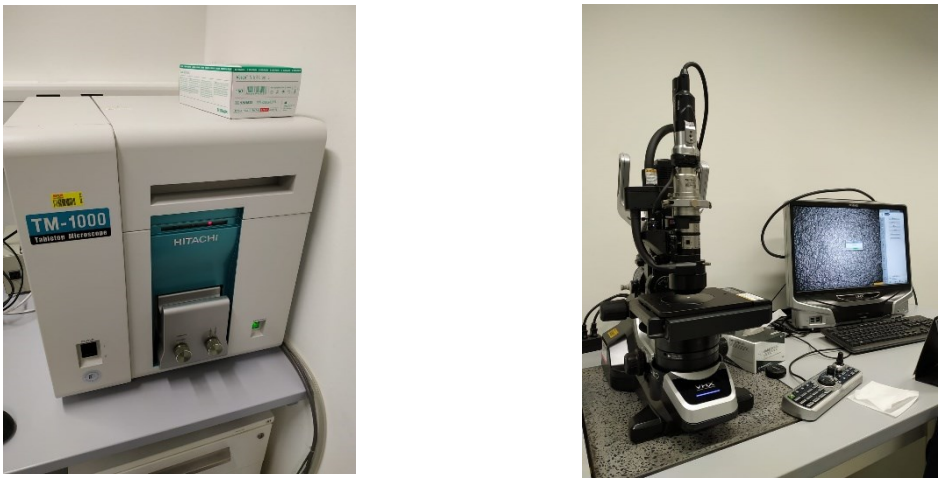

Figure 3.17: TM-1000 SEM (left), Keyence VHX-5000 (right)

4. Results and discussion

4.1 Analysis of front propagation

The general setup for thermal experiments explained in section 3.2.1 has been conducted in formulations which showed a propagating front through the thickness of the sample. The sample has been cut at 1,5 cm in order not to alter the temperature present in the third point (sp3). In some occasions, the temperature should be considered as an approximated value considering that a large amount of smoke is produced, especially at higher amount of photoinitiator. This can be due to the breakup of the ester group present in the monomer. Additionally, the relatively low boiling temperature of the resin (170 °C, from the technical data sheet from IGM resins) may lead to the presence of bubbles and smoke altering the value of the emanated temperature. Several images have been extrapolated from the recorded videos. The first image is extracted at "time zero" in which the light is switched on (0 sec), the second one is at the time in which the injection point occurs, then the other two images are extracted at the time when the propagation front passes through points sp2 and sp3. This condition is related to the formulation 5. (IOC8 SbF6 = 0,5%wt; TPED = 0,5%wt). Figure 4.1 illustrates the different points of interest in visible conditions, using a smartphone as recording device.

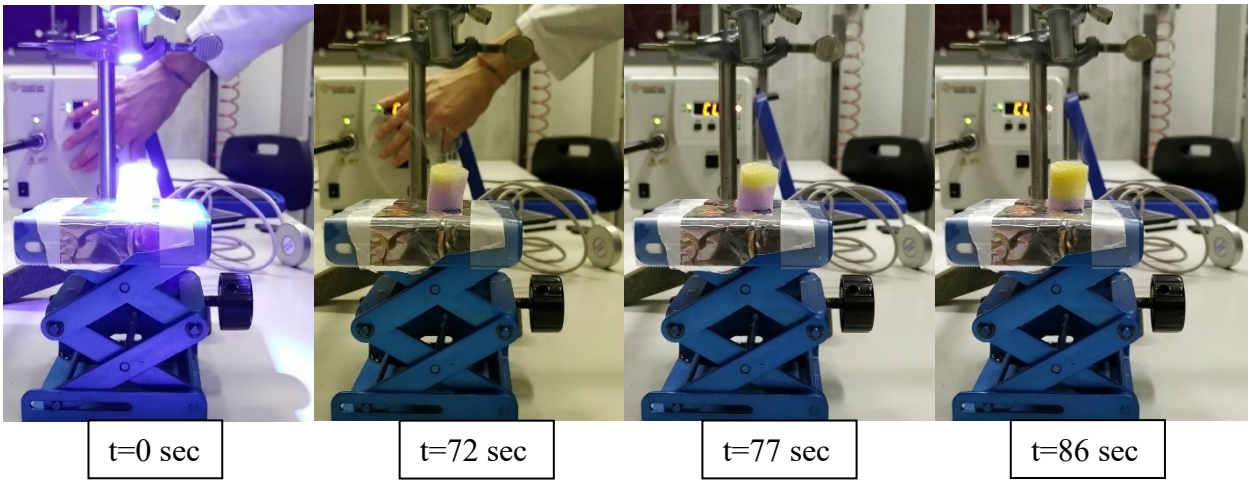

Figure 4.1: frame from the video recorded with the smartphone related to formulation 5. (IOC8 SbF6=0,5%wt, TPED=0,5%wt) At 40mW/cm²

The same experiment has been conducted with the IR thermal camera setup, and images at the same times have been extrapolated (Figure 4.2).

Figure 4.2: IR thermal images related to formulation 5. (IOC8 SbF6=0,5%wt, TPED=0,5%wt) At 40mW/cm²

The experiment was reproduced for all the formulations in triplicate in order to define a statistical behaviour.
The front velocity has been extrapolated as it was explained in section 3.3.2. (Figure 4.3)

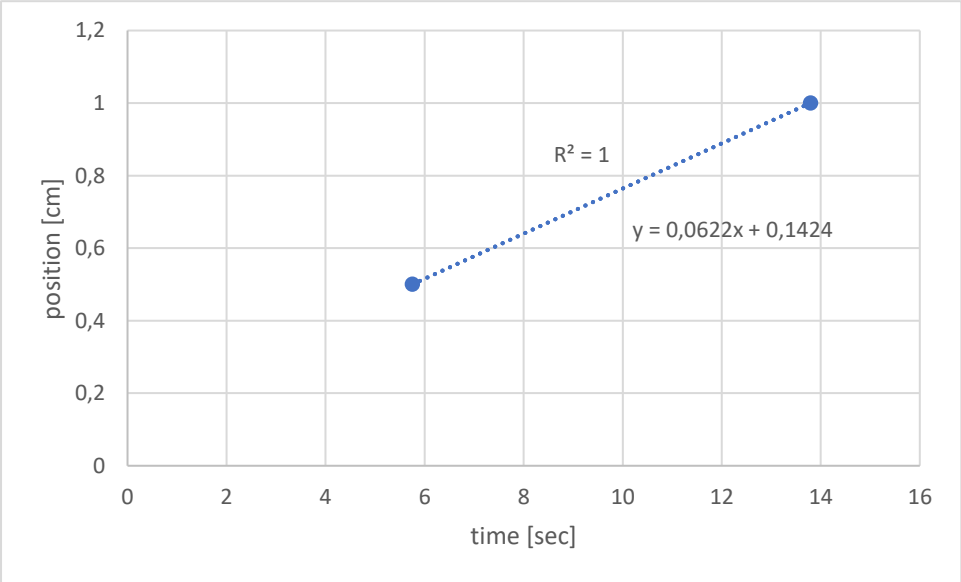

Figure 4.3: front velocity related to formulation 5. (IOC8 SbF6=0,5%wt, TPED=0,5%wt) At 40mW/cm²

In this way, multiplying the slope of the curve x60, the front velocity is determined in cm/min. E.g., for this run, the calculated front velocity is 3.73 cm/min.

In order to investigate the front behaviour through the thickness of the sample and to get useful data for stabilizing the propagating front, temperature versus time curves have been identified. Theoretically speaking, if a stable thermal front of polymerization is induced, the maximum temperature related to one position of the sample should identify a linear behaviour, increasing through time (Figure 4.14).

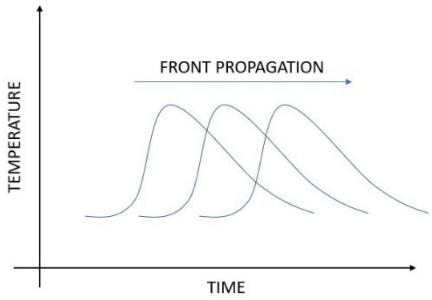

Figure 4.4: theoretical front propagation

These curves consider a stable front which propagates in a perfect horizontal line, manifestation of a perfect front stability.
The front behaviour has been studied for each formulation. Some anomalies have been found during this study, mostly due to the little portion of material studied in which the front doesn't have time to became stable in terms of temperature. In theory, a propagating front should be studied far away from the surface, in a region in which the front is stable, e.g. at least 0.5 cm far from the triggering point. In this regard, the small dimensions related to the first application considered (earbuds), doesn't allow to study the phenomenon in bigger samples. Other factor that may influence front stability may derive from changes in boundary conditions, such as the impregnation which become more difficult, as well as from the way in which the sample exchange the heat with the environment. The injection point wasn't recorded in correspondence to the first recording point (sp1) related to the centre of the surface, it is very likely that this is due to the heterogeneity of the used foam. This issue confirms the unpredictable behaviour present in the surface when the front starts and a delay between the moment in which the recording point related to the surface identifies a temperature higher than 250 °C and the considered onset time of the front (Figure 4.5).

Figure 4.5: example of the delaying of the starting point (2 seconds) formulation 6. At 40mW/cm²

However, other uncontrollable factors may reduce the front stability such as gas formation during curing or, again, foam structure heterogeneity (Figure 4.6).

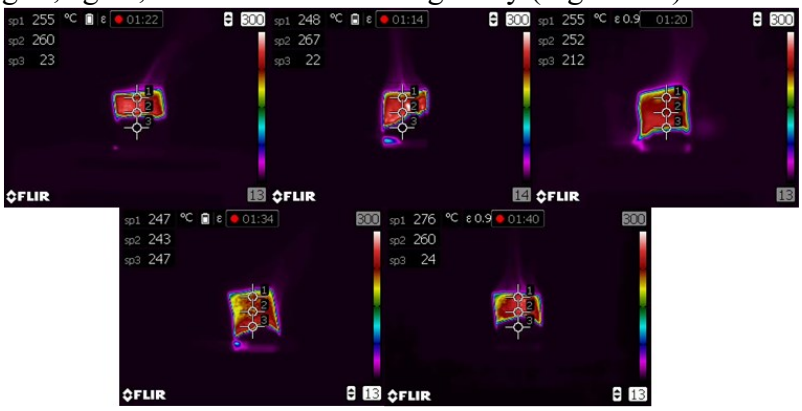

Figure 4.6: front instabilities examples

This issue may lead to anomalies between the maximum temperature recorded and the effective front position. Moreover, the possibility to identify the maximum temperature in the surface occurs in some occasion, confirming the effective presence of gasses which covers or alter temperature values in the other two recording points (sp2 and sp3). This confirms the extreme difficulty to link the behaviour recorded in this study with a stable propagating front for each formulation.

Anyway, an example of the propagating front in the three positions studied (blue = 0cm, orange = 0,5cm, grey = 1cm) in formulation 5. is plotted in Figure 4.7[1]. For each position and time, the temperature value was recorded and plotted against the corresponding time. Observing the blue curve related to the temperature, it is visible the short time in which the highest temperature is reached at the surface (blue graph) and at 0,5 cm (orange graph). The starting time of propagating front is set at 72 seconds, it is visible in this condition since the temperature greatly increase up to 257°C (75 sec). At 77 seconds, the front passed sp2 since

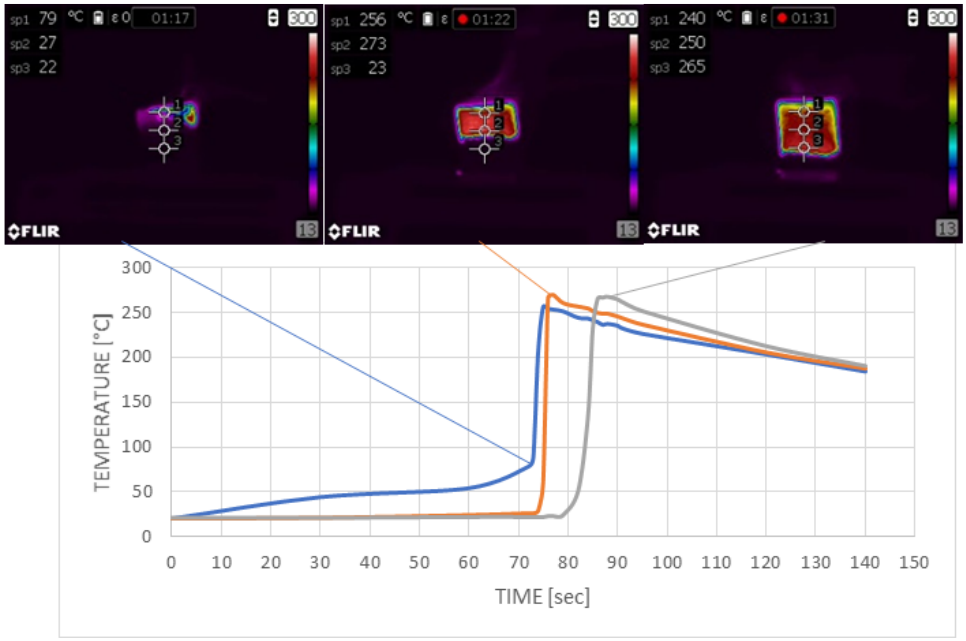

Figure 4.7: front behaviour for composition 5. At 40mW/cm²

[1] **NOTE: all pictures of the IR camera report the time with a second precision, all computations have been made using the video pixel therefore they are at a 1/100 seconds precision**

the temperature reaches higher values than 250°C and, at the same time, the maximum temperature (273°C) is attained. The injection process occurs from 72 seconds to 77 seconds: therefore, the injection time is of 5 seconds. At 86 sec, the front passed the third recording point with a corresponding temperature of 265 °C. This lead, as stated in the previous chapter, to a front velocity equal to 3.73 cm/min.
Same plot can be illustrated for formulation 6. (Figure 4.8), the starting time is set at 79 sec. In this condition, the highest temperature (295°C) value was recorded by the first recording point, two seconds later than the starting point of the front. Five seconds later (84 sec), the front completely passed the second recording point sp2. The injection time can be considered as 5 seconds in this condition. Then, at 90 seconds, the front visibly passed the third recording point, sp3. In this way, the calculated front velocity can be identified as 5.52 cm/min.

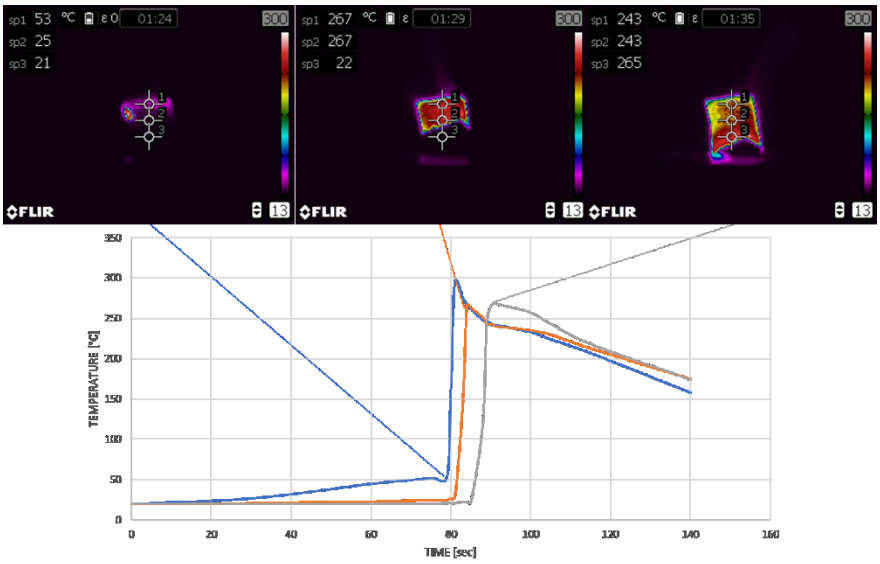

Figure 4.8: front behaviour for composition 6. At 40mW/cm²

Formulation 7. behaves as Figure 4.9 shows. The starting point of the front was set at 87 seconds, after this moment the temperature increased remarkably as the other formulations showed. After three seconds, the front passed the second recording point, reaching the

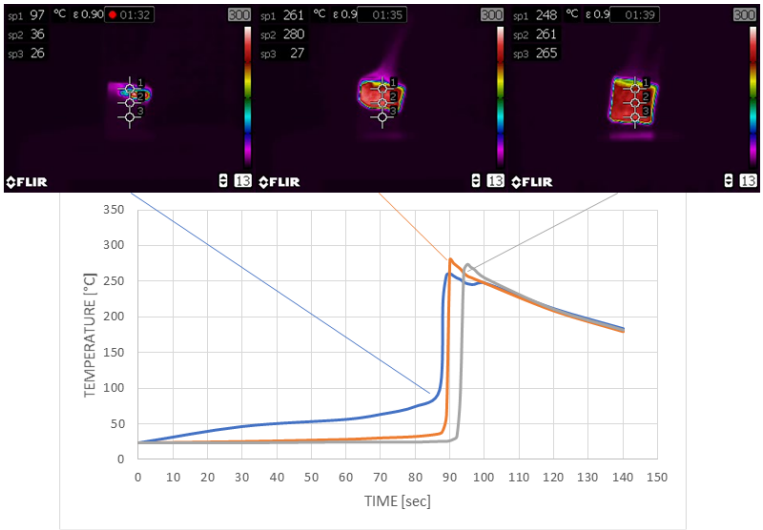

Figure 4.9: front behaviour for composition 7 At 40mW/cm²

highest temperature recorded (280°C). Finally, the front passed the third recording point at 94 seconds, leading to a front velocity of 6.383 cm/min.

Figure 4.10 shows the front behaviour for composition 8. In this condition, a relatively high temperature is recorded when the front is induced (66 seconds). This can be related to the possibility to have an injection point in a region that doesn't face directly the IR-camera. However, the same delay between the considered starting time and the time in which temperature higher than 250 °C is identified (2 seconds). After two seconds the front reached the second recording point and its related maximum temperature. At 73 seconds, the third recorded point related to the propagating front is considered. This will lead to a front velocity about 6.86 cm/min.

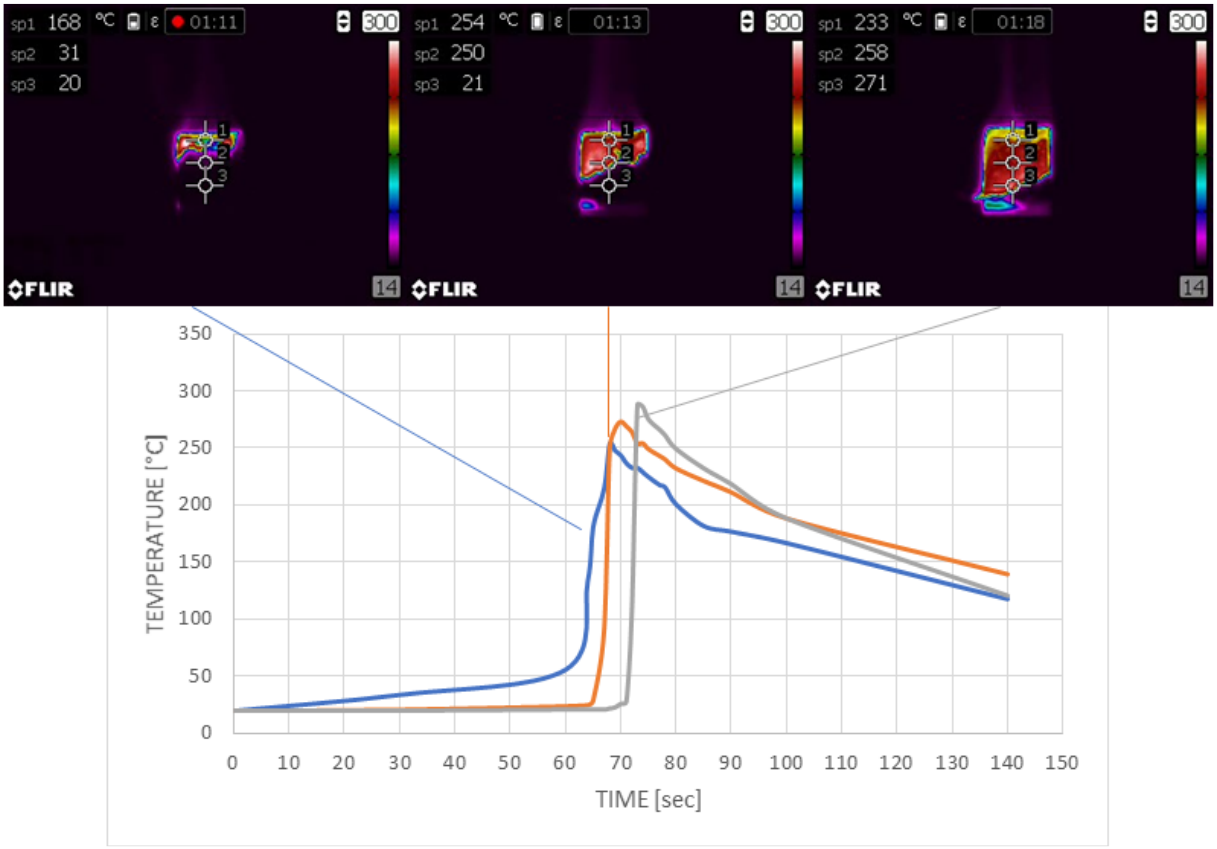

Figure 4.10: front behaviour for composition 8. At 40mW/cm²

Finally, front behaviour for composition 9. was investigated (Figure 4.11). In this condition, the starting time of the front was recorded at 73 seconds, afterwards the temperature increased exponentially as for formulation 5., 6. and 7. At 75 seconds, the maximum temperature (289°C) was recorded in correspondence of the first recording point. Then, at approximately 76 seconds, sp2 was reached by the propagating front identifying approximately the same value of temperature (284C). In the end, at 80 seconds, the front passed sp3, recording a temperature equal to 276 °C. leading to a front velocity equal to 7.44 cm/min. This absence of linearity between the maximum values of temperature at a given distance can be related to the production of gasses during photosensitive resin's boiling. Produced gasses will indeed change the value of the reflected temperature influencing the real object emanated temperature value. Since this phenomenon is uncontrolled, the linearity related to the maximum values of temperature at a given distance

and time cannot be statistically verified. In addition, structure heterogeneity may lead to uncertainties related to the front behaviour according to the dependence of the level of impregnation.

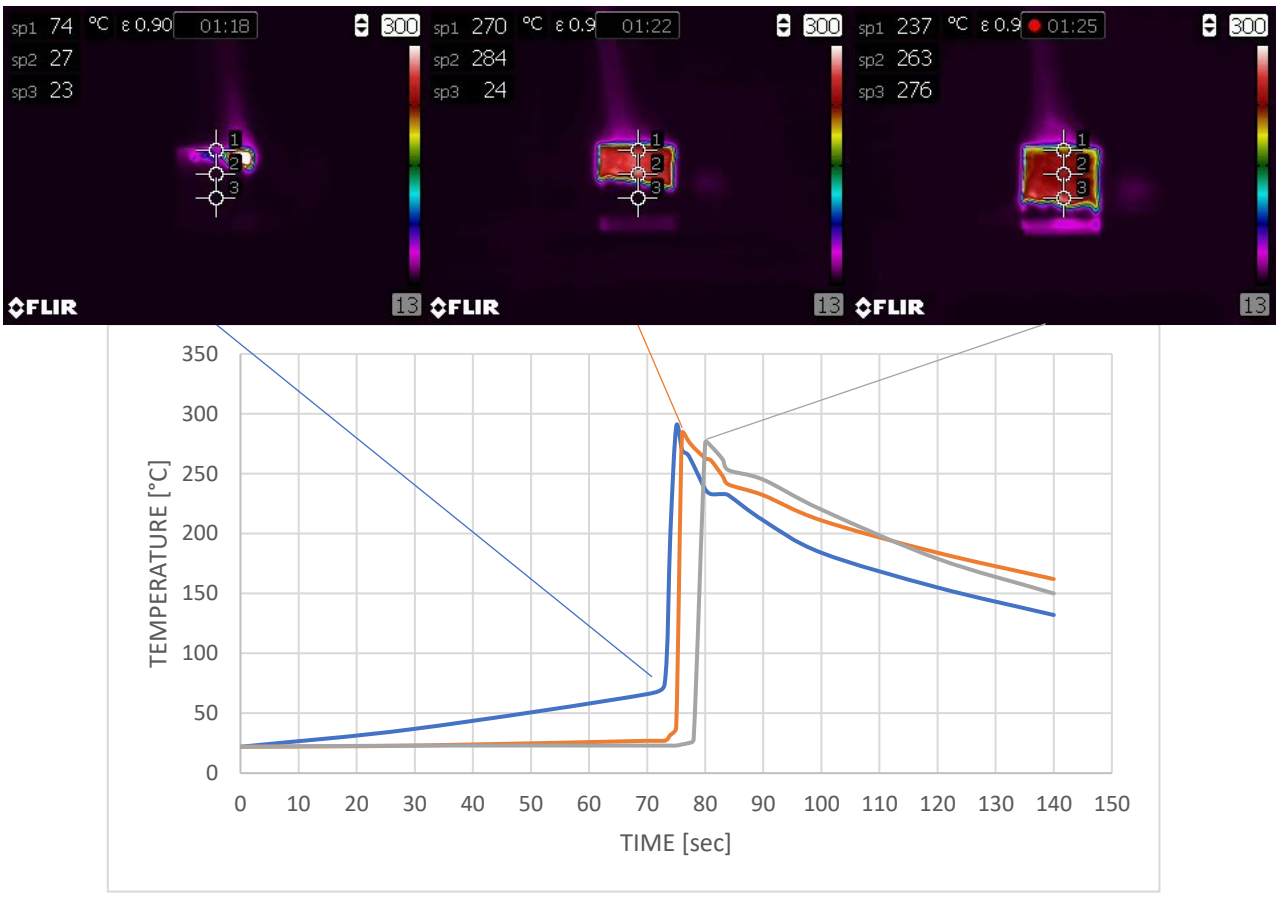

Figure 4.11: front behaviour for composition 8 At 40mW/cm²

As reported in literature, notwithstanding some anomalies, the shape of the curves is a clear manifestation that a frontal polymerization has occurred for all the compositions.
The front behaviour is characterized by a good level of homogeneity between sp2 and sp3. This has created the conditions to measure the front velocity with a good precision using computation and imagery mapping on the frames extracted by the video recorded.
In the contrary, the front behaviour is unpredictable between sp1 and sp2 and heavily affected by distortions between sp3 and the bottom of the samples.

4.1.1 Influence of photoinitiator

The study of the kinetic of the propagating front is conducted for all the formulations, focusing on the starting time of the front and the front velocity (Figure 4.12). From this graph, it is possible to conclude that the starting time of the front can be reduced at higher amount of photoinitiator. However, one limitation should be considered at 3%wt of photoinitiator because, when such treshold is exceded, the skin effect become important leading to a delay of the starting time of the front. Due to the reactivity's enhancement, the front velocity increases when the amount of photoinitiator is increased at 1,5%wt. Then, at higher amounts, a saturation occurrs and a plateau is visible, so the front velocity cannot be incrased anymore. This trend is similar to the one studied by Mariani et al., however the

absolute values registered in this study are slighlty higher, probably due to the usage of a different thermal inititator (Benzophenone).

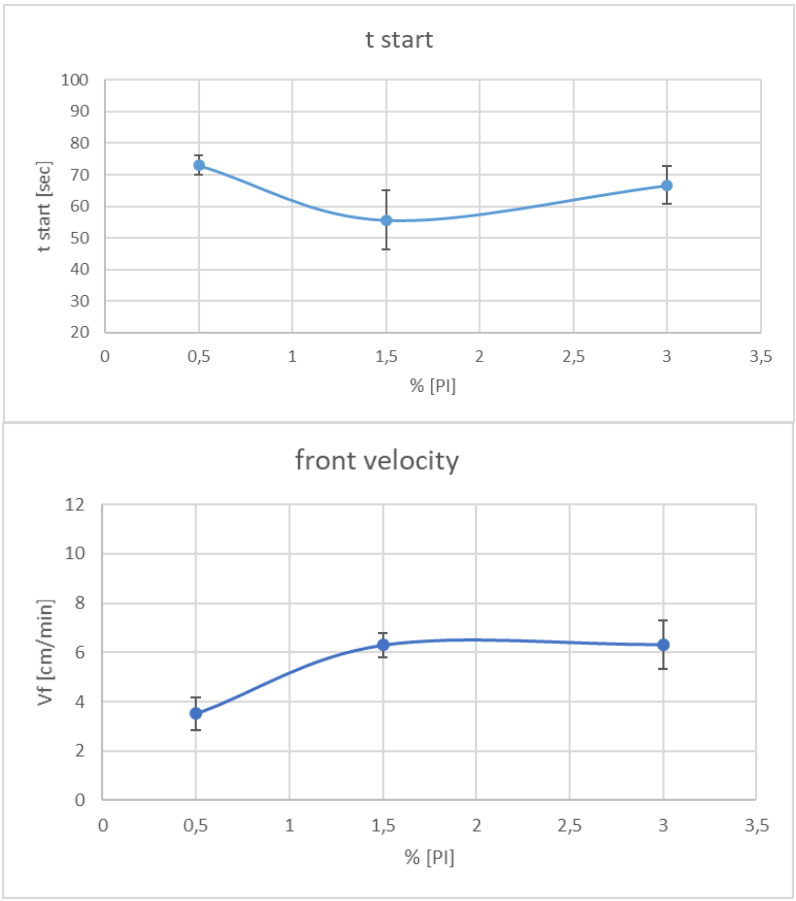

Figure 4.12: starting point (top), front velocity (bottom) at different amount of photoinitiator at 40mW/cm²

4.1.2 Influence of thermal initiator

With regard to different amount of thermal initiator, the kinetic of the propagating front is different (Figure 4.5). The starting front can be delayed increasing the amount of thermal initiator, this behaviour is clearly visible when the amount is maximum. This issue can be related to a screening effect of the thermal initiator due to the fact that it contains chromophore structures or due to a probable lack of dissolution which lead to scattering effects. The front velocity rises increasing the weight of thermal initiator up to 1,5%wt of TPED, for higher amounts of TPED the front velocity increases, even though with a low gradient. This might be due to a "saturation effect", in other words, after reaching a certain level/treshold, the front velocity is no more affected by higher percentage of TPED.

The result is partially in line with litterature. Both Bomze et al. and Mariani et al. have registered higher front velocity while increasing the concentration of thermal initiator. Mariani et al. have registered that "*for amount of initiator above 3.0 mol % no significant changes in front velocity and maximum temperature were observed*". What reported by Mariani et al. and the result of current testing, may sugegst that front velocity is not affected considerably by concentration of thermal initiator that goes above a certain treshold. This treshold is very likely to be a characteristic value of a specific formulation (resin and thermal initiator). In this study, the treshold is 1,5 %wt.

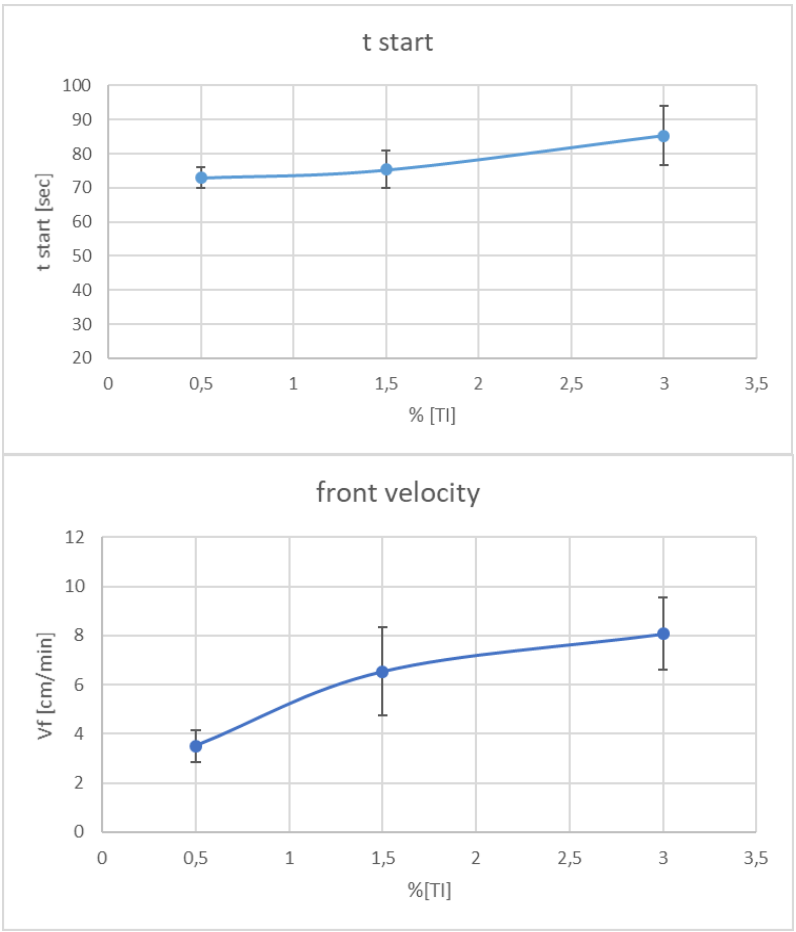

Figure 4.5: starting time of the front (top), front velocity (bottom) at different amount of thermal initiator at 40mW/cm²

4.1.3 Influence of thermal and photo initiators on process time and maximum temperature

The study has investigated the effect of diferent percentages of the two initiators on process time, a key parameter to determine the production rate of the studied process (Figure 4.6). As it is visible, it is possible to conclude that the only way to reduce the process time significantly is related to formulations in which the photoinitiator is between 0,5%wt and

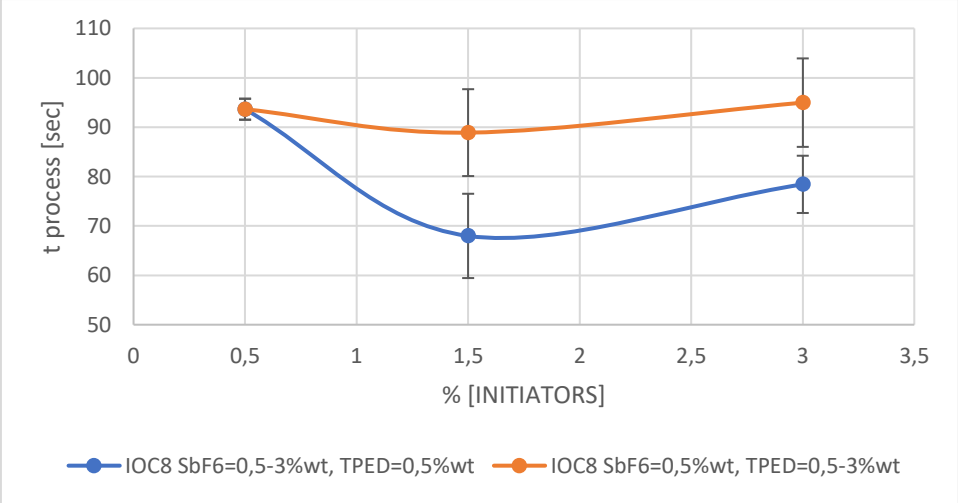

Figure 4.6: process time for 1.5cm thick foam

1,5%wt. This will lead to a decreasing in the starting time of the front considering that the skin effect is not influential condition that, in the countrary, is recorded at higher amount of photoinitiator. Variation in TPED percentage do not affect the process time.
As for the maximum temperature, it was measured in all formulations (Figure 4.7). At higher amount of photoinitiator, an higher exothermicity is identified, which leads to an increased value of maximum temperature. In this particular conditions, the huge production of smokes leads to many difficulties in the evaluation of the maximum temperature as high values related to the strandard deviations shows (Figure 4.8). However, recorded temperatures show an increase with respect to higher amount of photoinitiator as expected from higher reactivity of the formulation. Regarding the increasing amount of thermal initiator, a maximum value of temperature is recorded at 1,5%wt, while at higher amounts the temperature decreases. Again, this trend is similar to the one defined by Bomze et al. [27].

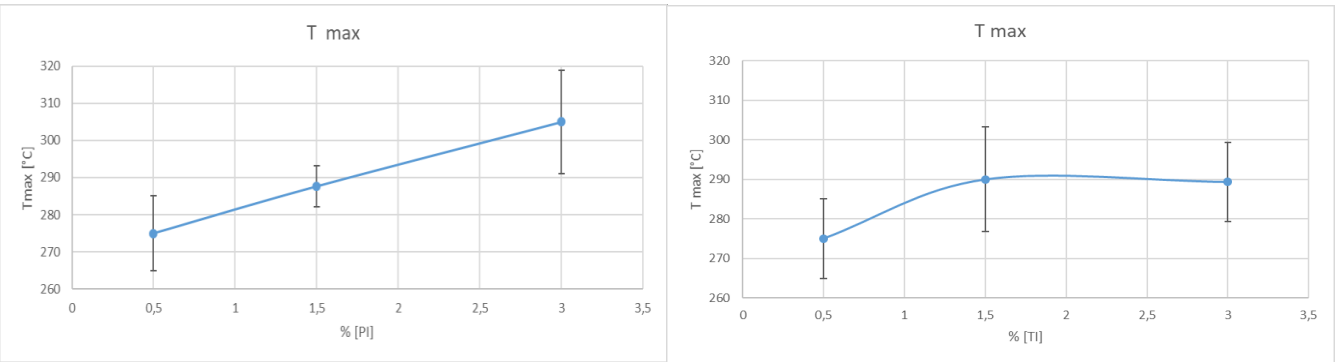

Figure 4.7: maximum temperature evaluation, different amount of IOC8SbF6 (left) and TPED (right)

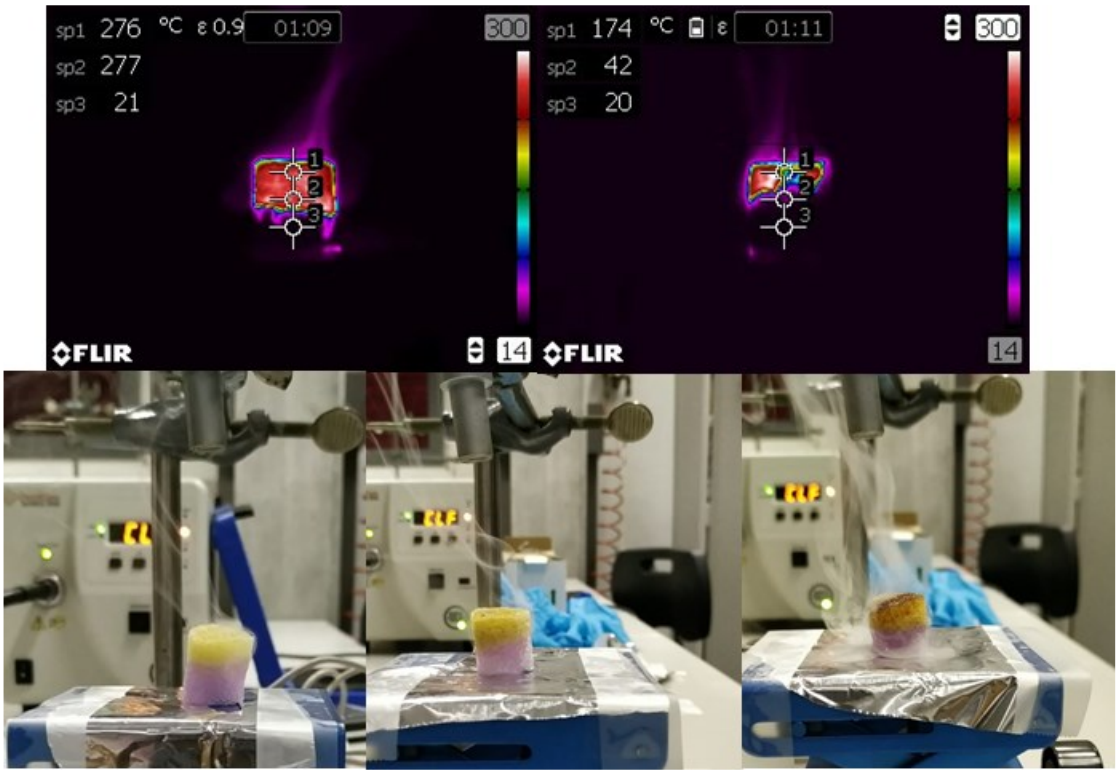

Figure 4.8: presence of smokes in 3%wt of IOC8 SbF6 and 0,5%wt of TPED (left) and 1,5%wt of IOC8 SbF6 and 0,5% TPED during IR tests (top). Visible presence of smokes at the lowest amount of both initiator (bottom, left), at higher amount of thermal initiator (formulation 6., bottom, centre), and at higher amount of photoinitiator (formulation 8., bottom, right) at 40mW/cm2

4.2 Morphology of impregnated and cured foams

4.2.1 Non confined impregnated foams

Internal inspection of the sample in formulations at higher amount of photoinitiator, shows that the polymer acquires an intense black colour: it is an indicator not only of the degradation of the foam, but also of the degradation of the created polymer network (Figure 4.9).

Figure 4.9: internal part of the formulation 9.

Finally, high values of temperature are reached very fast, as a consequence, an huge amount of gases are created in a very short time. These gases push the resin contained into the foam in the lower part of the sample till the point in which not cured resin is expelled from the bottom of the sample instead of being cured (Figure 4.10 and 4.11). This effect is more visible in formulations 8. and 9., when the amount of IOC8 SbF6 is higher.

Figure 4.10: external resin flow due to high heating rate. Composition 5. (left), composition 8. (centre), composition 9. (right)

In the contrary, variations in the amount of TPED showed different results. A less pronounced resin outflow from the bottom of the sample occurs. However, black colour is visible over the structure, especially when the amount of TPED is maximum: it is an

Figure 4.11: black colour and resin outflow present in formulation 5. (left), 6. (centre) and 7. (right)

indicator of a possible foam degradation as well as of thermal degradation of unreacted TPED.
Internal examination of samples has shown the possibility to obtain an uncured structure portion present in the centre of the sample (Figure 4.12).

Figure 4.12: uncured foam parts present into the sample for formulation 5.

This could be the result of the production of gasses which push the resin in the lower part of the sample, leaving the internal part uncured.
Said internal cavities may also be the outcome of a lack of impregnation in the deeper layers of the samples (as a minimum, in all samples at least 4 to 5 mm from the surface were surely impregnated). This can be the result of both poor impregnation based on infiltration conditions related to the used method (a simple squeezing of the foam chosen in order not to induce additional heterogeneity in an already heterogeneous structure) and high resin viscosity, which doesn't allow a complete and uniform foam impregnation.

4.2.2 Thermal stability analysis

Since temperatures reached are high, some investigations were conducted on the degradation behaviour of the materials involved.
Three subjects were studied: the foam used, the neat resin and the formulation 5.
Firstly, TGA measurement for the PU Supercell 2017 EUROFOAM foam from EUROSPUMA® has been conducted. The chosen range of temperature is from 30 °C to 400 °C and heating rate of 10 °C/min (Figure 4.18, top). The curve shows an onset temperature of 264.7 °C and two peak temperature of 283.03 °C and 345.19 °C. In this way, all conditions overcome the onset temperature. However, the first peak temperature has been overcome by all the compositions apart formulation 5., leading to a probable foam degradation. Investigating the structure for composition at higher amount of photoinitiator, it is possible to conclude that the temperature reached can be higher than 345.19 °C which correspond to the second temperature peak.

Same experiment has been conducted for the photosensitive cycloaliphatic epoxy resin Omnilane OC 1005 (Figure 4.18, bottom). In the same way, all the compositions overcome the onset temperature (239.69 °C). However, the peak temperature (290.04°C) has been overcame by all the formulations apart formulations 5. (maximum temperature: 275 ± 10.14 °C).

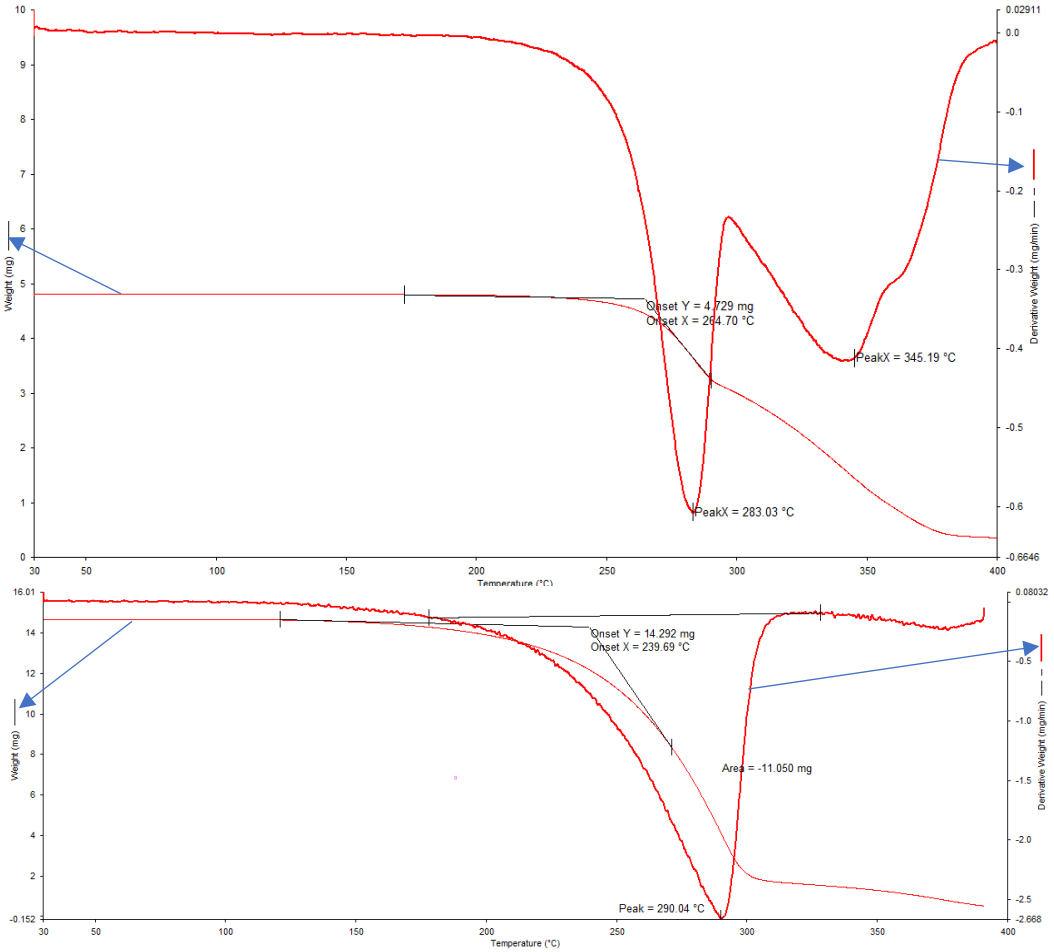

Figure 4.18: TGA PU supercell foam (top), TGA Omnilane OC 1005 (bottom)

Regarding formulation5, was necessary to use a different temperature range from 30°C to 500°C at 10°C/min (Figure 4.19). The different range choice was due to the fact that when a TPED is used it is the TPED to start the polymeric network.

The onset temperature is set at 366.84°C and the peak temperature at 411.4 °C. Considering that all the polymeric structure seems to be degraded in formulations at higher amount of

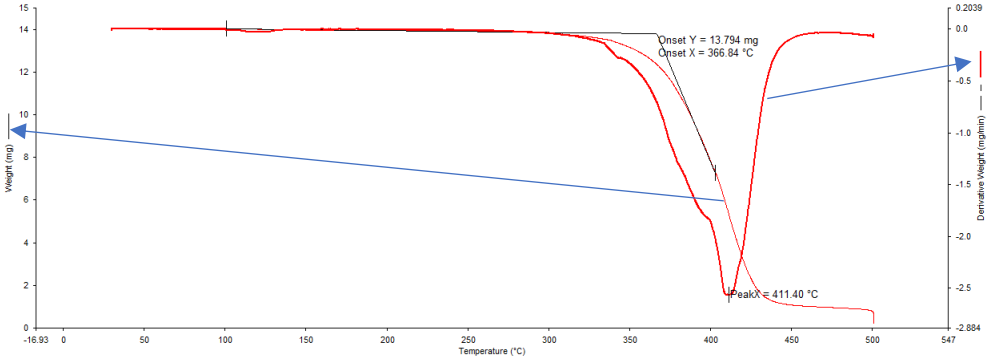

Figure 4.19: TGA formulation 5. IOC8 SbF6=0,5%wt, TPED=0,5%wt

photoinitiator, especially formulation 9., much higher values of temperature than the recorded ones should be considered.

4.2.3 Optical microscopy and SEM

Given the occurrence of degradation phenomena in some of the formulations studied, further investigations over the structure of the samples were conducted. The best and the worst results in matter of degradation were selected: formulation 5. (IOC8 SbF6 = 0,5%wt, TPED = 0,5%wt) and formulation 9. (IOC8 SbF6 = 3%wt, TPED = 0,5%wt). This selection was conducted according to colour, structure retention and a more controlled additional resin outflow from the bottom. Big differences in colour occurs in the sample surface (Figure 4.20) from yellow to ~~a~~ dark brown, the same colour difference is present throughout the entire structure of the sample. The foam structure is maintained in both formulations and some bubbles are visible in the formulations with the higher amount of photoinitiator, proving the resin boiling and the formation of gasses during curing.

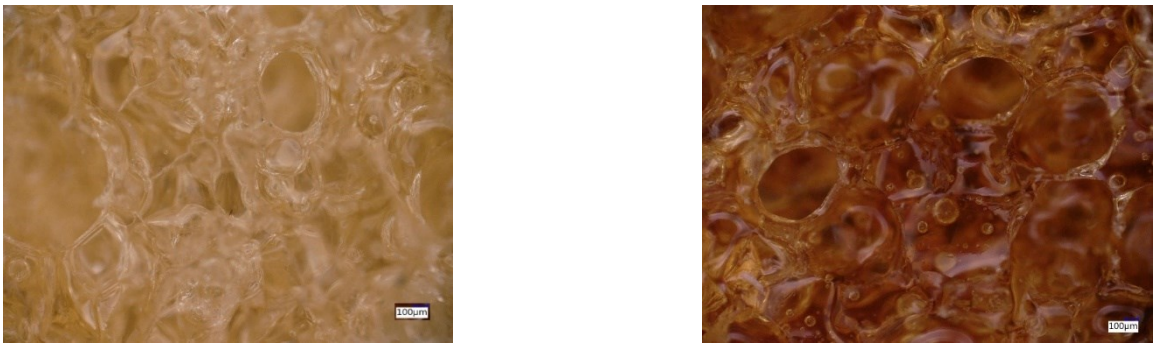

Figure 4.20: optical images at 50x of magnitude of cured foam impregnated with (left)Formulation 5. and (right) formulation 9.

For the same formulations, SEM images of sample surface have been taken for both of them (Figure 4.21). First signs of the breaking up of the overall structure when conditions become more critical are also visible in the surface.

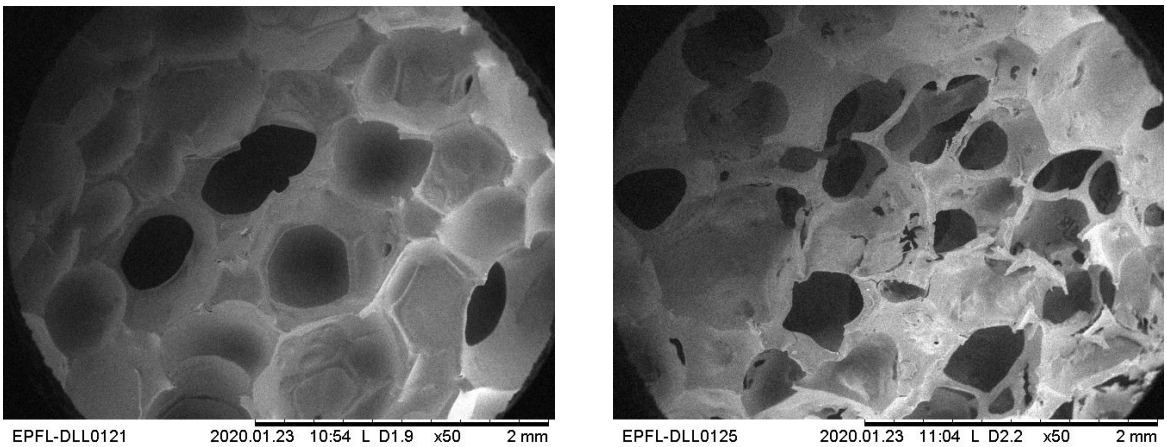

Figure 4.21: SEM images of formulation cured foam impregnated with 5. (left) and formulation 9. (right)

However, further investigations were conducted in the deeper layers from the surface of the material. The result is quite surprising because even in the formulation 5., considered as the one that controls better the exothermicity of the reaction, pores are present (Figure 4.22).

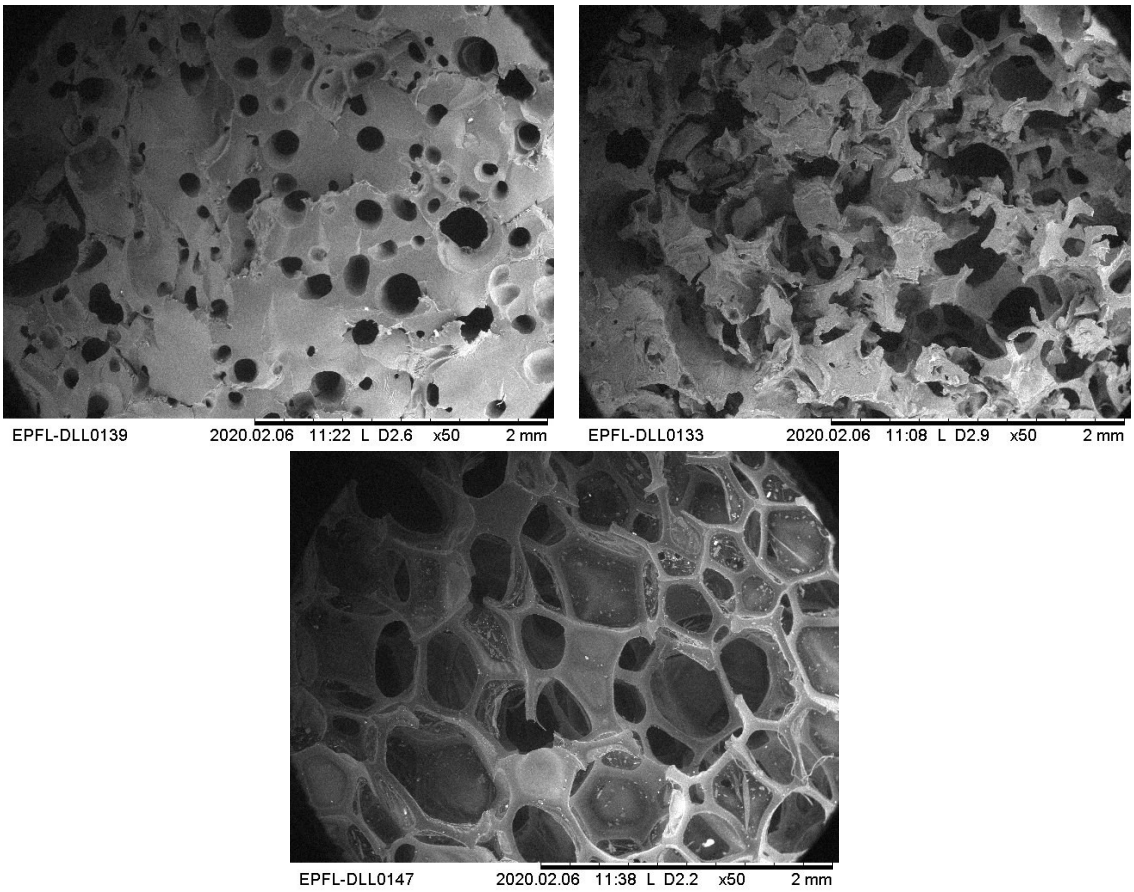

Figure 4.22: SEM images taken at deeper layers from the surface of formulation 5. (top left) and formulation 9. (top right). Unfilled foam (bottom)

This is mainly due to the formation of gasses during the front propagation since the boiling temperature (170 °C) is overcome. On the other hand, a complete disintegration of the structure is clearly visible in formulation 9. This can lead to serious problems, especially when a structural application is considered. Therefore, formulation in which the amount of initiator is minimum can be considered as the best solution among the tested ones, according to lower amount of gas produced, front stability and structure retention with no additional external flow produced. This is the result of a condition in which the outflow of the liquid resin is slower than the formation of each foam layer as well as of a better resin retention into the foam mould. Moreover, a freeze foamy structure is created, which may lead to improved thermal insulating properties. Considering the thermal conductivity of a cycloaliphatic epoxy resin (0,23 W/mK [53]), the presence of pores will induce a decreasing of the thermal conductivity according to the equation (4.1) [54]:

$$\lambda_p = \lambda_s(1 - P_c) \tag{4.1}$$

Where λ_s is the thermal conductivity of the solid, λ_p is the thermal conductivity of the porous structure and P_c is the cross-sectional pore fraction.
However, in order to be competitive with commercially available thermal insulator such as expanded polyurethane or mineral wool (λ= 0,020-0,040 W/mK) the value of P_c should be around 0,8-0,9. Moreover, as it was previously mentioned in the introduction, degradation

phenomena must be carefully controlled. As TGA confirmed, none of the studied compositions allowed a complete absence of degradation of the porous media. Therefore, the focus should be moved to different foams which don't meet any kind of degradation at this level of temperature, such as metallic foams.

4.2.4 DSC measurements

DSC measurements have been conducted in cured foam samples collected at 1 cm depth from the surface. This investigation has been performed in order to record exothermic peaks at relatively high temperatures, especially between 150°C and 200°C. This issue may be linked to an incomplete reaction after the propagating front. Two ramps have been conducted from 0 °C to 200 °C at 20 °C/min, both on the same sample. The first ramp investigates the presence of exothermic peaks, the second ramp checks if the reaction is complete and gives some information of the glass transition temperature of the material.
The first run of thermocurves involves samples with an increasing amount of photoinitiator (Figure 4.23).

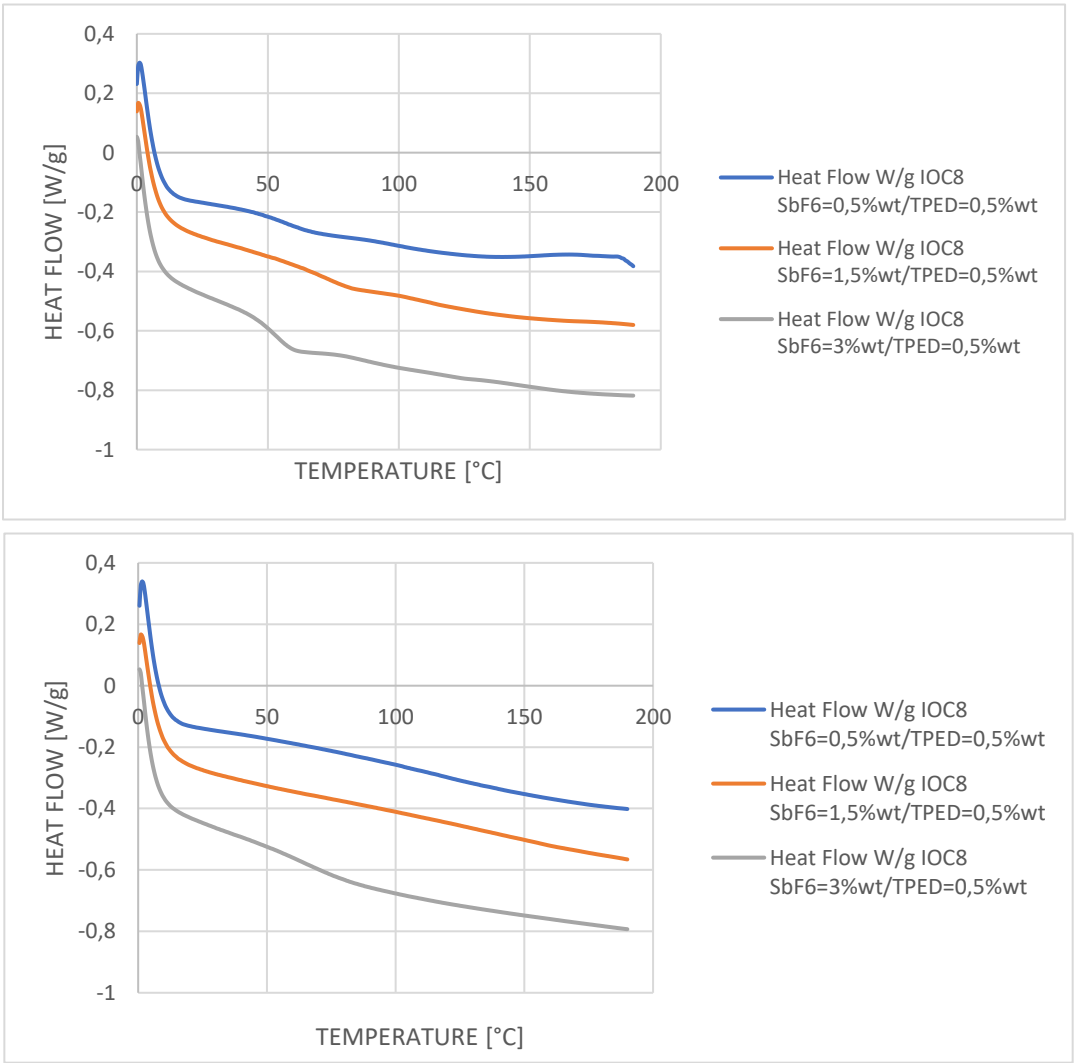

Figure 4.23: DSC thermogram for increasing amount of photoinitiator. First ramp (top), second ramp (bottom)

Only the curve related to formulation 5. (IOC8 SbF6=0,5%wt and TPED=0,5%wt) shows one little exothermic peak at 160 °C approximately. However, this peak can be negligible considering that it represents a conversion of 99,4%. The second run identifies that no more reactions occurred after the first ramp.

Same experiment was conducted on samples related to different amount of thermal initiator, maintaining constant the amount of photoinitiator at 0,5%wt.
In the same way, only compositions 5. and 6. showed a little exothermic peak, which can be considered as negligible (Figure 4.24).

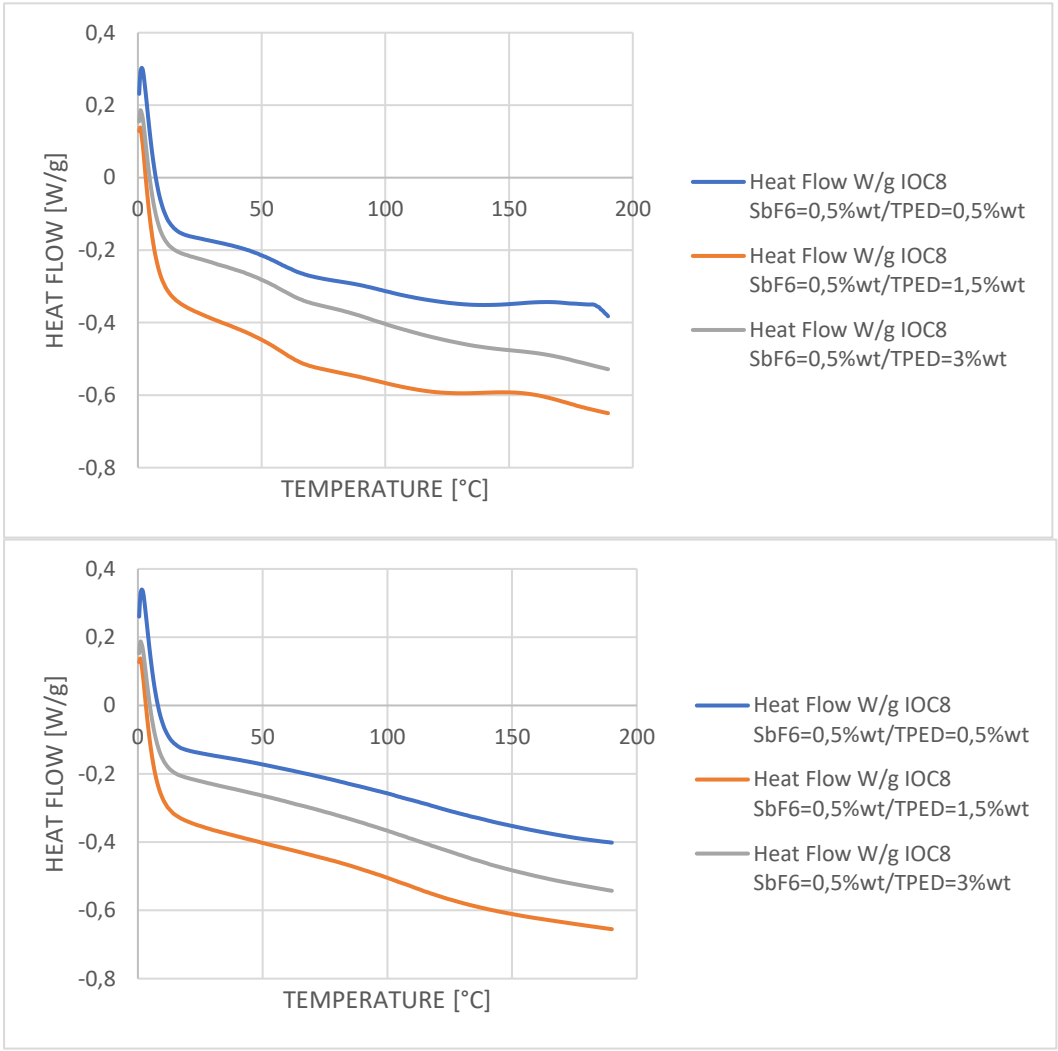

Figure 4.24: DSC thermogram for increasing amount of thermal initiator. First ramp (top), second ramp (bottom)

4.3 Analysis of front initiation

Further investigations re required in order to confirm what has been experienced through visual measurements of the frontal polymerization phenomenon. FTIR and Photo-DSC contribution are fundamental in order to investigate the kinetic and conversion phenomena of the very first photo-excited reaction. First, FTIR spectra of the liquid resin (orange curve) corresponding to formulation 5. and the cured sample of the same composition (blue curve) have been compared (Figure 4.25).

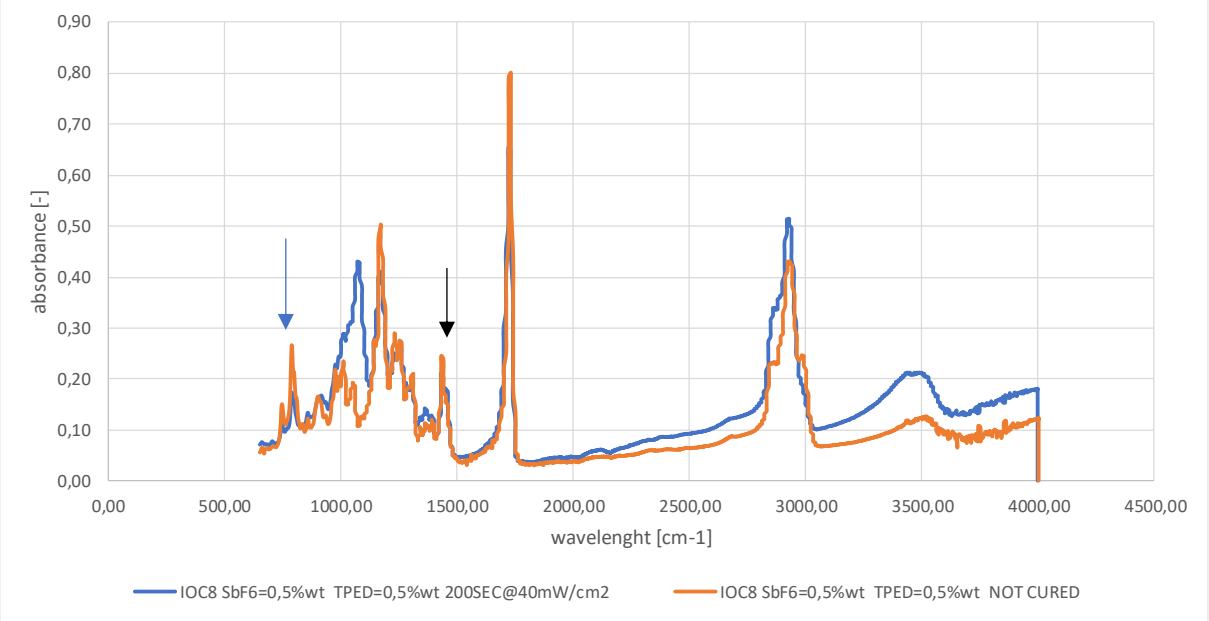

Figure 4.25: FTIR spectra not cured resin (orange) and cured sample (blue) related to formulation 5.

The cured sample has been obtained curing a thin film with a thickness of approximately 500µm at 40 mW/cm^2 for 200 seconds, which is the same exposure time and irradiance used for Photo-DSC measurements. Then, absorbance related to peaks of interest (epoxy ring, blue arrow) previously discussed in section 3.2.2 have been considered and divided per the absorbance of the reference peak (methylene group, black arrow) in order to identify the conversion of the epoxy ring (4.1):

$$A^*_{787,c} = \frac{A_{787,c}}{A_{1435,c}} = \frac{0.174}{0.211} = 0.8246 \quad ; \quad A^*_{787,0} = \frac{A_{787,0}}{A_{1435,0}} = \frac{0.268}{0.245} = 1.09387 \tag{4.1}$$

$$\alpha_e = 1 - \frac{A^*_{787,c}}{A^*_{787,0}}$$

In this way, the calculated conversion value is 24,6%. Considering the final value of the integral curve extrapolated from the Photo-DSC output (Figure 4.26), it is possible to calculate the enthalpy of reaction (4.2).

$$H_{cal} = \frac{H_{fin}}{\alpha_e} = 503{,}39 \text{ J/g} \tag{4.2}$$

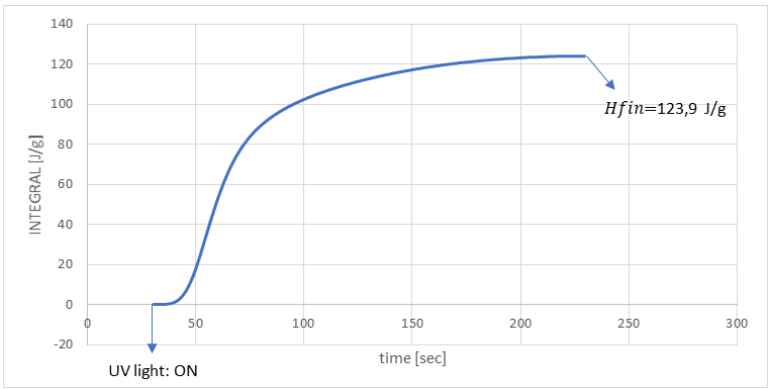

Figure 4.26: Integral curve extrapolated from formulation 5. Photo-DSC curve, UV light switched on after 30 seconds

According to Golaz et al. [48], the value related to the enthalpy of reaction of a slightly different cycloaliphatic epoxy resin (Genomer 7210 from Rahn, Switzerland) can be derived considering *"the weight concentration of epoxy functional monomers was divided by their average Epoxy Equivalent Weight (EEW) and multiplied by the theoretical enthalpy of 94.5 kJ/mol for one reacted epoxy group"*. Using the same approach, the reference value can be ascribed as 685,38 J/g (considering 99%wt of monomer concentration and 136,5 as the average Epoxy Equivalent Weight). The decrease regarding the calculated enthalpy of reaction from FTIR spectra and the value extrapolated from the monomer's features can be related to the presence of the thermal initiator too, which can influence the formulation's reactivity. However, is very common to find higher conversion values (so lower enthalpy values) than the ones measured by Photo-DSC. While an average conversion value representing the overall thickness of the sample is obtained by Photo-DSC, ATR-FTIR measures the conversion value of the surface of the sample. Finally, this phenomenon can be associated to a different photopolymerization behaviour between the surface, in which it is faster, and the bulk of the studied sample [55]. Same considerations can be stated for the reference value of full conversion for the studied monomer which can be calculated according to equation 4.3:

$$H_{th} = \frac{f E_a}{M_w} = 749{,}05\ J/g \tag{4.3}$$

Considering the difuncionality of the cycloaliphatic epoxy monomer (f=2) and its molecular weight of 232.32 g/mol. The value obtained with equation 4.3 was used as the reference value and Photo-DSC measurements were calibrated accordingly.

4.3.1 Influence of photoinitiator

First, the focus has been on the different amount of IOC8 SbF6 from formulation 1. to formulation 4. in which no thermal initiator has been added (blue curve). Then, t gel and $\dot{\alpha}$ values have been compared to formulation 5., 8. and 9. In order to investigate the same influence when the 0,5%wt of thermal initiator is added (orange curve) (Figure 4.27).

As it is visible from the curves, increasing the amount of IOC8 SbF6 an increasing on the t gel and a decreasing on $\dot{\alpha}$ occurs. This can be related to the skin effect, which occurs in these conditions. In addition, the formation of secondary aromatic species occurs which absorbs at similar wavelengths and affect the absorption efficiency of the photo acid generator reducing the amount of formed reactive species [56], [57], [58]. No differences, especially in the t gel, have been identified when 0,5%wt of thermal initiator is added, assuming no shield effect from the thermal initiator in these conditions. However, an increasing on the $\dot{\alpha}$ is visible comparing formulation 1. (0,5%wt of IOC8 SbF6) and formulation 5. (0,5%wt of both photo and thermal initiators) which leads to a certain reactivity caused by the presence of the thermal initiator too.

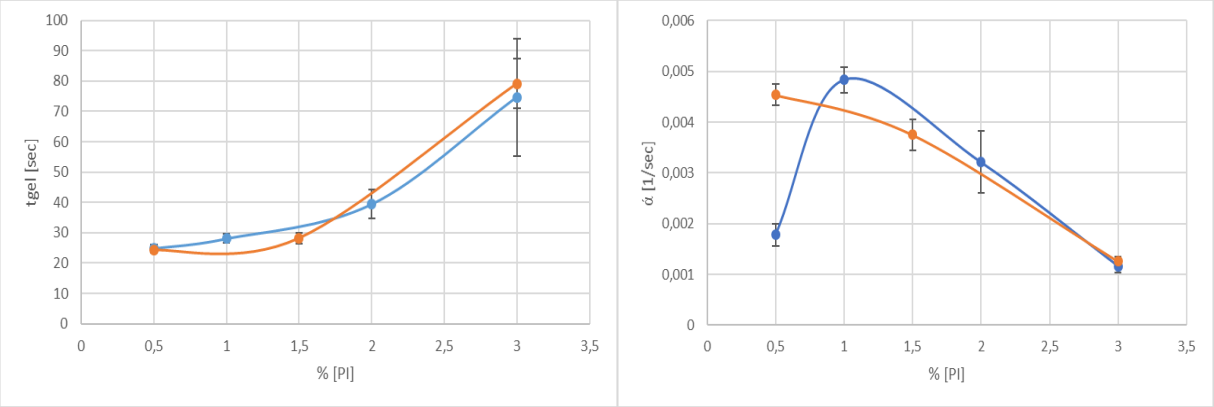

Figure 4.27: t gel (top) and ȧ (bottom) for different amount of photoinitiator. Blue curve: no thermal initiator added; orange curve: 0,5%wt thermal initiator added

.

4.3.2 Influence of thermal initiator

Same investigation has been conducted increasing the amount of TPED from 0%wt (formulation 1.) to 3%wt (formulation 5., 6., 7.) maintaining constant the value of photoinitiator at 0,5%wt (Figure 4.28).

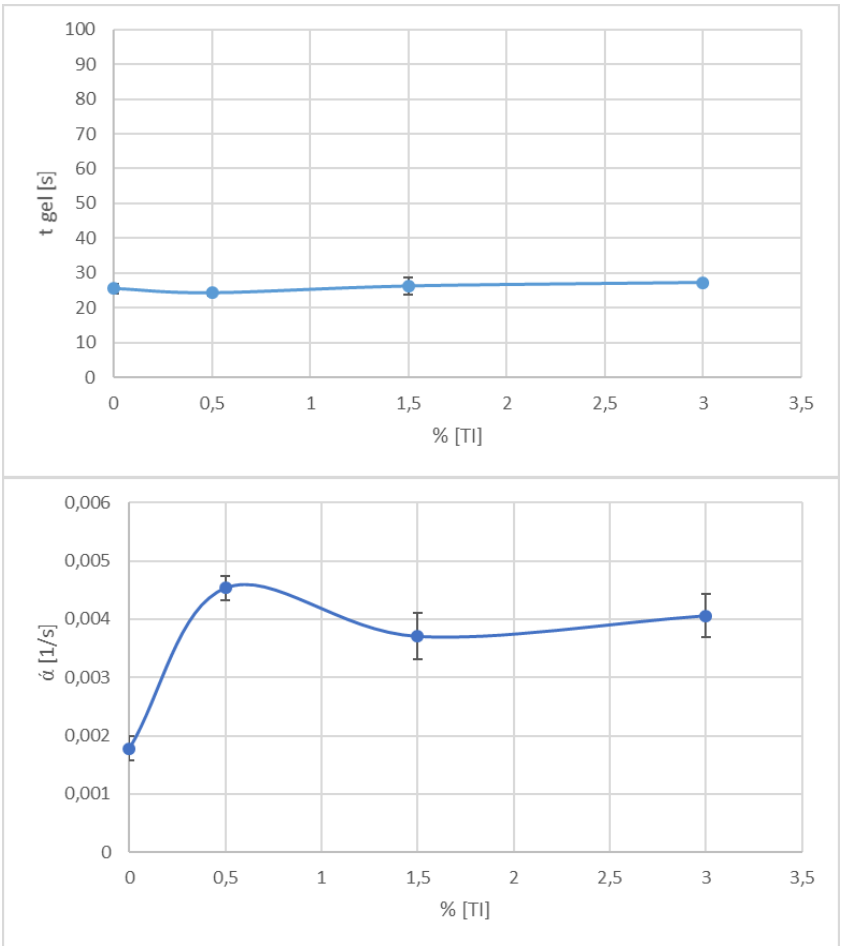

Figure 4.28: t gel (top) and ȧ (bottom) for different amount of thermal initiator TPED

No differences have been noticed regarding the t gel, however a decreasing on the maximum conversion rate is evident at higher amount of thermal initiator (1,5%wt and 3%wt) if compared with the formulation with the lowest amount of TPED. An hypothesis regarding the possibility of a screening effect related to the presence of higher amounts of thermal initiator can be expressed in light of absorption data below 400 cm^{-1} reported in table 4.

Table 4: absorption data for benzophenone and TPED (benzopinacol) [59]

Wavelength/cm^{-1}	Absorbance of benzophenone	Absorbance of benzopinacol
310	0.912	0.858
330	0.273	0.210
350	0.117	0.065
360	0.081	0.053

4.3.3 Correlation between front initiation and propagation

Finally, results obtained from Photo-DSC and thermography measurements were compared in order to identify a correlation between the initiation step and the front propagation. In particularly, t_{gel} , t_{start}, $\dot{\alpha}$ and front velocity were plotted (Figure 4.29).

The orange curve depicts the behaviour of the four parameters plotted at different percentages of thermal initiator: no peculiar correlation between initiation and propagation can be inferred, especially regarding $\dot{\alpha}$ vs V_f. In this condition, the outcome may be considered as to be "a cloud of point". The blue curve shows the behaviour of the four parameters at different percentages of photo initiator. The t_{start} vs t_{gel} plot suggests that the decreasing of the $\dot{\alpha}$ is due to the skin effect, which increases with increasing percentages of the photoinitiator. When the amount of photoinitiator is increased excessively, a delayed starting time of the front may occur: this is in line with the prominent increasing t_{gel} and a decreasing of $\dot{\alpha}$. Surprisingly, for concentrations of photoinitiator between 0,5%wt and 1,5%wt, the front velocity increases while $\dot{\alpha}$ decreases: this might be due to the fact that the skin effect blocks the creation of reactive species through the thickness of the sample, but an enhanced reactive species' creation occurs on the surface of the sample, therefore the initial part of the polymerization is characterized by a slower thermal diffusion. This may lead to both a decreasing on the starting time of the front and an higher front velocity since a better heat retention is induced [60], [61]. Moreover, the two phenomena (photo-induced

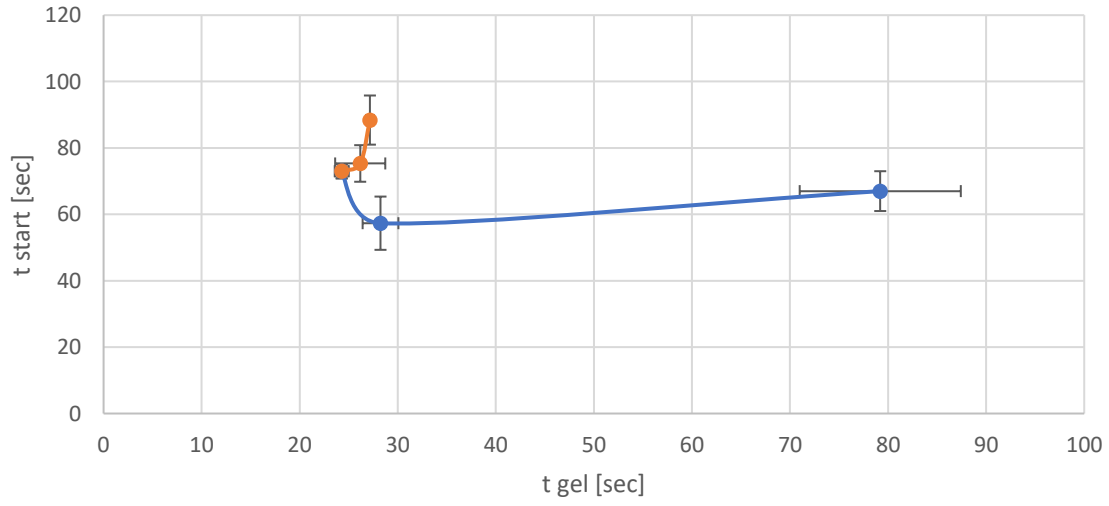

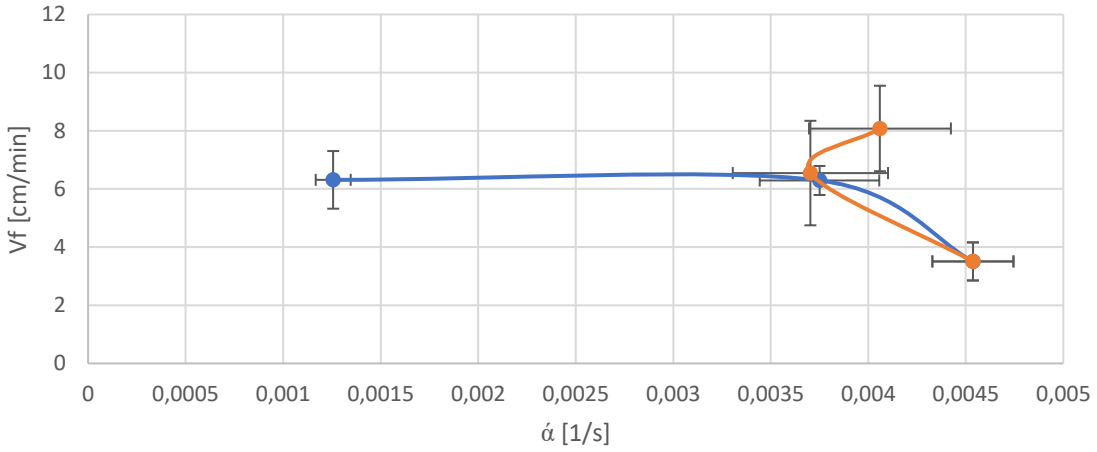

Figure 4.29: t_{start} vs t_{gel} (top), $\dot{\alpha}$ vs V_f (bottom). Orange curve: IOC8 SbF6=0,5%wt / TPED=0,5% - 3%wt. Blue curve: IOC8 SbF6=0,5% - 3%wt / TPED=0,5%wt

and thermal front polymerization) are influenced by different conditions. First, the photo-induced part can be influenced by skin effects or internal filter effects which, as previously stated, induce a decrease of ά in the studied composition range [58]. Second, thermal front velocity propagation can be influenced by other factors such as higher bubble formation and temperature, conditions arised at higher amount of photoinitiator, which leads to higher front velocity. For concentration higher than 1,5%wt, said phenomenon was not registered due to a probable "initiator burnout" which may lead to a plateau of front velocity values [3]. Finally, further studies must be conducted on the correlation between the photo-initiation and thermal propagation behaviour of the polymerization front focusing on a more detailed range of composition within the optimal range (from 0,5%wt to 1,5%wt of IOC8 SbF6 and 0,5%wt of TPED).

4.4 RICFP in aluminium foam

As stated in section 3.1.4, the possibility to combine benefits related to UV technology with those related to Interpenetrating Phase Composites may lead to outstanding economical, manufactural and final advantages. The first challenge was the foam impregnation. In order to facilitate resin impregnation through the porous media, one aluminium foam characterized by big pores size and a cylindrical shape of 3 cm diameter was selected. A composition of 1%wt of both initiators was prepared following the method proposed in order to ensure the front propagation through the porous media.
The formulation was poured into a silicon mould until half of it was filled and then the aluminium foam with the precise dimension of the mould was placed and pushed into the mould in order to obtain the impregnation in deep layers. Then, additional formulation was poured into the mould in order to obtain the impregnation in superficial layers. Afterwards, the light guide was placed very close to the sample, the lamp power was set at 100% and, finally, the light was switched on. According to this first experiment, any propagating front has been recorded and only a surface curing of the formulation occurred (Figure 4.30, left). This result is mainly because the minimal layer thickness, fundamental condition in order to obtain a propagating front of polymerization, wasn't reached. Moreover, the porous media used influences light absorption efficiency of the UV-curable formulation because of light absorption and scattering phenomena. Therefore, another strategy was adopted: the foam was cut at a lower thickness than the one of the mould. Then the impregnation step was the same as for the previous test, with the difference of the presence of a surface layer composed of only the curable formulation. In this way, the presence of the minimal layer thickness in order to trigger the frontal polymerization was guaranteed and the influence on absorption efficiency of the curable formulation by the aluminium foam was eliminated. The success of this second experiment is clear and an IPC was produced (Figure 4.30, right). The resin outflow from the mould is even more evident by the presence of additional cured resin on the top. The cured resin presents a foam structure which can be an issue if a structural application is required. However, an increase in energy absorption can be predicted, of primary importance when high impact protection must be high. In addition, compressive strength, thermal and acoustic insulation properties could be improved significantly. Nevertheless, as stated in section 2.4 many parameters and conditions should be further considered in order to characterize in a reasonable way the produced material (e.g., the interface between the cured resin and the aluminium foam, the suitable phases' volume fraction, the influence of the amount of initiators on the cured resin structure as well as a different resin with higher boiling temperature which doesn't run into gas formation and create a thick and homogeneous structure).

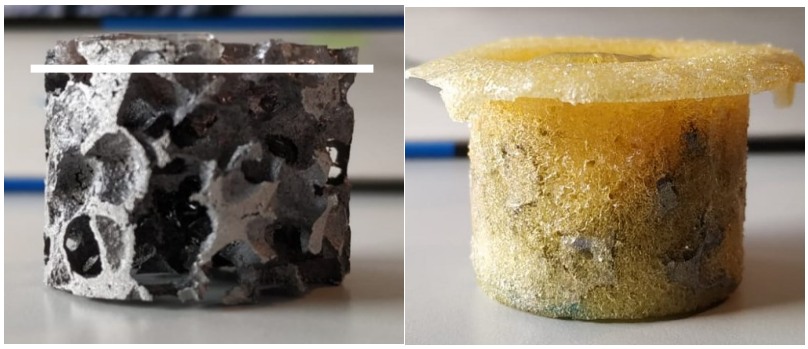

Figure 4.30: surface curing (white line) visible in the first experiment (left), IPC obtained by RICFP technique (right)

5. Conclusions

In the present study, a screening of the main properties and phenomena involved in an RICFP process in impregnated open cell foam is performed in order to characterize a system/material that induces the shape acquisition in a very fast way. For doing that, several measurements were performed focusing on front kinetic (via infrared thermography), structure (using SEM and optical microscopy) and degradation (employing thermogravimetric analysis) behaviours for various percentages of both. Firstly, a proof of fact has been conducted in order to assure that only the combination of photo and thermal initiator is suitable to induce a frontal polymerization (FP) under UV exposure. Minimal amount of both initiators in order to induce FP has been identified at 0,5%wt for both of them. In the following phase, two sets of experiments have been proposed: the first one is characterized by increasing the amount of photoinitiator (0.5%wt, 1,5%wt and 3%wt) maintaining unchanged the amount of thermal initiator at the lowest possible level (0,5%wt); the second one was conducted by the opposite criterion.

As reported in literature, notwithstanding some anomalies, a frontal polymerization as occurred for all the compositions. The front behaviour is characterized by a good level of homogeneity in the middle part of the samples (about 0,5cm away from the upper and lower surfaces). This has created the conditions to measure the front velocity with a good precision using computation and imagery mapping on the frames extracted by the video recorded. In the contrary, the front behaviour is unpredictable in the upper and lower portion of the samples, where it is affected by distortions.

As expected, by increasing the amount of photoinitiator between 0,5%wt and 1,5%wt higher reactivity into the system is induced, recording higher temperature and front velocity values, higher concentration of photoinitiator (higher than 1,5%wt) do not affect the kinetic of the process while affect the exothermicity (maximum values of temperature have reached 305±13.89°C). Furthermore, higher percentage of photoinitiator brings to a more pronounced skin effect, which led to a delay of the starting time of the front. In the contrary, front behaviour is different when percentage of thermal initiator is changed. Maximum temperature increased proportionally with the increasing of thermal initiator, up to 1.5% wt, for higher concentration, the maximum temperature decreases. On the other hand, front velocity increases proportionally to the thermal initiator concentration up to 1,5%wt, for higher concentrations the front velocity does not increase ranging at about 8,079 ±1.469 cm/min. The starting time of the front showed increasing values at higher amount of thermal initiator, suggesting the existence of a shield effect produced by the presence of chromophores group in its structure. Regarding the structure retention, visually, best result has been obtained in the formulation in which the amount of both initiators is minimum (0,5%wt). Samples of this composition showed better conditions in terms of structure retention, and reduced external outflow and exothermicity.

Since high temperature values were recorded, it was deemed necessary to conduct investigations on internal degradation phenomena. In this way, three TGA measurements were performed on the degradation behaviour of the: unfilled foam, neat resin and formulations containing both initiators. In all tests, the actual temperatures reached levels higher than the onset temperature. This condition led to the presence of degradation in all studied samples, but the one with the lowest amount of initiators, in which this issue seems to be more controlled, such outcome was confirmed by SEM images. Images show that a foamy structure was maintained because a foaming agent (gasses originating from the resin boiling) was produced during curing. This may lead to an improvement of the thermal insulation behaviour of the studied material. However, more parameters should be

considered in order to prove its effective low thermal conductivity such as porosity control, which can't be identified in performed tests conditions.
FTIR, Photo-DSC and DSC measurements were conducted in order to characterize kinetic and conversion phenomena. Photo-DSC measurements confirmed the skin effect present at higher amount of photoinitiator; in fact, the existence of skin effect is confirmed by the increasing of t_{gel} and the decreasing of $\dot{\alpha}$. This phenomenon is further confirmed by the delay of the measured starting point of the front, appreciable in formulation with the highest amount of photoinitiator (from 1,5%wt and above). Surprisingly, for concentrations of photoinitiator between 0,5%wt and 1,5%wt, the front velocity increases while $\dot{\alpha}$ decreases: this might be due to the fact that the skin effect blocks the creation of reactive species through the thickness of the sample, but an enhanced reactive species' creation occurs on the surface of the sample, therefore the initial part of the polymerization is characterized by a slower thermal diffusion. This may lead to both a decreasing on the starting time of the front and an higher front velocity since a better heat retention is induced. In addition, the two phenomena, photo-induced polymerization and thermal polymerization front, are respectively influenced by different conditions such as the skin effects or the internal filter effects (lowering the maximum conversion rate) and higher bubble formation and temperature (increasing the front velocity). Photo-DSC measurements regarding the different amount of thermal initiator showed a decreasing of the maximum conversion rate at concentration higher than 0,5%wt. This may conduct to speculate the possibility of the presence of a screening effect connected with the presence of higher amounts of thermal initiator. Analogue speculation was made for the thermographic analysis.
DSC measurements have been done in order to investigate conversion in deeper layers of the sample obtained by RICFP. None of the studied formulations revealed important exothermic peaks identifying a completed reaction, confirming the high reactivity associated to the studied photosensitive resin.
Since high temperatures and degradation phenomena occurs, no valuable application can be considered for the obtained final system taking also into account that the mechanical stability cannot be reached. Moreover, many difficulties have been observed trying to control the process such as front instabilities, production of gasses and even possible lack of impregnation. Those difficulties are mainly due to the heterogeneity of the foam structure and to impregnation method based only on infiltration. Controlling these features will lead to higher accuracy level. For example, in order to improve the impregnation step, it is possible to consider a functionalization of the foam surface by photografting or taking advantage of surfactants. Moreover, degradation phenomena and bubble formation should be considered carefully in these more critical conditions, especially for structural applications.
Finally, another porous media, an aluminium foam, was cured taking advantage of the studied process. This could open a wide new chapter on ultralightweight composites field maintaining all the advantages related to UV curing process. The envisaged high production rates, low energy consumption, solvent free and easy to produce formulations are important features which can lead to remarkable benefits in composite production. Further studies must be done in order to identify the best compromise for this process firstly focusing on the amount of initiator considered and the related production rate. According to the results obtained from the studied system, a way to reduce the process time and to maximize the production rate is to increase the amount of photoinitiator. However, this could be cost intensive because the photoinitiator is the most expensive compound added in the formulation.
Another parameter, which hasn't been altered in this study and maintained at low levels in order to investigate possible applications which involves skin contact, is the initial

irradiance. Increasing this value will lead to a faster polymerization rate related to the first UV dependent step according to equation 2.5. This will reduce the starting point of the front leading to an increased production rate.
In summary, the study led to the characterization of the application of the RICFP methodology for the occlusion of small cavities with the particular objective of manufacturing an earbud. The RICFP technique used with polyurethane foam is characterized by:

- certainty of the realization of a polymerization front;
- high and non-reducible exothermicity, this prevents its use for medical use and, in particular, makes this technique unsuitable for the creation of a personalized earbud;
- presence of irregular and non-predeterminable phenomena in the trigger area;
- high process temperatures that lead to degradation phenomena of the foam, the boiling of the resin with the consequent formation of hot gases which endanger the homogeneity of the polymerized product with the evident negative consequences on mechanical stability and on thermal and acoustic insulation.

The results of laboratory experiments made it possible to determine that the optimal percentages of initiators are between 0.5% wt and 1.5% wt of photoinitiator while the thermal initiator must be kept at the value of 0.5% wt.
Further investigations applied to this application could be:

- study a different resin with higher boiling temperature which doesn't allow the presence of bubbles during curing;
- study a way to reduce temperature, which is mostly related to the selected resin;
- find a balance between the percentage of initiators and the initial irradiance, in order to obtain the best efficiency from the process;
- investigate how the front of polymerization behaves when bigger dimensions of the manufact are required, focusing on how much it can be fed and how much gasses and bubbles production is expected;
- improve foam impregnation taking advantage of functionalization techniques, this enhancement can be related to all kind of used foams, both polymeric and metallic;
- investigate mechanical, physical and chemical properties of the Interpenetrating Phase Composite produced with RICFP technique.

Acknowledgement

First of all I would like to thank the Politecnico di Torino and the École polytechnique fédérale de Lausanne for the great opportunity provided to me to study and learn in an highly competent study and research environment, from which I learned important lessons.

My most sincere thanks to the supervisor of this project, Dr. Yves Leterrier, and to the thesis supervisor, Prof. Marco Sangermano, for giving me the opportunity to face an intriguing challenge, for the constant and enlightened guide and tuition and for providing me the insight from their experiences.

I thank all the members of the Laboratory for Processing of Advanced Composites for their continued availability and assistance, even outside normal working hours. I would like to express my special thanks to Jeroen Staal for his help and continued availability especially regarding the Photo-DSC measures.

I would like to thank Eurofoam for the foam sample provided to me.

Finally, my deepest gratefulness to all the study colleagues, to my friends, to my family and to my girlfriend Susanna, whose support was fundamental for the realization of this project.

6. References

[1] Fouassier, J. (1995). Photoinitiation, photopolymerization, and photocuring : fundamentals and applications. München: Hanser.

[2] Crivello JV and Dietliker K, Photoinitiators for Free Radical, Cationic and Anionic Polymerization, 2nd edn. Wiley, New York, p. 479 (1998).

[3] Pojman JA (2012) Frontal Polymerization. In: Matyjaszewski K and Möller M (eds.) Polymer Science: A Comprehensive Reference, Vol 4, pp. 957–980. Amsterdam: Elsevier BV

[4] KHAN, Akhtar M.; POJMAN, John A. The use of frontal polymerization in polymer synthesis. Trends in Polymer Science, 1996, 8.4: 253-257

[5] https://it.decorexpro.com/montazhnaya-pena/skolko-sohnet/

[6] https://www.lettera43.it/howto/quanto-tempo-ci-mette-il-silicone-ad-asciugare/

[7] J. Vuorio, V. Nikkilä, V. Teivastenaho, J. Peltola, J. Partanen, P. Kiviluoma, and P. Kuosmanen,"Additive manufacturing with UV light cured resin," 9th Int. Conf. DAAAM Balt. Ind. Eng. DAAAMBaltic 2014, vol. 2014–Janua, no. April, pp. 317–322, 2014

[8] Colpani, Alessandro & Fiorentino, Antonio & Ceretti, Elisabetta. (2018). 3D printing for health & wealth: Fabrication of custom-made medical devices through additive manufacturing. AIP Conference Proceedings. 1960. 140006. 10.1063/1.5034998.

[9] I. Gibson, "The changing face of additive manufacturing," J. Manuf. Technol. Manag., vol. 28, no. 1, pp. 10–17, 2017.

[10] Filingeri, Davide. (2016). Neurophysiology of Skin Thermal Sensations. Comprehensive Physiology. 6. 10.1002/cphy.c150040.

[11] https://www.shsu.edu/chm_tgc/chemilumdir/JABLONSKI.html

[12] Megson, N. J. L. (1956). Epoxide resins. Nature, 177(4517), 962–964. https://doi.org/10.1038/177962a0

[13] Klikovits, N., Liska, R., D'Anna, A., & Sangermano, M. (2017). Successful UV-Induced RICFP of Epoxy-Composites. macromolecular Chemistry and Physics.

[14] Sangermano, M., Antonazzo, I., Sisca, L. and Carello, M. (2019), Photoinduced cationic frontal polymerization of epoxy–carbon fibre composites. Polym. Int., 68: 1662-1665. doi:10.1002/pi.5875POLITECNICO DI TORINO.docx

[15] Mohamad Ali Tehfe, Fanny Louradour, Jacques Lalevée, Jean-Pierre Fouassier Photopolymerization Reactions: On the Way to a Green and Sustainable Chemistry, Appl. Sci. 2013, 3, 490-514; doi:10.3390/app3020490

[16] Crivello, J.V.; Reichmamis, E. Photopolymer materials and processes for advanced technologies. Chem. Mater. 2014, 26, 533–548.

[17] Sangermano, M. (2012). Advances in cationic photopolymerization. Pure and Applied Chemistry, 84(10), pp. 2089-2101. Retrieved 2 Feb. 2020, from doi:10.1351/PAC-CON-12-04-11.

[18] M. Atif, R. Bongiovanni & J. Yang (2015) Cationically UV-Cured Epoxy Composites, Polymer Reviews, 55:1, 90-106, DOI: 10.1080/15583724.2014.963236

[19] Sangermano, M., Pegel, S., Pötschke, P. and Voit, B. (2008), Antistatic Epoxy Coatings With Carbon Nanotubes Obtained by Cationic Photopolymerization. Macromol. Rapid Commun., 29: 396-400. doi:10.1002/marc.200700720

[20] Yang, Long & Yang, Jinliang & Nie, Jun & Zhu, Xiaoqun. (2017). Temperature controlled cationic photo-curing of a thick, dark composite. RSC Adv.. 7. 4046-4053. 10.1039/C6RA25346F.

[21] Atif, M., Yang, J., Yang, H., Jun, N., & Bongiovanni, R. (2016). Effect of novel UV-curing approach on thermo-mechanical properties of colored epoxy composites in outsized dimensions. Journal of Composite Materials, 50(22), 3147–3156. https://doi.org/10.1177/0021998315616174

[22] Bomze, D., Knaack, P., & Liska, R. (2015). Successful radical induced cationic frontal polymerization of epoxy-based monomers by C–C labile compounds. Polymer Chemistry, 6(47), 8161–8167. https://doi.org/10.1039/C5PY01451D

[23] Chechilo, N. M.; Enikolopyan, N. S. Dokl Phys Chem 1975, 221, 392–394.

[24] Chechilo, N. M.; Enikolopyan, N. S. Dokl Phys Chem 1976, 230, 840–843.

[25] Davtyan, Sevan & Tonoyan, Anahit. (2018). The Frontal Polymerization Method in High Technology Applications. Review Journal of Chemistry. 9. 432-455. 10.1134/S2079978018040039.

[26] Mariani, A., Bidali, S., Fiori, S., Sangermano, M., Malucelli, G., Bongiovanni, R. and Priola, A. (2004), UV-ignited frontal polymerization of an epoxy resin. J. Polym. Sci. A Polym. Chem., 42: 2066-2072. doi:10.1002/pola.20051

[27] Bomze, D., Knaack, P., Koch, T., Jin, H. and Liska, R. (2016), Radical induced cationic frontal polymerization as a versatile tool for epoxy curing and composite production. J. Polym. Sci. Part A: Polym. Chem., 54: 3751-3759. doi:10.1002/pola.28274

[28] Knaack, Patrick & Klikovits, Nicolas & Tran, Anh Dung & Bomze, Daniel & Liska, Robert. (2019). Radical induced cationic frontal polymerization in thin layers. Journal of Polymer Science Part A: Polymer Chemistry. 57. 10.1002/pola.29375.

[29] Rusu, M., Block, C., Van Assche, G., & Mele, B. (2012). Influence of temperature and UV intensity on photo-polymerization reaction studied by photo-DSC. Journal of Thermal Analysis and Calorimetry, 110. https://doi.org/10.1007/s10973-012-2465-5

[30] Terrones, G., & Pearlstein, A. J. (2001). Effects of optical attenuation and consumption of a photobleaching initiator on local initiation rates in photopolymerizations. Macromolecules, 34(10), 3195–3204. https://doi.org/10.1021/ma001235y

[31] Artavia, L. D., & Macosko, C. W. (1994). Polyurethane flexible foam formation BT - Low density cellular plastics: Physical basis of behaviour. In N. C. Hilyard & A. Cunningham (Eds.) (pp. 22–55). Dordrecht: Springer Netherlands. https://doi.org/10.1007/978-94-011-1256-7_2

[32] Obi, B. E. (2018). Fundamentals of Polymeric Foams and Classification of Foam Types. Polymeric Foams Structure-Property-Performance. https://doi.org/10.1016/b978-1-4557-7755-6.00005-7

[33] B. Croop, H. Lobo, and N. DatapointLabs, "Selecting material models for the simulation of foams in LS-DYNA," Proc. 7 th LS-DYNA …, 2009

[34] Gooch, J. W. (2010). Encyclopedic Dictionary of Polymers. Springer. Retrieved from https://books.google.ch/books?id=HRgy8iHQtdwC

[35] Sakam7oto, K., Lochhead, R. Y., Maibach, H. I., Yamashita, Y., & Nakama, Y. (2017). Surfactants. Cosmetic Science and Technology, 231–244. https://doi.org/10.1016/B978-0-12-802005-0.00015-X

[36] Ma, Z., Gao, C., Yuan, J., Ji, J., Gong, Y. and Shen, J. (2002), Surface modification of poly-L-lactide by photografting of hydrophilic polymers towards improving its hydrophilicity. J. Appl. Polym. Sci., 85: 2163-2171. doi:10.1002/app.10803

[37] Wegner, L. D., & Gibson, L. J. (2000). Mechanical behaviour of interpenetrating phase composites - I: Modelling. International Journal of Mechanical Sciences, 42(5), 925–942. https://doi.org/10.1016/S0020-7403(99)00025-9

[38] Jhaver, R., & Tippur, H. (2009). Processing, compression response and finite element modeling of syntactic foam based interpenetrating phase composite (IPC). Materials Science and Engineering A, 499(1–2), 507–517. https://doi.org/10.1016/j.msea.2008.09.042

[39] Liu, Y., & Gong, X. L. (2006). Compressive behavior and energy absorption of metal porous polymer composite with interpenetrating network structure. Transactions of Nonferrous Metals Society of China (English Edition), 16(SUPPL.). https://doi.org/10.1016/S1003-6326(06)60229-X

[40] Marx, J. C., Robbins, S. J., Grady, Z. A., Palmieri, F. L., Wohl, C. J., & Rabiei, A. (2020). Polymer infused composite metal foam as a potential aircraft leading edge material. Applied Surface Science, 505(May 2019), 144114. https://doi.org/10.1016/j.apsusc.2019.144114

[41] Voytekunas, V. Y., Ng, F. L., & Abadie, M. J. M. (2008). Kinetics study of the UV-initiated cationic polymerization of cycloaliphatic diepoxide resins. European Polymer Journal, 44(11), 3640–3649. https://doi.org/10.1016/j.eurpolymj.2008.08.043

[42] Fouassier, J. P., Allonas, X., & Burget, D. (2003). Photopolymerization reactions under visible lights: Principle, mechanisms and examples of applications. *Progress in Organic Coatings*, *47*(1), 16–36. https://doi.org/10.1016/S0300-9440(03)00011-0

[43] http://www.eurospuma.com/en/

[44] http://www.flirmedia.com/MMC/THG/Brochures/RND_059/RND_059_US.pdf

[45] Harrap MJM, Hempel de Ibarra N, Whitney HM, Rands SA. 2018 Reporting of thermography parameters in biology: a systematic review of thermal imaging literature. R. Soc. open sci. 5: 181281. http://dx.doi.org/10.1098/rsos.181281

[46] https://www.engineeringtoolbox.com/emissivity-coefficients-d_447.html

[47] González, M. G., Cabanelas, J. C., & Baselga, J. (2012). Applications of FTIR on epoxy resins-identification, monitoring the curing process, phase separation and water uptake. Infrared Spectroscopy-Materials Science, Engineering and Technology, 2, 261–284.

[48] Golaz, B., Michaud, V., Leterrier, Y., & Mnson, J. A. E. (2012). UV intensity, temperature and dark-curing effects in cationic photo-polymerization of a cycloaliphatic epoxy resin. Polymer, 53(10), 2038–2048. https://doi.org/10.1016/j.polymer.2012.03.025

[49] Corcione, C., Malucelli, G., Frigione, M., & Maffezzoli, A. (2009). UV-curable epoxy systems containing hyperbranched polymers: Kinetics investigation by photo-DSC and real-time FT-IR experiments. Polymer Testing - POLYM TEST, 28, 157–164. https://doi.org/10.1016/j.polymertesting.2008.11.002

[50] Decker, C., Nguyen Thi Viet, T. and Pham Thi, H. (2001), Photoinitiated cationic polymerization of epoxides. Polym. Int., 50: 986-997. doi:10.1002/pi.730

[51] https://www.thermofisher.com/it/en/home/industrial/spectroscopy-elemental-isotope-analysis/spectroscopy-elemental-isotope-analysis-learning-center/molecular-spectroscopy-information/ftir-information/ftir-sample-handling-techniques/ftir-sample-handling-techniques-attenuated-total-reflection-atr.html

[52] Thomas Vidil, François Tournilhac, Simone Musso, Agathe Robisson, Ludwik Leibler. Control of reactions and network structures of epoxy thermosets. Progress in Polymer Science, Elsevier, 2016, 62, pp.126-179.

[53] Chinkanjanarot, Sorayot. (2018). MULTISCALE MODELING: THERMAL CONDUCTIVITY OF GRAPHENE/CYCLOALIPHATIC EPOXY COMPOSITES.

[54] FRANCL, J. and KINGERY, W.D. (1954), Thermal Conductivity: IX, Experimental Investigation of Effect of Porosity on Thermal Conductivity. Journal of the American Ceramic Society, 37: 99-107. doi:10.1111/j.1551-2916. 1954.tb20108.x

[55] Rusu, M., Block, C., Van Assche, G., & Mele, B. (2012). Influence of temperature and UV intensity on photo-polymerization reaction studied by photo-DSC. *Journal of Thermal Analysis and Calorimetry*, *110*. https://doi.org/10.1007/s10973-012-2465-5

[56] Maurizio F., Stefano P., & Davide R. (2019). Photoorganocatalysis In Organic Synthesis. World Scientific Publishing Comp. pp. 508 [ISBN 978-1786-34606-3]

[57] Kabatc, J., Ortyl, J., & Kostrzewska, K. (2017). New kinetic and mechanistic aspects of photosensitization of iodonium salts in photopolymerization of acrylates. RSC Advances, 7(66), 41619–41629. https://doi.org/10.1039/C7RA05978G

[58] Boey, F., Rath, S.K., Ng, A.K. and Abadie, M.J.M. (2002), Cationic UV cure kinetics for multifunctional epoxies. J. Appl. Polym. Sci., 86: 518-525. doi:10.1002/app.11041

[59] Potey, L. C., Kosalge, S. B., & Sarode, R. S. (2014). Synthesis and Analysis of Benzopinacol from Benzophenone by Photoreduction in Green Chemistry. International Journal of Pharmaceutics and Drug Analysis, 2(1), 55–58. http://ijpda.com/admin/uploads/nwTfHj.pdf

[60] Hennessy, M. G., Vitale, A., Cabral, J. T., & Matar, O. K. (2015). Role of heat generation and thermal diffusion during frontal photopolymerization. Physical Review E -

Statistical, Nonlinear, and Soft Matter Physics, 92(2). https://doi.org/10.1103/PhysRevE.92.022403

[61] Nason, C., Roper, T., Hoyle, C., & Pojman, J. A. (2005). UV-induced frontal polymerization of multifunctional (meth)acrylates. *Macromolecules*, *38*(13), 5506–5512. https://doi.org/10.1021/ma048569y